DRAFT

EVALUATION OF UNCERTAINTIES IN SCDAP/RELAP5 STATION BLACKOUT SIMULATIONS

by

C. D. Fletcher
R. M. Beaton

Information Systems Laboratories, Inc.
Idaho Falls, Idaho and Rockville, Maryland

prepared for

U. S. Nuclear Regulatory Commission
Office of Nuclear Regulatory Research
Washington DC 20555

NRC Project Officer
Donald Helton
NRC Technical Advisor
Christopher F. Boyd

under

Contract No. NRC-04-05-064
Continuation of Support for System Code Analysis to Predict
Severe Accident Conditions Leading to Containment Bypass

JCN Number Y6198
RES ID: RES-C05-340

August 2006

ABSTRACT

The U. S. Nuclear Regulatory Commission has been conducting studies to evaluate the risk associated with steam generator tube failure following low probability severe accidents in pressurized water reactors. The issue relates to the sequence in which the various reactor coolant system boundary structures fail. Failures of hot leg piping, pressurizer surge line piping and the reactor vessel wall lead to discharge of fission products into the containment. Failures of steam generator tubes lead to discharge of fission products into the steam generator secondary system, from where they may be discharged to the environment through the main steam safety or secondary system power operated relief valves. Prior reports have evaluated the extent of steam generator tube structural strength degradation required to cause tube failures to precede hot leg or pressurizer tube failure for a station blackout event in a typical Westinghouse PWR as well as other plants. This report estimates the uncertainties in key SCDAP/RELAP5-calculated output parameters for a base case severe accident station blackout event sequence in a Westinghouse four-loop PWR. The key output parameters are those identified by a Phenomena Identification and Ranking Table (PIRT) evaluation as being important for representing the plant behavior during the specific accident event sequence. An uncertainty evaluation is performed using a sensitivity-study approach in which the base case simulation is repeated, except with model changes implemented to represent variations in important phenomena, which are also identified through PIRT evaluation.

CONTENTS

LIST OF FIGURES

LIST OF TABLES

EXECUTIVE SUMMARY

A natural circulation of highly superheated steam can develop in the reactor coolant system (RCS) of pressurized water reactors during specific low probability station blackout (SBO) events that progress to severe accident conditions. This steam circulation can transfer significant heat from the reactor core to portions of the RCS outside of the reactor vessel. Since the pressure in the RCS can remain elevated during a SBO event sequence, introducing highly superheated steam into the hot leg, pressurizer surge line and steam generator (SG) tube regions of the RCS poses potential challenges for the pressure boundaries in these components. The potential for SG tubes to fail is of particular importance since their failure represents the opening of a flow path from the RCS into the SG secondary system, where the pressure relief valves could provide a direct path for the passage of core fission products to reach the environment.

The Nuclear Regulatory Commission (NRC) has been pursuing thermal-hydraulic studies to evaluate SG tube integrity. Several previous reports have documented base case and sensitivity SCDAP/RELAP5 simulations for station blackout event sequences in a typical Westinghouse plant. This report documents a study estimating the uncertainties in key SCDAP/RELAP5-calculated output parameters.

The key parameters are those SCDAP/RELAP5 output variables (temperatures, heat transfer coefficients and scoping SG tube failure safety margins) which others in the project are using in the performance of detailed piping stress analyses and probabilistic risk analyses. These key parameters represent the dependent variables for the uncertainty study.

The uncertainties are estimated using a sensitivity-study approach. Variations in important parameters are individually implemented into the SCDAP/RELAP5 model and the results from sensitivity runs which include the variations are compared with the results of the base case run. The important parameters (the independent variables for the uncertainty study) are identified using a Phenomena Identification and Ranking Table (PIRT) evaluation of the thermal-hydraulic phenomena, physical processes and behavior important for simulating the base case station blackout event sequence in the typical plant. The differences between the sensitivity and base case values for the dependent variables are used to estimate the uncertainties present in the SCDAP/RELAP5 simulation of those variables.

Nineteen SCDAP/RELAP5 sensitivity calculations are performed for the purpose of estimating the uncertainties in eight key SCDAP/RELAP output variables. An additional 12 SCDAP/RELAP5 sensitivity calculations are performed for the purpose of evaluating various other modeling, plant configuration and accident event-sequence issues.

The results from the uncertainty study are the standard deviations for the eight key SCDAP/RELAP5 output variables. The standard deviations are calculated with four different approaches: using equal-weighting and biased-weighting of the independent-variable terms and with and without consideration of the effects of uncertainty in the mean.

The recommended standard deviations are those calculated using biased-weighting of the independent variable terms. This approach takes advantage of information regarding the likelihood for independent variable changes in one direction versus the other direction. The information comes from plant operating experience, assessment of SCDAP models against specific severe accident experiments and assessment of RELAP5 models against a much-larger set of general reactor safety thermal-hydraulic experiments.

The recommended standard deviations are also those calculated with the consideration that the 20 SCDAP/RELAP5 runs collectively (rather than the base case run alone) best represents the mean behavior of the dependent variables.

The recommended standard deviations for the key SCDAP/RELAP5 output variables are tabulated in Section 8.

Data for the input, output and plot files for the SCDAP/RELAP5 calculations described in this report are provided on DVDs which are available to recipients of this report. Additional output data from the SCDAP/RELAP5 calculations are also provided on the DVDs to facilitate analyses performed by others involved in the project.

NOMENCLATURE

AC	alternating current
ACRS	Advisory Committee on Reactor Safeguards
AFW	auxiliary feedwater
CCFL	counter-current flow limiting
C_D	hot leg discharge coefficient
CE	Combustion Engineering
CFD	computational fluid dynamics
C_v	flow coefficient
D	diameter
DVD	digital video diskette
FSAR	final safety analysis report
FW	feedwater
HL	hot leg
INEEL	Idaho National Engineering and Environmental Laboratory
ISL	Information Systems Laboratories, Inc.
MFW	main feedwater
NRC	U. S. Nuclear Regulatory Commission
PIRT	phenomena identification and ranking table
PORV	power operated relief valve
PRA	probabilistic risk assessment
PWR	pressurized water reactor
RCP	reactor coolant pump
RCS	reactor coolant system
RV	reactor vessel
SBO	station blackout
SG	steam generator
SL	pressurizer surge line
SRV	safety relief valve
σ	standard deviation

FOREWORD

The analyses presented in this report are performed to evaluate plant behavior during hypothetical event sequences with potential for leading to a severe accident. The occurrence of the event sequences is extremely unlikely due to multiple assumed concurrent failures of systems and components. A few of the key assumptions for the station blackout base case accident sequence are:

- Loss of off-site power for an extended period
- Failure of all diesel-electric generators to start
- Failure of the turbine-driven auxiliary feedwater system to operate
- 21 gpm (equivalent hole size) reactor coolant pump shaft seal leakage
- Steam leakage causes all steam generators to depressurize

These assumptions result in a “high-dry” condition with all four steam generators depressurized by the time any primary system ruptures are predicted to occur. No operator intervention for mitigating the accident is accounted for.

The analyses therefore do not represent best-estimate plant behavior, nor do the results indicate the most-likely outcomes of the event sequences. The results can only be put into perspective with appropriate consideration for the probability of such events occurring. The predicted results apply only for the specific analysis assumptions and may vary considerably as assumptions are changed (for example, greater reactor coolant pump shaft seal leakage rates can eliminate steam generator tube failures which are predicted at smaller leakage rates). These considerations must ultimately be accounted for in an integrated probabilistic risk assessment of severe accident induced steam generator tube failures

1.0 INTRODUCTION

The U. S. Nuclear Regulatory Commission (NRC) has for the past several years been conducting studies to evaluate the risk associated with steam generator (SG) tube failure following severe accidents in pressurized water reactors (PWRs). For PWRs with U-tube SGs, the natural circulation of superheated steam in the loop piping during severe accidents could result in sufficient heating of the SG tubes to induce creep rupture failure prior to hot leg or surge line failure. To examine the risk impacts of induced SG tube rupture and the effects of changes in the regulatory requirements for SG tube integrity, the NRC has performed severe accident thermal-hydraulic analyses to examine the pressure and temperature conditions imposed on the SG tubes. These evaluations have focused on tube integrity during station blackout (SBO) severe accident scenarios wherein the reactor coolant system (RCS) remains at high pressure, the SG water inventory is lost and no source of feedwater is assumed available. This type of event exposes the SG tubes to highly-superheated steam at the high RCS pressures associated with the opening setpoint pressures of the pressurizer power operated relief valves (PORVs) and safety relief valves (SRVs), coincident with low-pressure conditions in the SG secondary system.

Because the SBO event represents a significant risk contributor among sequences that progress to core damage and poses a threat to SG integrity, that event has been the assumed accident initiator for all of the analyses performed to date using the system code SCDAP/RELAP5 (Reference 1). The extent of the prior analyses has been considerable. The Idaho National Engineering and Environmental Laboratory (INEEL) evaluated SBO events in several PWRs (Reference 2). Subsequently, the INEEL refined a SCDAP/RELAP5 model of a typical Westinghouse four-loop plant for simulating this accident sequence (Reference 3). Information Systems Laboratories, Inc. (ISL) evaluated the effects on the results of variations in the accident sequence and modeling assumptions (References 4 and 5). The SCDAP/RELAP5 models for SBO events represent the average tubes in the SGs. ISL developed a method (Reference 6) based on Westinghouse 1/7th-scale experimental data (Reference 7) by which the temperatures and failure criteria for the hottest SG tube can be estimated using the average SG tube output data from the SCDAP/RELAP5 calculation. ISL then extensively documented a revised base case calculation for the Westinghouse four-loop plant using the upgraded model that included the hottest tube response (Reference 8). ISL performed an extensive set of sensitivity studies evaluating various changes in SCDAP/RELAP5 modeling options, event sequence assumptions and plant configuration (Reference 9). Subsequently, additional modifications of the Westinghouse four-loop plant model were incorporated to improve the model performance, better represent the physical response of the plant and provide additional output data to facilitate analyses performed by others in the project. Reference 10 fully documents the current SCDAP/RELAP5 Westinghouse four-loop plant model and the results of a revised station blackout base case calculation.

This report develops estimates for the uncertainties present in SCDAP/RELAP5 simulations of SBO accident event sequences in a typical Westinghouse PWR. The base case calculation from Reference 10 serves as the nominal case for the uncertainty evaluation. It is noted that this base case calculation does not necessarily represent a best-estimate simulation of the most-likely SBO accident scenario.

Section 2 of this report provides an overview description of the SCDAP/RELAP5 system model. Section 3 describes the base case SBO event sequence and summarizes the results of the SCDAP/RELAP5 SBO base case calculation from Reference 10. Section 4 describes a Phenomena Identification and Ranking Table (PIRT) evaluation of the important phenomena, processes and plant behavior for the base case event sequence. The PIRT was employed to identify the dependent variables (the figures of merit) and the independent variables (the important thermal-hydraulic phenomena affecting the figures of merit) for the uncertainty evaluation. Section 5 describes the selection of the sensitivity case calculations (variations on the base case calculation) that were run to generate data for the uncertainty evaluation and to address various other modeling, event sequence assumption and plant configuration issues. The results from the sensitivity runs are given in Section 6. Estimates for the uncertainties in the calculated results for the figures of merit are developed in Section 7. The conclusions from the work described in this report are given in Section 8 and references are listed in Section 9. Appendix A provides a list of the SCDAP/RELAP5 calculation channel identifiers for which additional output data from the calculations is provided on DVDs that are available to project participants.

2.0 SCDAP/RELAP5 MODEL DESCRIPTION

The SCDAP/RELAP5 plant model is fully documented in Reference 10. The model represents the fluid volumes and structures in the core, reactor vessel and primary and secondary coolant system regions of the plant. The model also includes a simple representation of the containment. As discussed in the introduction, this plant model has been developed by INEEL and ISL over a period of many years for the specific purpose of evaluating the SBO event in a Westinghouse PWR.

The SCDAP/RELAP5 computer code (Reference 1) calculates the overall RCS thermal-hydraulic response for severe accident situations that include core damage progression and reactor vessel heat up and damage. The computer code is the result of a merging of the RELAP5 and SCDAP computer codes. Models in RELAP5 calculate the overall RCS thermal-hydraulics, control system interactions, reactor kinetics and the transport of non-condensable gases. The RELAP5 code is based on a two-fluid (steam/noncondensible mixture and water) model allowing for unequal temperatures and velocities of the fluids and the flow of fluid through porous debris and around blockages caused by reactor core damage. Models in SCDAP calculate the progression of damage in the reactor core, including the heat up, oxidation and meltdown of fuel rods and control rods, ballooning and rupture of fuel rod cladding, release of fission products from fuel rods and the disintegration of fuel rods into porous debris and molten materials. The SCDAP models also calculate the heat up and structural damage of the reactor vessel lower head which results from the slumping of reactor core material with internal heat generation.

SCDAP also includes models for calculating the creep rupture failure of structural components. Specifically important for this project is the calculation of creep failure for stainless steel and Inconel based on the creep rupture theory of Larson and Miller (Reference 11 and Reference 1, Volume 2, Section 12.0). This creep rupture failure model is employed in the system model to predict failure times for the hot legs, pressurizer surge line and SG tubes. The model allows one to specify a stress multiplier, wherein a multiplier of 1.0 provides a creep failure prediction for a structure with no material degradation, and multipliers greater than 1.0 may be used to represent conditions of degraded structural strength. In the plant model, creep rupture failure calculations are performed for the average SG tubes and hot legs in all four coolant loops, and for the pressurizer surge line and hottest SG tube in the pressurizer-loop SG. A stress multiplier of 1.0 is used for the hot leg and surge line structure calculations while stress multipliers from 1.0 to 7.5 are used for the SG tube calculations. The SCDAP/RELAP5-calculated predictions of structural failures are intended to provide a reasonable “first look” into that issue, not to supplant structural failure evaluations using more detailed analysis tools.

The SCDAP/RELAP5 calculations presented in this report were performed with code Version 3.3de, which contains the SCDAP source taken from SCDAP/RELAP5/MOD3.3, Version 3.3ld.

The nodalization diagrams for the revised SCDAP/RELAP5 plant model are provided in Figures 1 through 4. In these diagrams, the open areas typically represent fluid regions with arrows indicating flow paths and shaded regions represent the structures included in the model (such as fuel rods, vessel internals and piping walls). The reader is cautioned that for practical reasons

the sub-structure of some components in the model cannot be accurately shown in these diagrams. For example, the upgraded model currently uses 40 axial nodes over the heated length of the core, not 10 nodes as shown in Figure 1.

The SCDAP/RELAP5 SBO calculations are performed in four sequential steps, which are described as follows.

In Step 1 (steady state) a model using the reactor vessel nodalization in Figure 1 and the coolant loop nodalization in Figure 2 is used to establish full-power steady-state conditions from which the SBO transient accident sequence is initiated. Note that Figure 2 shows the nodalization for only one of the coolant loops; identical models are used for all four coolant loops (with the exception of the pressurizer and surge line, which are connected only on Loop 1).

In Step 2 (time reset), the same model is used to perform a brief restart calculation only for the purpose of resetting the problem time to zero at the start of the SBO accident sequence.

In Step 3 (event initiation), the model continues using the nodalization schemes shown in Figures 1 and 2, but model features and changes are implemented to initiate the SBO accident sequence (such as tripping the reactor, the turbine and the reactor coolant pumps and disabling feedwater). This model is run from the time of SBO event initiation until the time when the core uncovers and superheated steam begins to enter the coolant loops.

In Step 4 (post core uncovery), significant modeling changes are made so as to permit the simulation of the two different coolant loop natural circulation modes shown in Figure 5. The mode shown on the right side of Figure 5 represents a countercurrent flow situation wherein hot steam is passed through the upper halves of the hot legs to the SG inlet plenum where mixing occurs (which results in a counter flow of hot and cool steam through the SG tubes) and cool steam is returned to the reactor vessel via flow through the lower halves of the hot legs. The mode shown on the left side of Figure 5 represents a flow of steam from the reactor vessel upper plenum, through the hot legs and completely around the coolant loop to the reactor vessel downcomer. The model selects the coolant loop circulation mode based upon whether or not the reactor coolant pump cold leg loop seal (Component 116 in Figures 2 and 3) is filled with water, a condition which blocks steam flow around the coolant loop. This selection is made independently for each of the four coolant loops of the model. The model therefore is capable of representing both the “recirculating” and “normal” coolant loop flow behaviors shown in Figure 5. In the typical plant examined, the pressurizer surge line connects on the side of the Loop 1 hot leg. Figure 4 shows the hot leg-to-surge line connection scheme employed for joining the surge line to the upper and lower sections of Hot Leg 1.

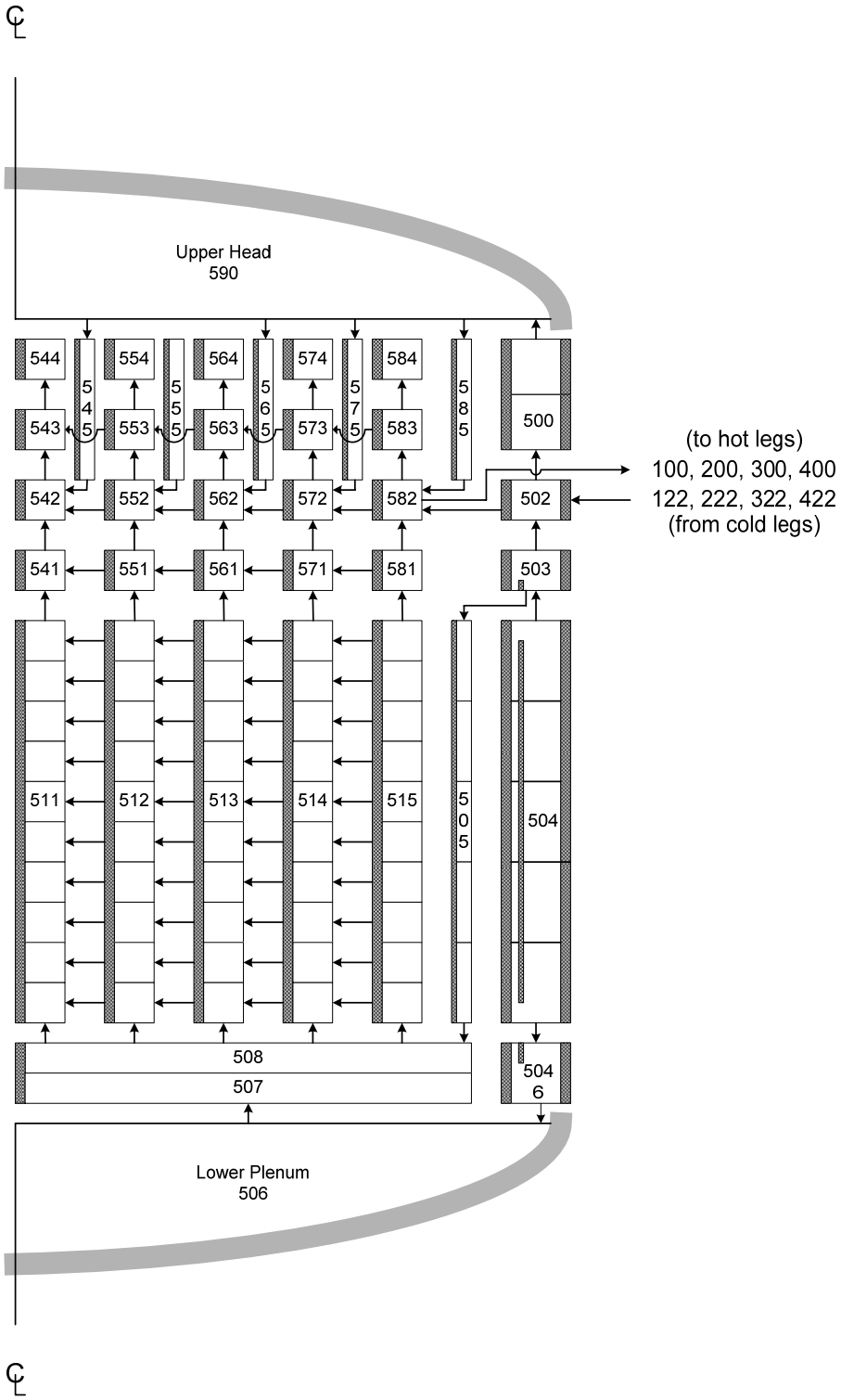

Figure 1. Reactor Vessel Nodalization.

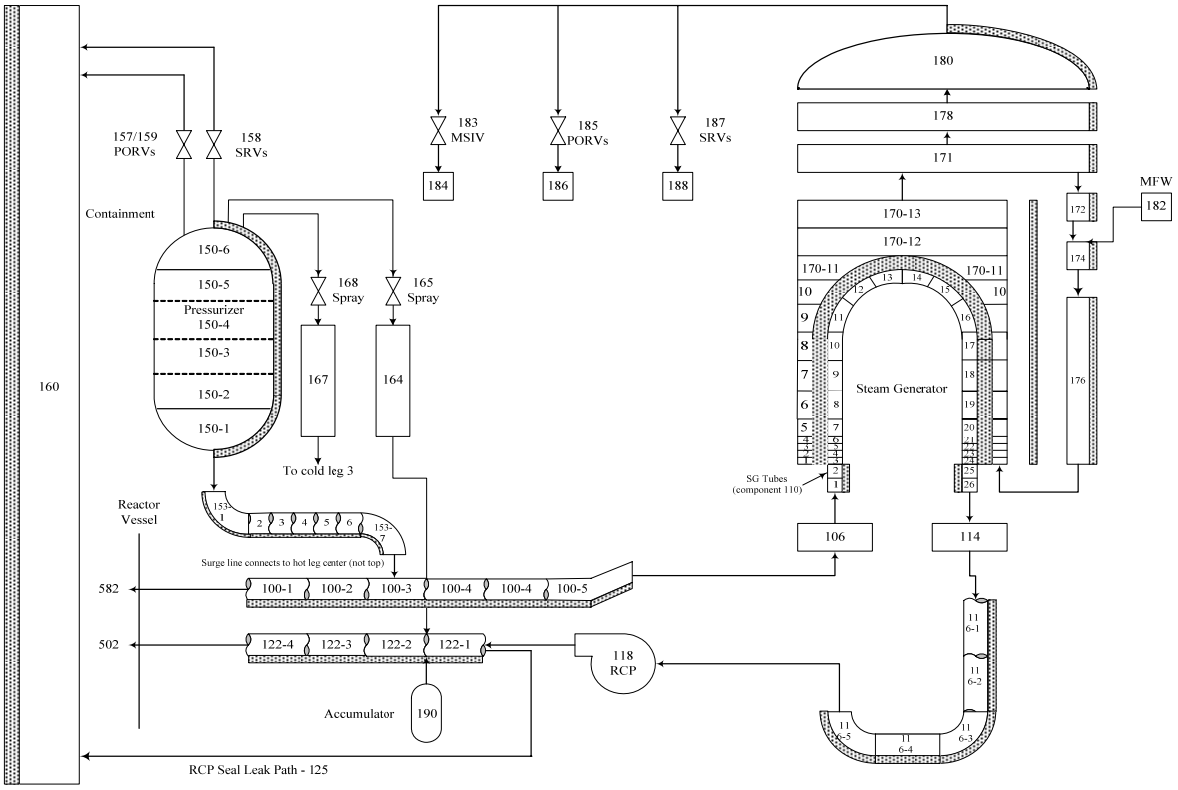

Figure 2. Loop Nodalization Excluding Provisions for Countercurrent Natural Circulation.

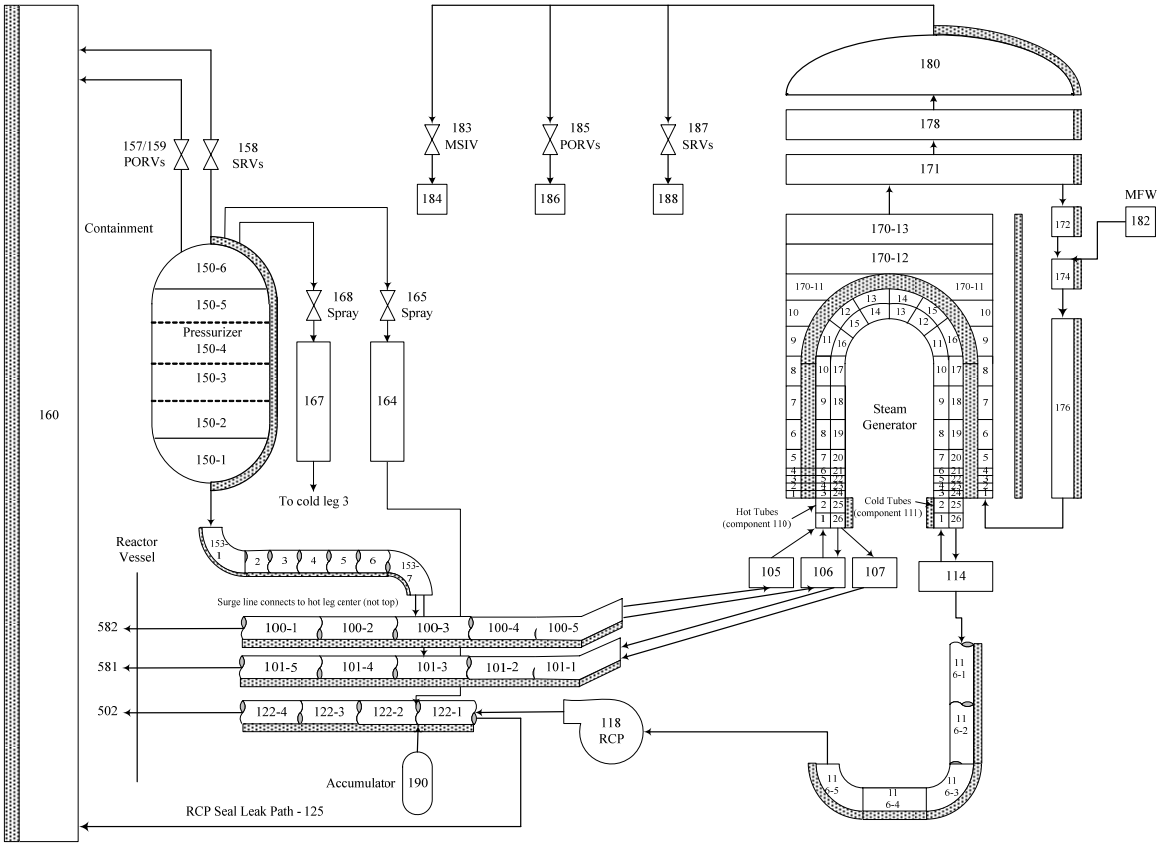

Figure 3. Loop Nodalization With Provisions for Countercurrent Natural Circulation.

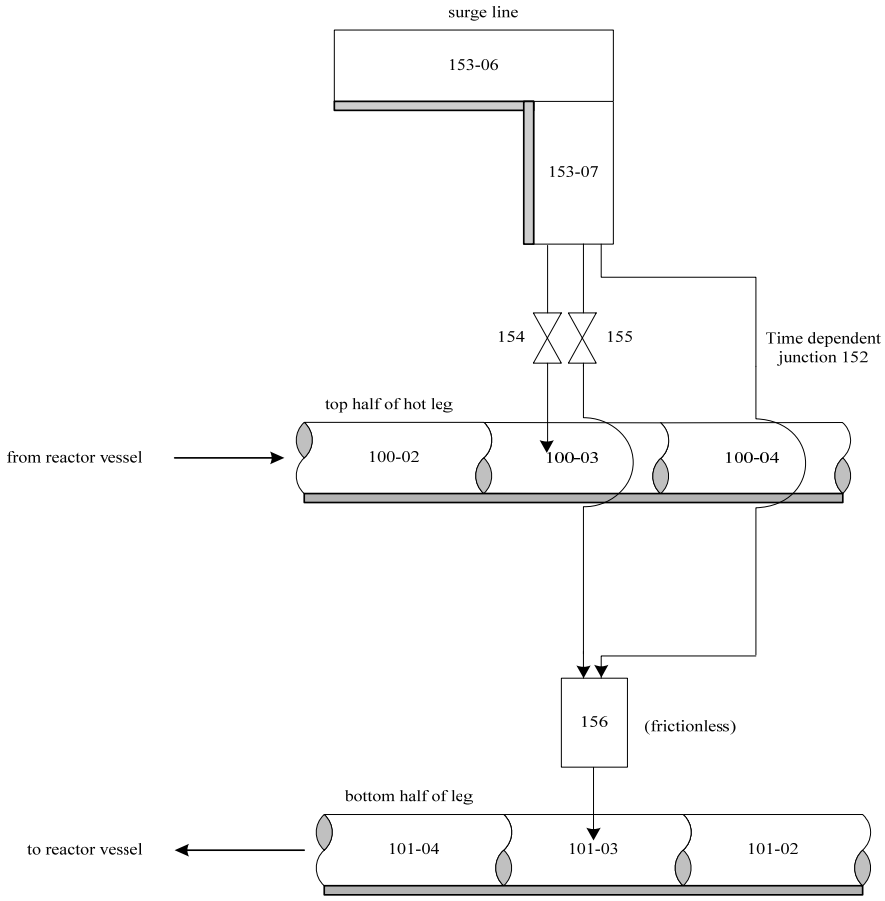

Figure 4. Surge Line Connections to the Split Hot Leg During Natural Circulation.

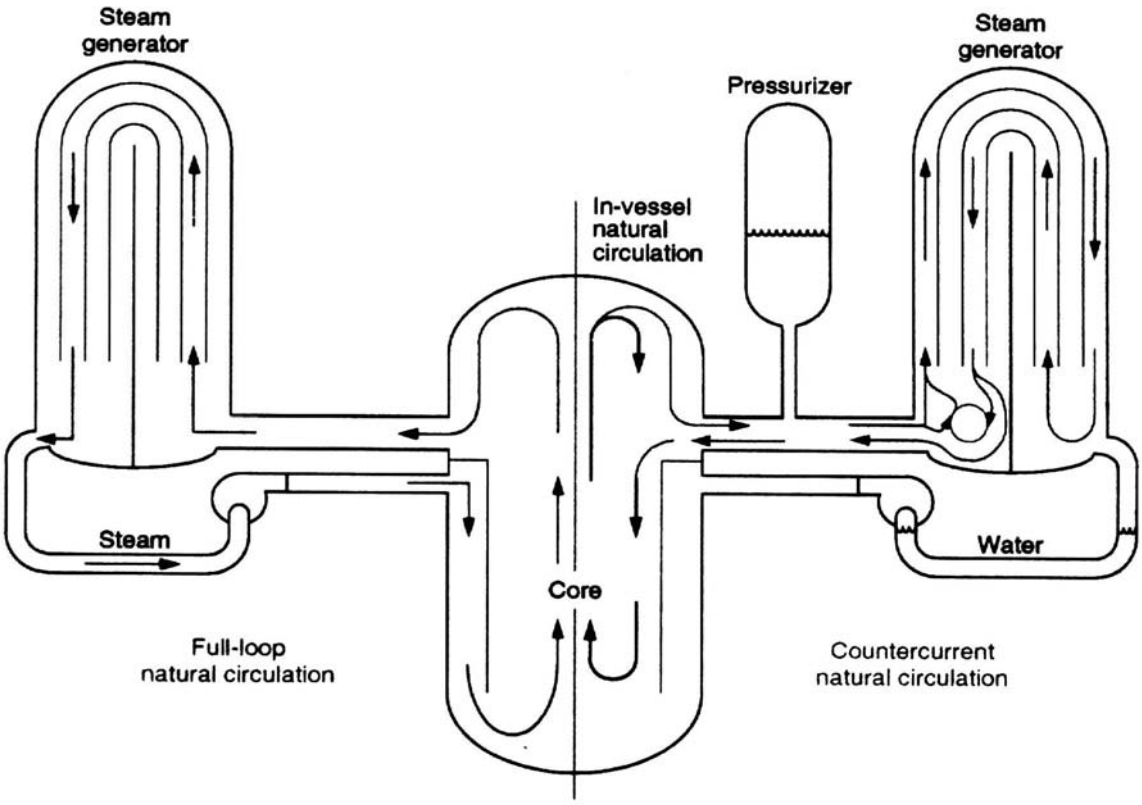

Figure 5. Natural Circulation Flow Patterns that Develop During Severe Accidents in PWRs with U-Tube Steam Generators.

3.0 BASE CASE EVENT SEQUENCE DESCRIPTION AND CALCULATION RESULTS

This section documents the SCDAP/RELAP5 SBO base case calculation which is used as the reference case for the uncertainty evaluation. Section 3.1 describes the base case station blackout accident event sequence. Section 3.2 describes the calculation of steady state conditions from which the transient SBO event sequence is begun. Section 3.3 describes the results of the transient base case calculation.

3.1 Event Sequence Description

The sequence of events simulated in the SCDAP/RELAP5 SBO base case transient calculation is summarized as follows.

A loss of off-site AC power occurs when the reactor is operating at full power and with a 10% tube plugging condition in each of the four steam generators (SGs). The diesel-electric generators fail to start and as a result all AC plant power sources are lost. The loss of AC power results in reactor and turbine trips and the coast-down of the four reactor coolant pumps (RCPs). The letdown flow is isolated and the charging system functions of pressurizer level control and RCP seal injection are lost. The high and low pressure safety injection systems are not available because of the AC power loss. The accumulator systems are available for injecting coolant into the cold legs should the reactor coolant system (RCS) pressure fall below the initial accumulator pressure, 4.24 MPa (615 psia). The main feedwater flow stops and the motor-driven auxiliary feedwater (AFW) system is unavailable as a result of the AC power loss. The turbine-driven AFW system has an independent failure-to-start assumption in the event sequence being modeled, so no feedwater is available following the loss of AC power. A station battery life of four hours is assumed; after that time motor operated valves, such as the pressurizer and SG power operated relief valves (PORVs) are considered inoperable.

The SG secondary system pressures rise because the feedwater and steam flow paths are isolated at the beginning of the event sequence. The SG PORVs open to limit the pressure increase. Minor steam leak paths from the SGs are assumed which have the effect of slowly depressurizing all four SGs over a period of about two hours after the SG water inventory has boiled off. A steam leak flow area of 3.23 cm^2 (0.5 in^2) is assumed in each SG.

The event sequence assumes that the loss of RCP seal injection cooling flow results in partial failures of the RCP shaft seals in all four coolant pumps at the time the SBO event begins. An initial 21 gpm per pump leak rate of RCS liquid around the shaft seals into the containment is assumed. The seal leak path characteristics and flow areas are not changed over the course of the event sequence and the leak flow rates are determined by the transient fluid conditions calculated in the pumps and containment.

This low-probability event sequence results in a severe accident because none of the systems that provide normal core cooling are assumed to be operable. For a while, buoyancy-driven coolant-loop natural circulation carries hot water from the core through the SGs, transferring heat to the SG secondary water inventory. The SG water inventory is boiled and the steam is released

through the SG PORVs. Since none of the feedwater systems are available, the secondary water inventory declines and is eventually fully depleted. After that time, the core decay power heats and swells the RCS water, increasing its temperature and pressure. During this process, the RCS pressure increase is limited by the opening of the pressurizer PORVs and the pressurizer safety relief valves (SRVs). The RCS fluid lost through those valves is not recoverable so the RCS inventory continuously declines. Eventually, the RCS inventory loss becomes extreme, the core uncovers and the fuel starts to heat up. The fuel heat up leads to an exothermic oxidation process between the steam and the fuel rod cladding that adds heat to the fuel in addition to the heat produced from the fission decay process.

The basic physical processes of this event sequence during the period when the steam temperatures are rising regard the transport of hot steam from the core outward into the other regions of the reactor vessel and coolant loops. Of main concern is which structural components first reach their high-temperature failure points. A failure of SG tubes leads to discharge of radioactivity from the RCS into the SG secondary system, from which it may be released to the atmosphere via flow through SG PORVs or SRVs. This type of release is referred to as "containment bypass." A failure of the reactor vessel or reactor coolant piping (such as the hot legs or pressurizer surge line) leads to discharge of the reactivity into the containment, from which the potential releases to the atmosphere are significantly lower. Further, a failure of the reactor vessel or reactor coolant piping depressurizes the RCS, which reduces stresses on the SG tubes and likely prevents their failure. Even in the event of SG tube failures subsequent to other RCS component failures, the reduced pressure inside the tubes will not result in a significant containment bypass release to the atmosphere.

3.2 Steady State Calculation of Initial Conditions

The SCDAP/RELAP5 model was run to a steady solution over a period of 1,500 s. The file name of the input deck for the steady-state run is "uncbases1.i". The file name of a short SCDAP/RELAP5 restart calculation from the end point of the steady-state run (to reset time to zero) is "uncbases2.i". These are Steps 1 and 2 of a sequential four-step SCDAP/RELAP5 calculation process, as described in Section 2.

The calculated conditions from the end of the SCDAP/RELAP5 steady-state run are compared with the target values for the plant full-power operating conditions in Table 1. The comparison indicates that the code-calculated parameters are in excellent agreement with the desired plant values. The calculated steady-state solution therefore represents an acceptable set of initial conditions from which to start the transient SBO accident simulation.

3.3 Transient Station Blackout Calculation Results

The transient SBO event sequence described in Section 3.1 was simulated using the SCDAP/RELAP5 model, starting from time zero at the time of the loss of off-site power. The transient calculation is performed as Steps 3 and 4 of a four-step SCDAP/RELAP5 modeling process as described in Section 2. The file name of the Step 3 input model, which is used from time zero until the time when the core uncovers, is "uncbases3.i". The file name of the Step 4

input model, which incorporates the split hot leg and SG tube modeling configuration after the time when the core uncovers, is "uncbases4.i".

The SCDAP/RELAP5 calculated sequence of events for the SBO base case is shown in Table 2. The calculated time history results for key parameters are shown in Figure 6 through Figure 27 and are summarized as follows. A more detailed analysis of the base case calculation transient results is provided in Reference 10.

The RCS pressure response is shown in Figure 6. The pressure initially declines in response to the cooling provided by heat removal to the SGs and by the RCP shaft seal leaks. Figure 7 shows the SG secondary pressure responses and Figure 8 shows the RCP leak flow responses. The RCS depressurization continues until the SG secondary liquid inventories, as shown in Figure 9, have been boiled and released to the atmosphere through the SG PORVs. Afterward, the cooling afforded by system heat loss to containment and pump shaft seal leak flow is insufficient to remove the RCS heat load and the RCS pressure increases to the opening setpoint pressures of the pressurizer PORVs and SRVs, as shown in Figures 10 and 11. The most challenging RCS pressure conditions are experienced when the pressurizer fills with water, as shown in Figure 12.

The mass lost through the pressurizer PORVs and SRVs and through the RCP shaft seal leakage paths depletes the RCS inventory, the core uncovers and superheated steam flows out from the reactor vessel into the coolant loops starting at 9,222 s. Water remains trapped in the cold leg RCP-suction loop seal piping, thus blocking the path for the steam to flow all the way around the coolant loops. This blockage provides the conditions necessary for countercurrent flow through the hot legs and SG tubes. Figure 13 shows the void fractions calculated in the bottom cells of the loop seal piping. The loop seal piping in all four loops remains water filled during the period of maximum RCS pressurization, with only minor bubbling of steam through the loop seals.

Following core uncovery, countercurrent flow of superheated steam is calculated through two circulation flow paths within each coolant loop. In one circulation path, hot steam flows upward from the SG inlet plenum through a portion (41%) of the SG tubes and cool steam returns from the SG outlet plenum through the remaining portion of the SG tubes, flowing downward as it reaches the SG inlet plenum. In the other circulation path, hot steam flows through the upper half of the hot leg to the SG inlet plenum and cooler steam is returned from the SG inlet plenum to the reactor vessel through the lower half of the hot leg. Mixing between these two circulation paths occurs in the SG inlet plenum. In Coolant Loop 1, which contains the pressurizer, steam may be diverted from the hot leg into the pressurizer surge line, and the behavior of parameters shown in the time-history plots is generally affected by the cyclic opening and closing of the pressurizer PORVs.

The flow rates in the SG 1 forward-flowing (hot) and reverse-flowing (cold) average tube sections are shown in Figure 14. The flow around this circulation path is driven by the buoyancy head created from the difference in steam densities (resulting from different temperatures) between the hot and cold tube sections.

The flow rates in the Loop 1 upper and lower hot leg sections are shown in Figure 15. Unlike the SG tube circulation path where the flow rates in the hot and cold sections are the same, in the Loop 1 hot leg circulation path the flow through the upper section is greater than that in the lower section during periods when the pressurizer PORV is open. The flow around the hot leg circulation path is driven by the buoyancy head created by the steam temperature and density differences between the two sections over the vertical portion of the hot leg and within the SG inlet plenum.

In addition to the SG tube and hot leg flow circulations, there are also flow circulations within the reactor vessel. The difference in densities between the hot steam leaving the vessel to the upper hot leg sections and cool steam returning to the vessel through the lower hot leg sections sets up circulation paths within the vessel. The cooler steam returning from the lower hot leg sections tends to flow downward through the peripheral core regions and then upward through the central core regions. Another circulation path also sets up in the reactor vessel upper plenum region, with hotter steam flowing from the core channel exits across the upper regions to reach the entrances to the upper hot leg sections and with cooler steam flowing from the exits of the lower hot leg sections toward the reactor vessel centerline. The vessel circulation is characterized in Figure 16, which shows the mass flow rates near the tops of one of the upward-flowing central core regions and one of the downward-flowing peripheral core regions.

The flow resistances of the SCDAP/RELAP5 model in the regions of the SG inlet plenum are preset so as to match the behavior of the mixing and flow parameters (hot leg discharge coefficient, recirculation ratio, hot mixing fraction and cold mixing fraction) observed during Westinghouse 1/7th-scale experiments and CFD analyses simulating station blackout behavior. Definitions for the mixing and flow parameters are provided in Reference 10. Figures 17 through 20 show the SCDAP/RELAP5-calculated responses for the inlet plenum mixing and flow parameters and Table 3 compares the smoothed SCDAP/RELAP5-calculated values for these parameters (averaged over the four coolant loops) with their nominal target values at 13,000 s. The table shows excellent agreement between the calculated and desired target values for the mixing and flow parameters. See Reference 10 for a more detailed analysis of the calculated mixing and flow parameter results.

The responses of the SG power fractions are shown in Figure 21 and included in Table 3. This parameter represents the ratio of the heat removed to each SG (to the tubes, tubesheet, inlet plenum wall and outlet plenum wall) to the total core heat (fission product decay and fuel rod oxidation heat), calculated on an integrated basis and starting at the time of core uncovery. In prior analyses, a target value for the SG power fraction was employed. However, in the current analyses this has been replaced by the hot leg discharge coefficient and SG power fraction data are provided here only for purposes of comparison with prior analyses.

The hydrogen generation rate response is shown in Figure 22. The oxidation process begins gradually as a result of metal water reaction on the exterior of the fuel rod cladding in the highest-power core regions. The oxidation rate increases rapidly as fuel temperatures climb and the process spreads into lower power regions of the core. The peak core oxidation power is 334.1 MW and during the period of its peak the oxidation power is the dominant contributor to the system heatup. To place the significance of the oxidation power into perspective, at the time

of its peak the oxidation power is 11.2 times the fission product decay power and 10.3% of the normal-operation full rated thermal power.

Figure 23 compares the thermal responses for the key structures in Loop 1. The data shown represent the average temperatures across the structure thickness at the hottest axial locations. As the hot leg steam temperatures rise, the rates at which the structure temperatures increase vary, depending on the structure thickness. The temperatures of the thin-wall SG tubes respond quickly to an increasing steam temperature, while the temperature of the thicker pressurizer surge line responds more slowly and the still-thicker hot leg structure temperature responds even more slowly.

The start of the pressurizer surge line heatup is delayed until the pressurizer empties. Before then, liquid intermittently draining out of the pressurizer into the surge line during periods when the pressurizer PORVs are closed cools the steam inside the surge line and the surge line wall. After the pressurizer empties, the pressurizer PORVs continue to cycle and hot steam is drawn upward through the surge line without the cooling benefit afforded by liquid draining downward. The surge line wall is much thinner than the hot leg wall and, once pressurizer draining is complete, this difference causes the pressurizer surge line wall to heat up more rapidly than the hot leg wall. Pressurizer PORV cycling ceases at 14,400 s (four hours after event initiation) when the station batteries are assumed to be depleted. Afterward, the RCS pressure increases, but not sufficiently to open the pressurizer SRVs (see Figures 6 and 11) until the very end of the transient calculation, when slumping of molten core material into the reactor vessel lower head region causes the RCS pressure to spike upward. The turnover in the surge line structure temperature in Figure 23 reflects the cessation of surge line steam flow. With neither the pressurizer PORVs nor SRVs opening, the flow of increasingly-hotter steam through the surge line stops and the heat loss from the outside of the surge line to the containment cools the surge line wall. Figure 24 shows a detailed view of the structure temperature responses from Figure 23 overlaid with the SCDAP/RELAP5-calculated failure times for the structures.

Figures 25 through 27 compare the Larson-Miller creep rupture damage indexes for the surge line, hot leg and SG tube structures. The damage index indicates the accumulation of creep damage as a fraction of the creep that will produce structural failure (i.e., failure occurs at the time the index value reaches 1.0). The creep rupture model allows use of a stress multiplier that represents the effect on the creep calculation corresponding to a specific degree of degradation in the strength of a structure due to other factors, such as cracks that were present before the accident event sequence started. For the surge line and hot leg structures only a stress multiplier of 1.0 is used. A set of stress multipliers from 1.0 to 7.5, in increments of 0.5, is used for the SG tube structures as a means to introduce tube material strength degradation as an analysis variable.

Figure 25 compares the damage indexes for the pressurizer surge line and the four hot legs. The failure of Hot Leg 1 occurs first, followed by failures of Hot Legs 2, 3 and 4 and then by the failure of the surge line (the calculated creep rupture failure times for all structures in the model are listed in Table 4).

Figure 26 compares the damage indexes for Hot Leg 1 and the average tubes in SG 1. The figure shows that an average tube with a stress multiplier of 2.0 or lower is predicted to fail after the

time when Hot Leg 1 fails. In other words, tubes that are subjected to the average steam conditions on the inside are not expected to fail before Hot Leg 1 as long as degradation of the tube strength has not progressed past the point where a tube will fail when subjected to a stress of only (1.0 / 2.0 =) 50% of the stress that would fail a non-degraded tube.

Figure 27 compares the damage indexes for Hot Leg 1 and the hottest tube in SG 1. This figure and the event times in Table 4 indicate that the hottest tube with a stress multiplier of 1.0 is predicted to fail 155 s prior to the time when Hot Leg 1 fails. In other words, even non-degraded tubes that are subjected to the hottest steam conditions on the inside are expected to fail before Hot Leg 1. See Reference 10 for more information regarding how the model represents the hottest tube behavior.

Note that the structural damage predictions provided with SCDAP/RELAP5 are intended to represent only rough indications of damage occurrence. These indications are useful when, for example, comparing the damage potential for one accident sequence with the damage potential of another sequence. Damage predictions from which major project conclusions will be drawn will be made by other project participants, using the SCDAP/RELAP5-calculated pressures, steam temperatures and heat transfer coefficients as boundary conditions in detailed stress analysis models.

The SCDAP/RELAP5 base case calculation continued beyond the times of the hot leg and pressurizer surge line structural failures. A relocation of molten control rod absorber to the reactor vessel lower head is calculated (starting at 15,548 s), followed by a relocation of molten core fuel (starting at 17,038 s and representing approximately 15% of the core fuel) to the reactor vessel lower head region. The run failed at 17,189 s as a result of steam explosion effects caused by the molten core fuel slumping into the liquid-filled reactor vessel lower head region.

Section 4 describes a Phenomena Identification and Ranking Table (PIRT) evaluation performed for the purpose of identifying the dependent variables (figures of merit) and independent variables (the important thermal-hydraulic phenomena affecting the figures of merit) for the uncertainty evaluation. Table 5 lists the values for the PIRT-identified dependent variables from the SCDAP/RELAP5 base case calculation; these will be used as the nominal, reference-case output data against which the sensitivity case results are compared. For the purpose of comparing results among many similar runs, it is necessary to both smooth the output in time and use an evaluation-time selection criterion that can adjust for the effects of event sequence timing differences among the runs. The specific definitions for the uncertainty study dependent variables and the smoothing and evaluation-time selection approaches used are described in Section 5.1

To facilitate analyses performed by others in the project, data for selected output channels from the SCDAP/RELAP5 station blackout base case calculation (and for the sensitivity case calculations) are provided on DVDs which are available to others in the project. The selected additional data channels are identified in Appendix A.

Table 1. SCDAP/RELAP5 Full-Power Steady State Results.

Parameter	Target Value	SCDAP/RELAP5 Calculated Value
Reactor power (MW_t)	3,250	3,250
Pressurizer pressure (MPa)	15.51	15.509
Pressurizer water/steam volume (%)	60/40	61.1/38.9
Total RCS coolant loop flow rate (kg/s)	17,010	17,010
Cold leg temperature (K)	549.9	549.90
Hot leg temperature (K)	585.5	585.45
SG secondary pressure (MPa)	4.964	4.892
Feedwater temperature (K)	493.5	493.48
Steam flow rate per SG (kg/s)	440.9	439.9
Liquid volume per SG (m^3)	52.05	52.27

Table 2. Sequence of Events from the SCDAP/RELAP5 SBO Base Case Calculation.

Event Description	Event Time (s)
TMLB' SBO event initiation (loss of AC power, reactor trip, turbine trip, feedwater flow stops, reactor coolant pump trip, reactor coolant pump shaft seal leaks begin, steam generator steam leaks begin).	0
Reactor coolant pump rotors coast to a stop, coolant loop natural circulation begins	106
SG dry-out (99% void in bottom secondary cell), SG1 / SG2 / SG3 / SG4.	5,905 / 5,983 / 5,983 / 6,018
Pressurizer PORV cycling begins.	7,148
First pressurizer SRV cycle, open/close.	8,605 / 8,714
Loop natural circulation flow interrupted by steam collecting in SG tube U-bends, SG1 /SG2 /SG3 / SG4.	8,673 / 8,579 / 8,595 / 8,618
Second pressurizer SRV cycle, open / close.	9,033 / 9,087
Collapsed liquid level falls below the top of the fuel heated length (6.323 m above bottom of lower head).	9,150
Steam at the core exit begins to superheat, hot leg countercurrent circulation begins.	9,222
Collapsed liquid level falls below the bottom of the fuel heated length (2.666 m above bottom of lower head).	10,079
Pressurizer empties	10,637
Onset of fuel rod oxidation.	10,733
First control rod cladding failure.	12,150
First fuel rod cladding rupture.	13,003
Peak fuel rod oxidation rate reached.	13,417
Hottest SG tube creep rupture failure (SG 1, non-degraded, 1.0 stress multiplier).	13,475
Hot Leg 1 fails by creep rupture.	13,630
Hot Legs 2, 3 and 4 fail by creep rupture.	13,700
Pressurizer surge line fails by creep rupture.	13,960
Station batteries assumed to be depleted, motor operated valves are no longer operable.	14,400
Average SG tube creep rupture failure (SG 1, non-degraded, 1.0 stress multiplier).	14,590
First relocation of control rod absorber material to reactor vessel lower head.	15,548
Approximately 15% of core fuel relocates to the reactor vessel lower head.	17,038
End of calculation. Run fails due to steam explosion resulting from molten core slumping into the water-filled reactor vessel lower head.	17,189

Table 3. Comparison of Target and SCDAP/RELAP5-Calculated SG Inlet Plenum Mixing and Flow Parameters.

Parameter	Target Value	SCDAP/RELAP5 Calculated Value
Assumed Split of SG Tubes into Hot/Cold Regions	41%/59%	41%/59%
Average Hot Leg Discharge Coefficient	0.12	0.1207
Average Hot Mixing Fraction	0.85	0.853
Average Cold Mixing Fraction	0.85	0.847
Average Recirculation Ratio	2.0	1.982
Portion of the Integrated Total Core Heat Addition which is Absorbed in the Four SGs	Not Applicable	28.4%

Table 4. Summary of Calculated Creep Rupture Failure Times from the SBO Base Case Calculation.

Structure		Calculated Failure Time (s)
Pressurizer surge line		13,960
Hot Leg 1 / Hot Leg 2 / Hot Leg 3 / Hot Leg 4		13,630 / 13,700 / 13,700 / 13,700
SG 1 / SG 2/ SG 3 / SG 4		
Average SG Tube, Stress Multiplier:	1.0	14,590 / 14,650 / 14,630 / 14,650
	1.5	13,930 / 13,970 / 13,960 / 13,970
	2.0	13,660 / 13,675 / 13,670 / 13,675
	2.5	13,510 / 13,525 / 13,520 / 13,525
	3.0	13,410 / 13,420 / 13,420 / 13,425
	3.5	13,355 / 13,365 / 13,360 / 13,365
	4.0	13,225 / 13,240 / 13,235 / 13,240
	4.5	13,150 / 13,170 / 13,160 / 13,170
	5.0	13,115 / 13,135 / 13,125 / 13,135
	5.5	13,095 / 13,115 / 13,105 / 13,115
	6.0	13,085 / 13,105 / 13,095 / 13,105
	6.5	13,080 / 13,100 / 13,090 / 13,100
	7.0	13,075 / 13,095 / 13,085 / 13,095
	7.5	13,075 / 13,095 / 13,085 / 13,095
SG 1		
Hottest SG Tube, Stress Multiplier:	1.0	13,475
	1.5	13,395
	2.0	13,320
	2.5	12,950
	3.0	12,590
	3.5	12,325
	4.0	12,170
	4.5	12,080
	5.0	12,045
	5.5	12,025
	6.0	12,015
	6.5	12,010
	7.0	12,005
	7.5	12,005

Table 5. Base Case Values of the Uncertainty Study Dependent Variables.

Uncertainty Study Dependent Variable	SCDAP/RELAP5 Model Parameter(s)	Evaluation Time for Base Case Value	Base Case Value
Average SG Tube Failure Margin	DCREPH 2, DCREPH 6-19	Not Applicable	2.10
Hottest SG Tube Failure Margin	DCREPH 2, DCREPH 62-75	Not Applicable	< 1.00 Failure of non-degraded hottest tube precedes hot leg failure by 155 s
Average SG Tube Metal Temperature	CNTRLVAR 701	13,630 s	1021.7 K
Hottest SG Tube Metal Temperature	CNTRLVAR 706	13,630 s	1239.6 K
Hot Leg Steam Temperature	CNTRLVAR 714	13,517 s	1776.0 K
Hot Leg Wall Inside Surface Heat Transfer Coefficient	CNTRLVAR 720	13,517 s	423.1 W/m^2-K
Pressurizer Surge Line Steam Temperature	CNTRLVAR 727	13,517 s	1373.0 K
Pressurizer Surge Line Wall Inside Surface Heat Transfer Coefficient	CNTRLVAR 732	13,517 s	490.9 W/m^2-K

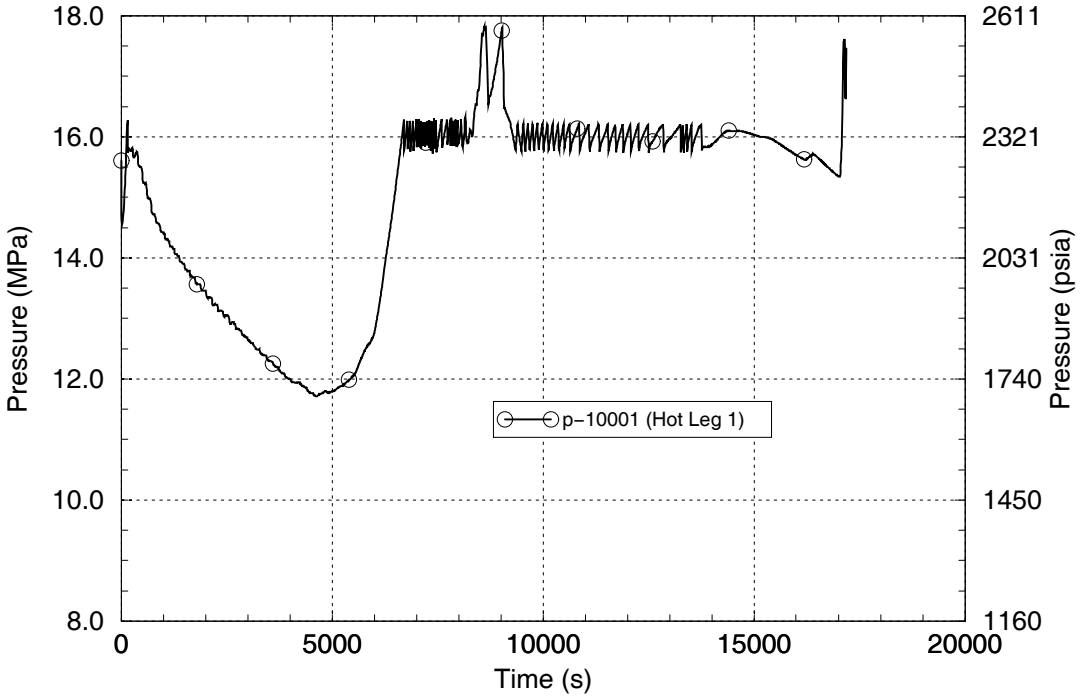

Figure 6. Reactor Coolant System Pressure.

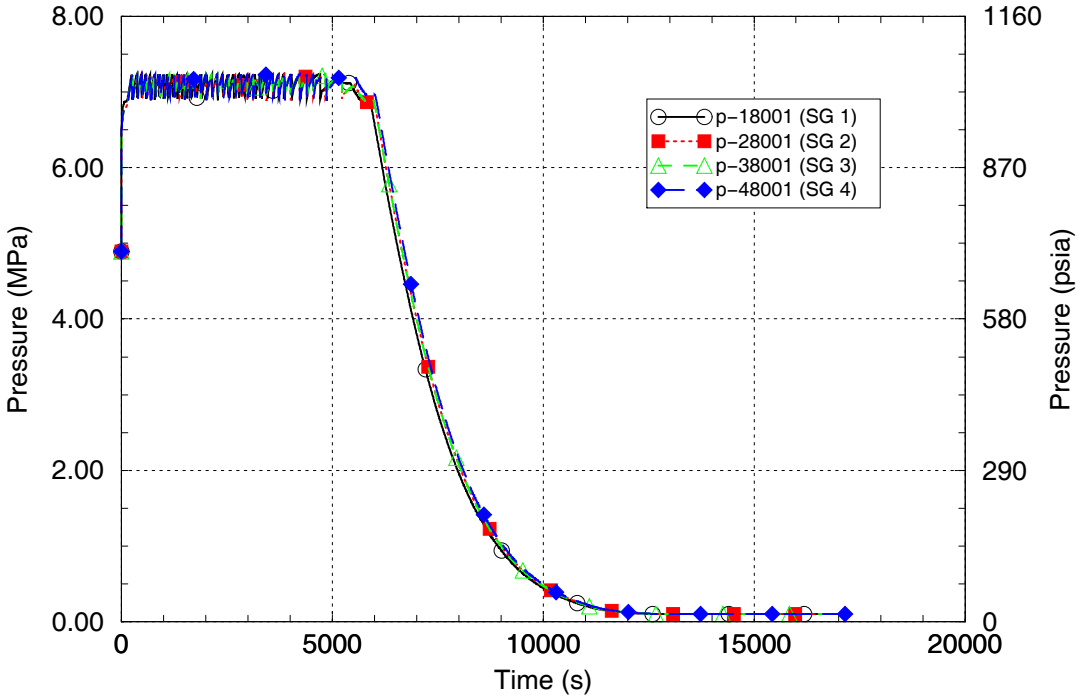

Figure 7. Steam Generator Secondary Pressures.

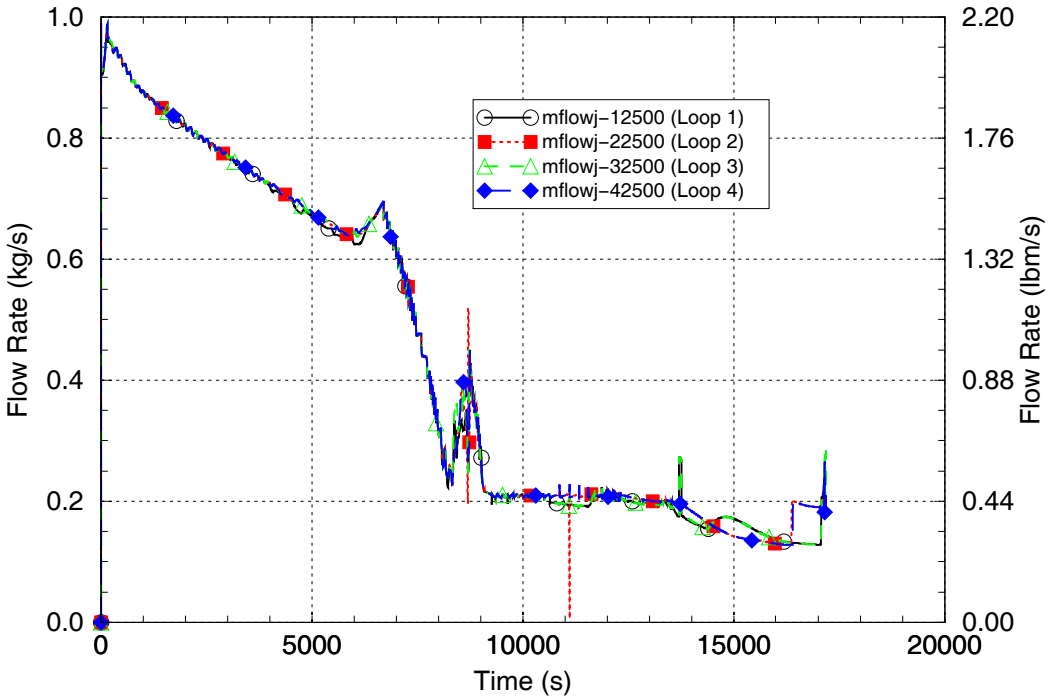

Figure 8. Reactor Coolant Pump Shaft Seal Leakage Flows.

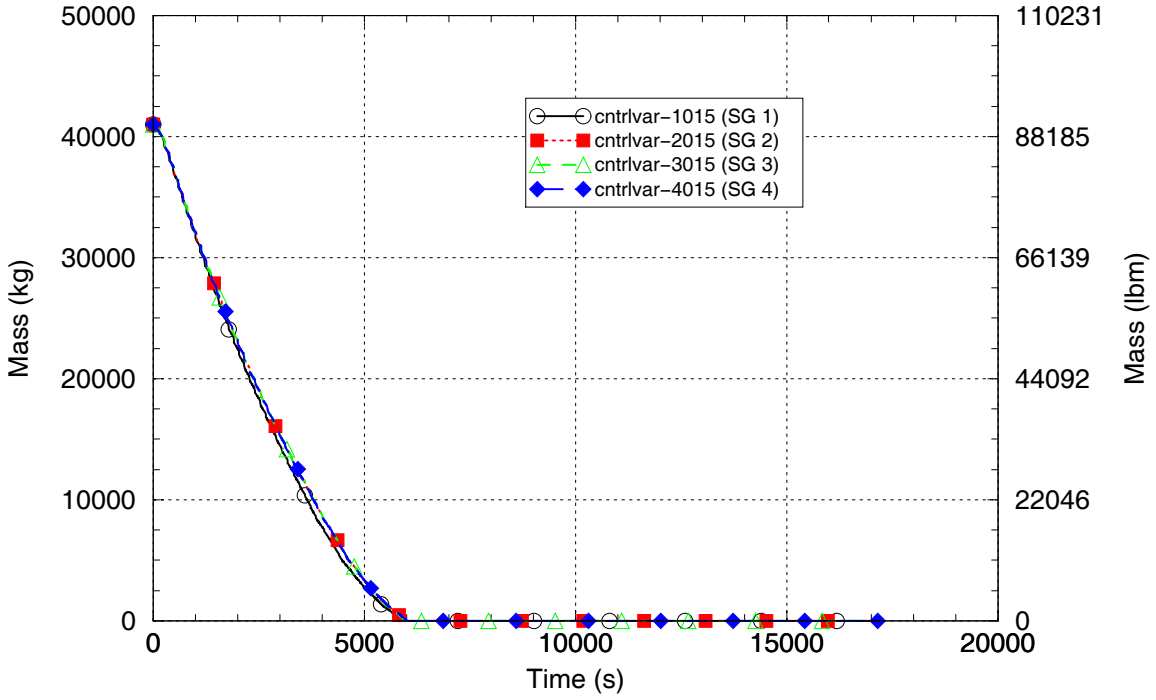

Figure 9. Steam Generator Secondary Liquid Masses.

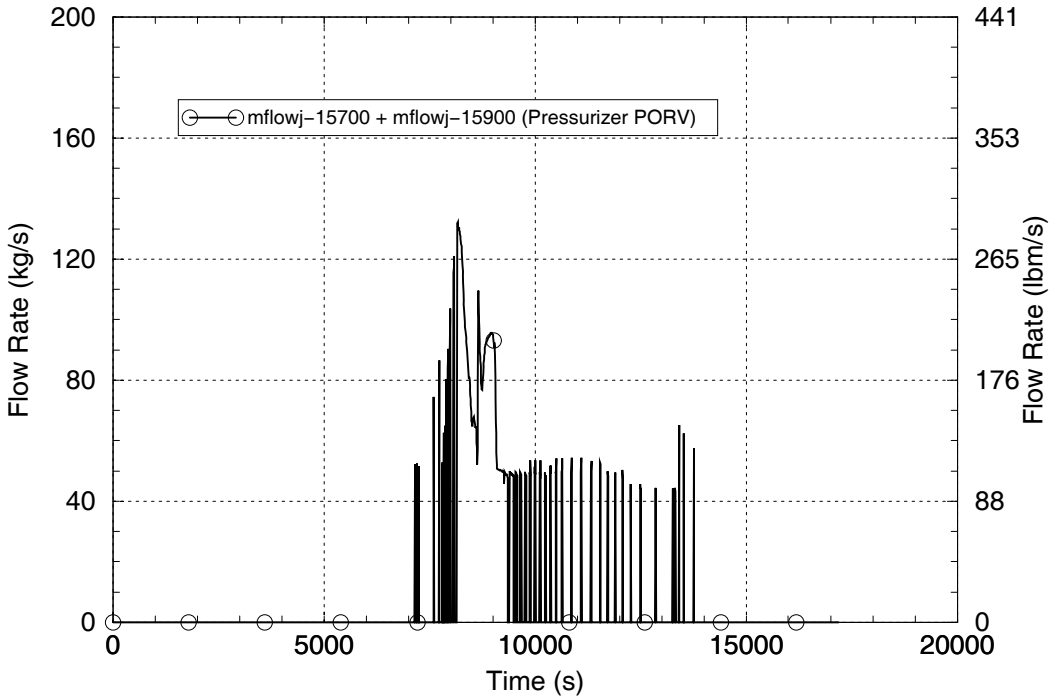

Figure 10. Total Pressurizer PORV Flow.

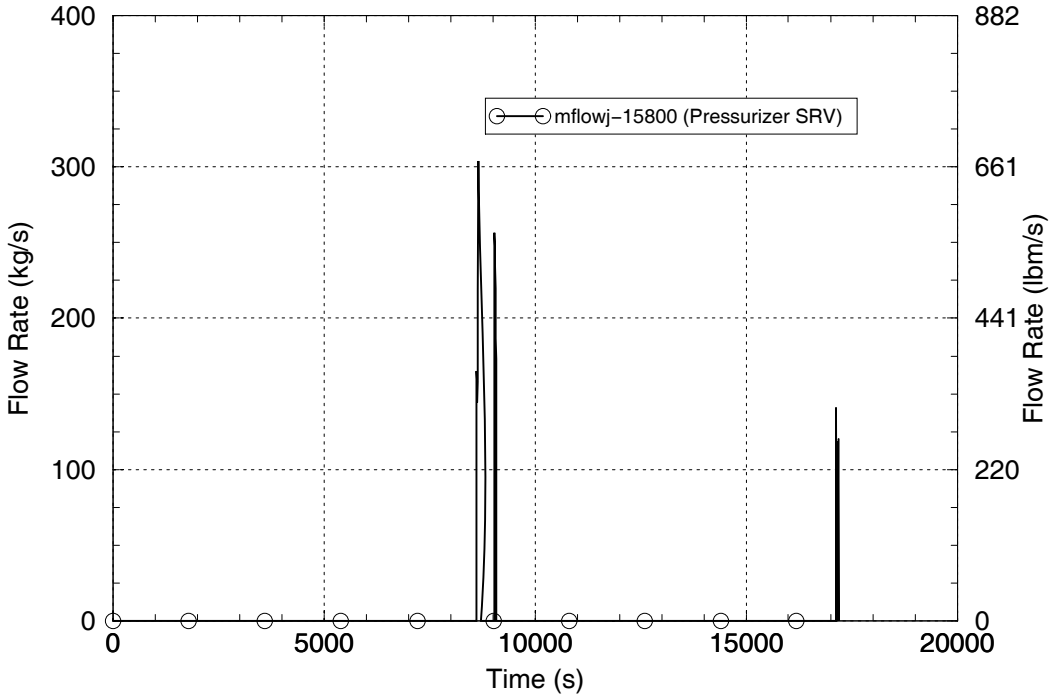

Figure 11. Pressurizer SRV Flow.

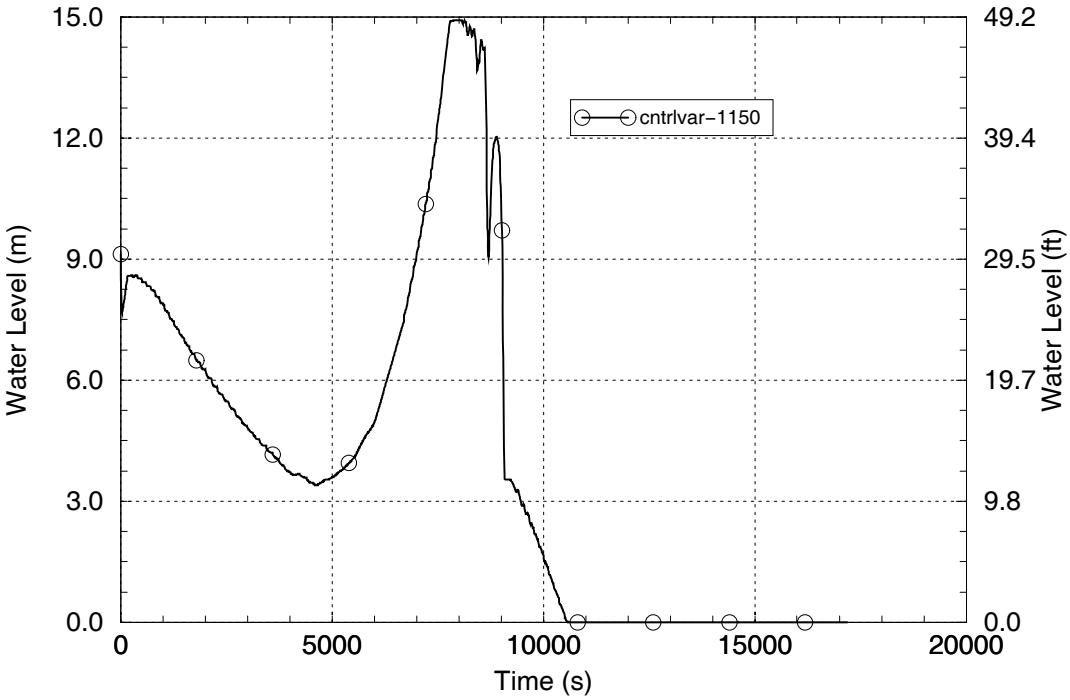

Figure 12. Pressurizer Level.

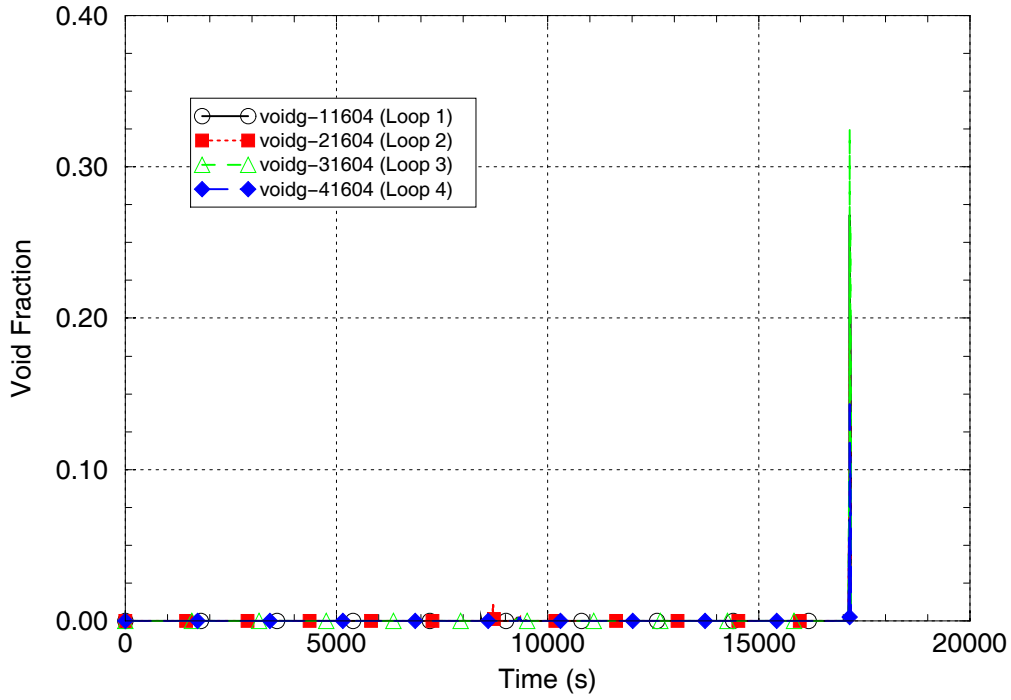

Figure 13. Reactor Coolant Pump Loop Seal Void Fractions.

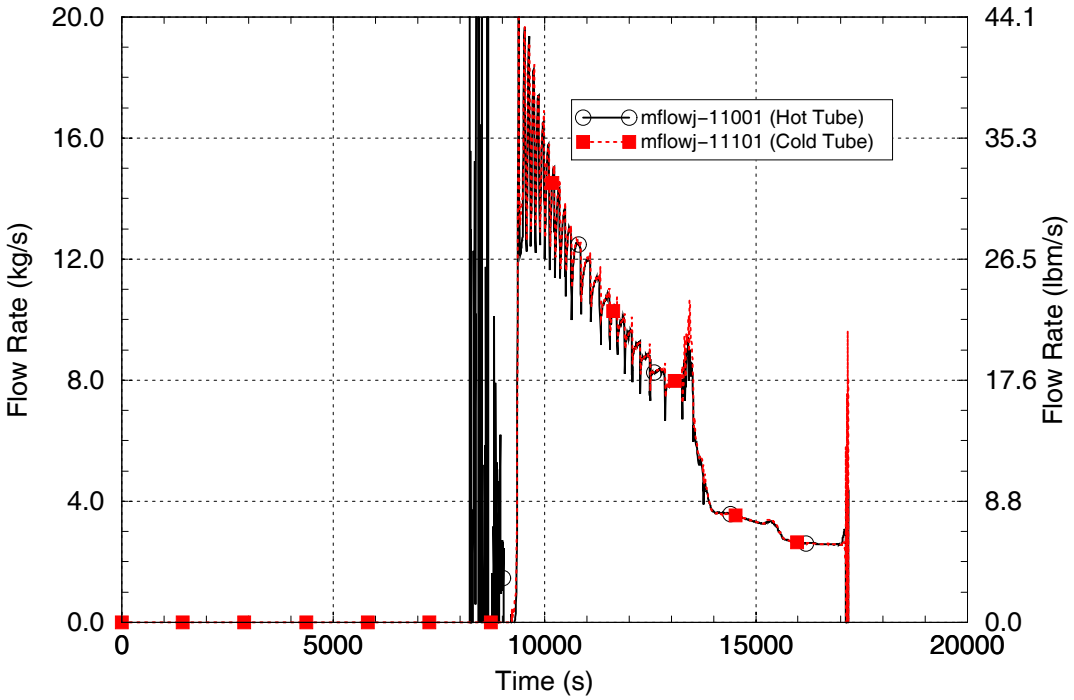

Figure 14. SG 1 Hot and Cold Average Tube Flows.

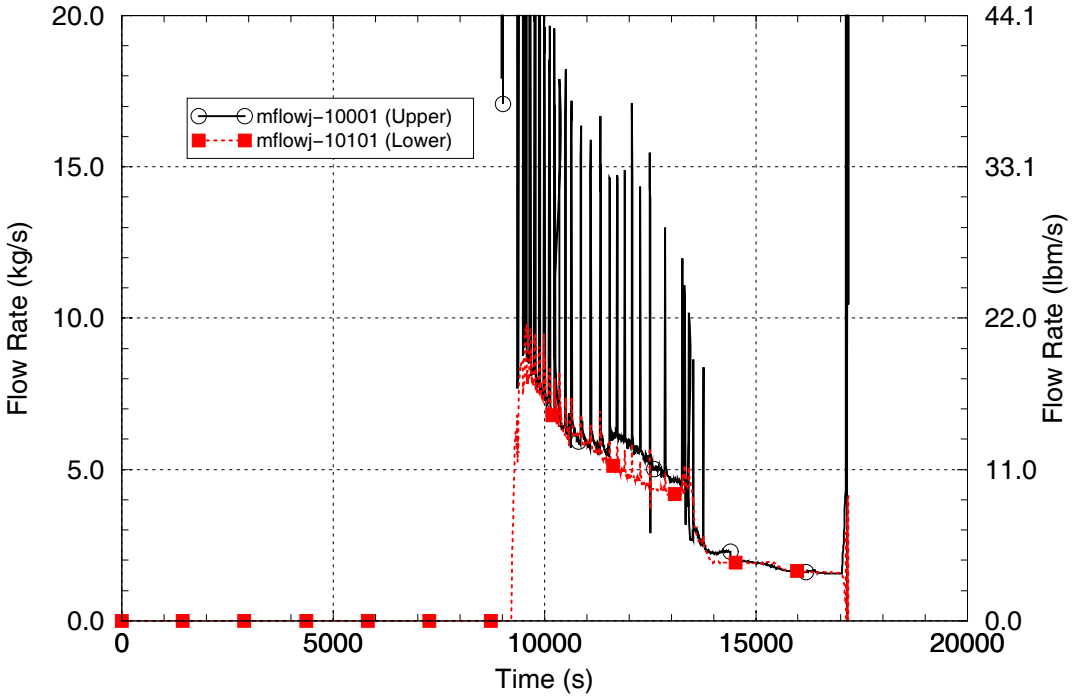

Figure 15. Hot Leg 1 Upper and Lower Section Flows.

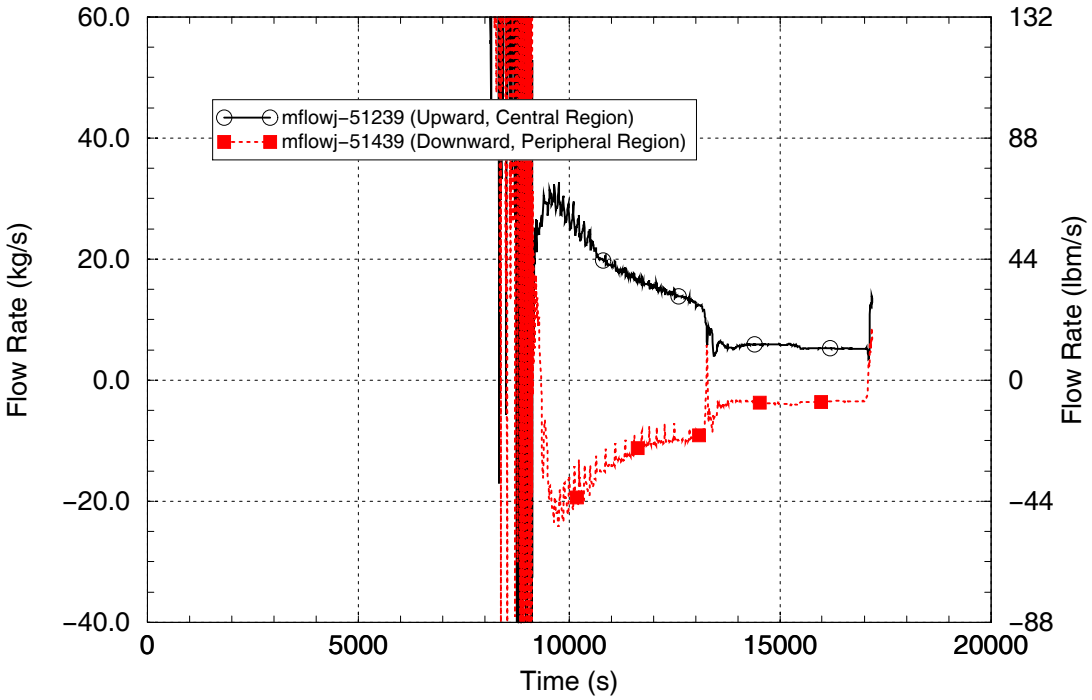

Figure 16. Vessel Circulation Flows.

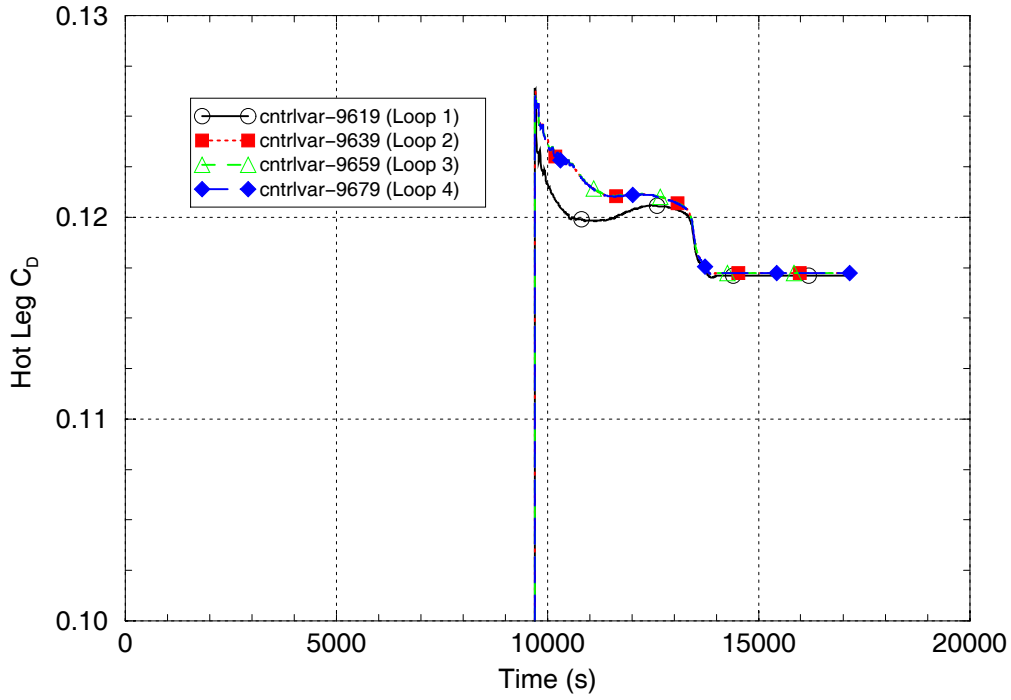

Figure 17. Hot Leg Discharge Coefficients.

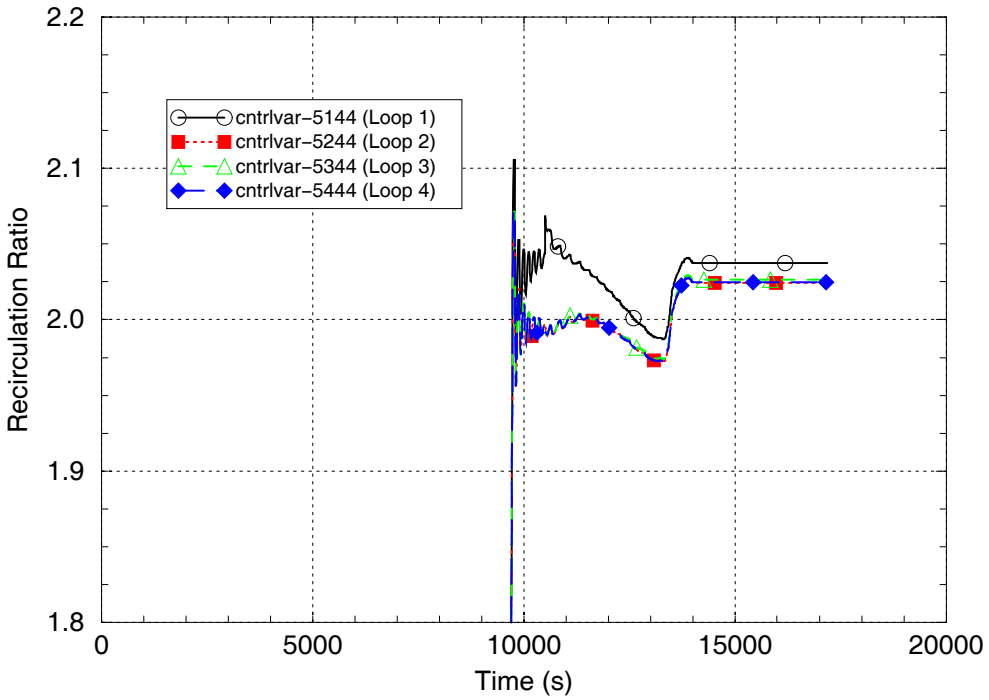

Figure 18. Recirculation Ratios.

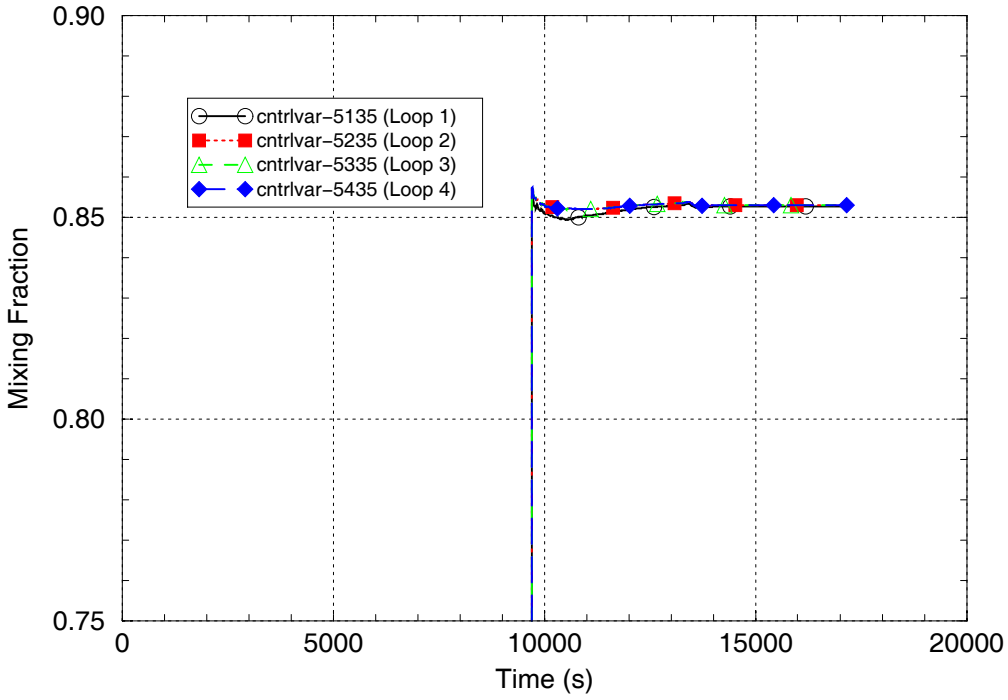

Figure 19. Hot Mixing Fractions.

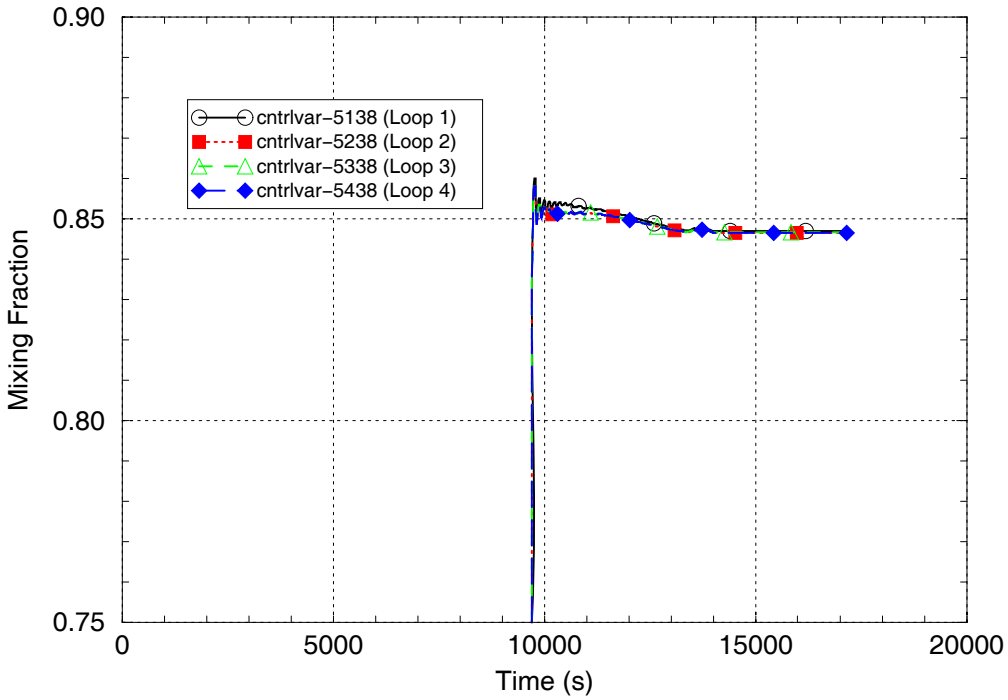

Figure 20. Cold Mixing Fractions.

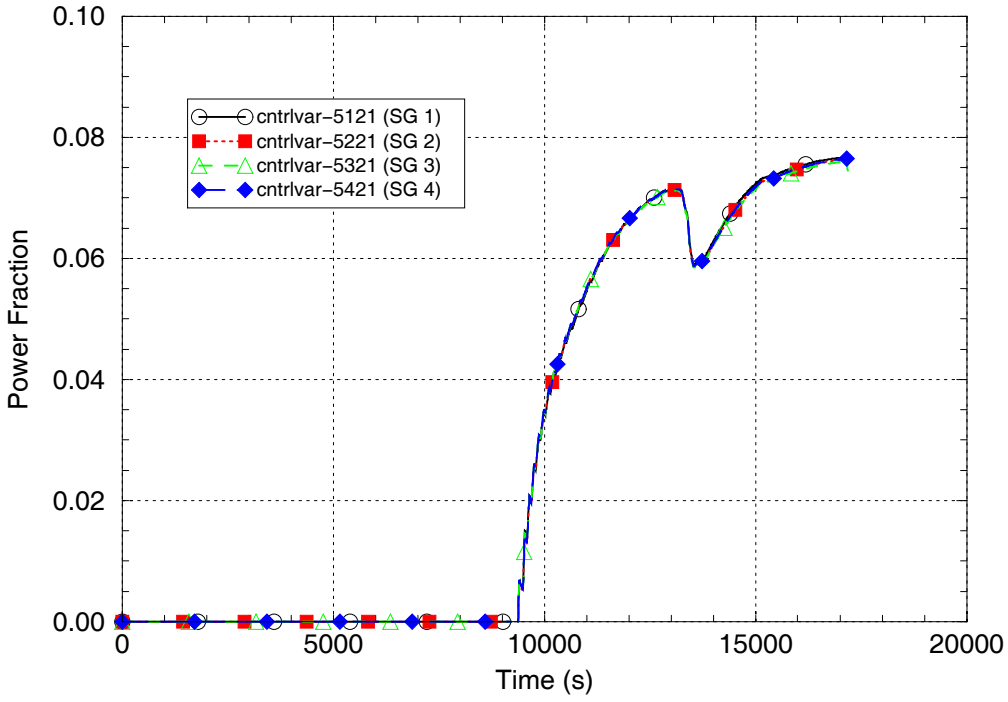

Figure 21. SG Power Fractions.

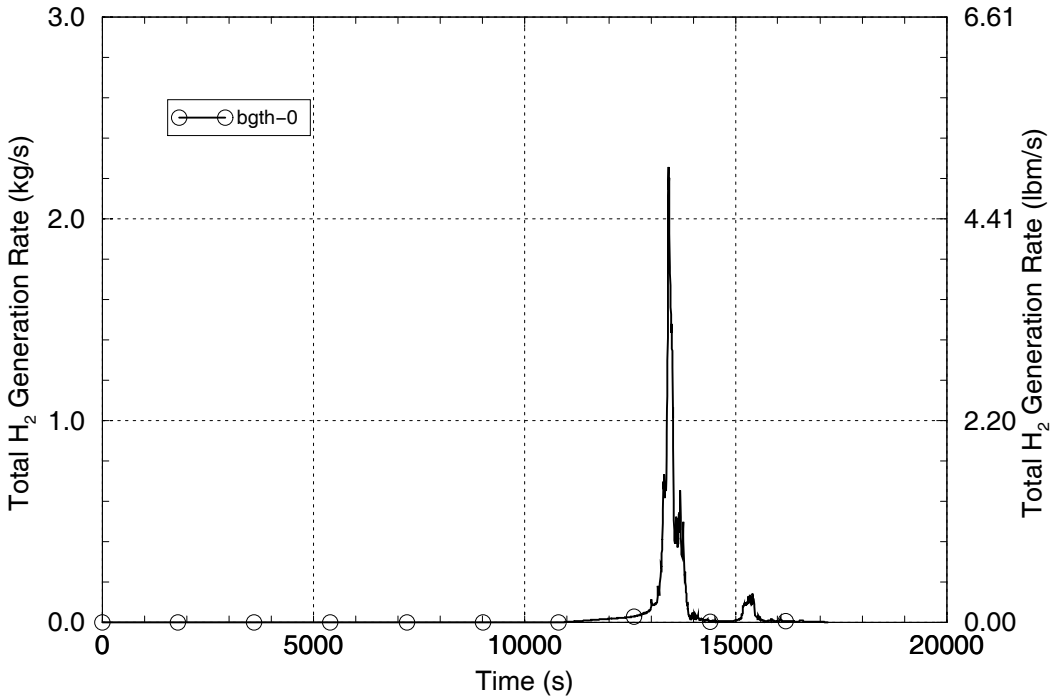

Figure 22. Hydrogen Generation Rate.

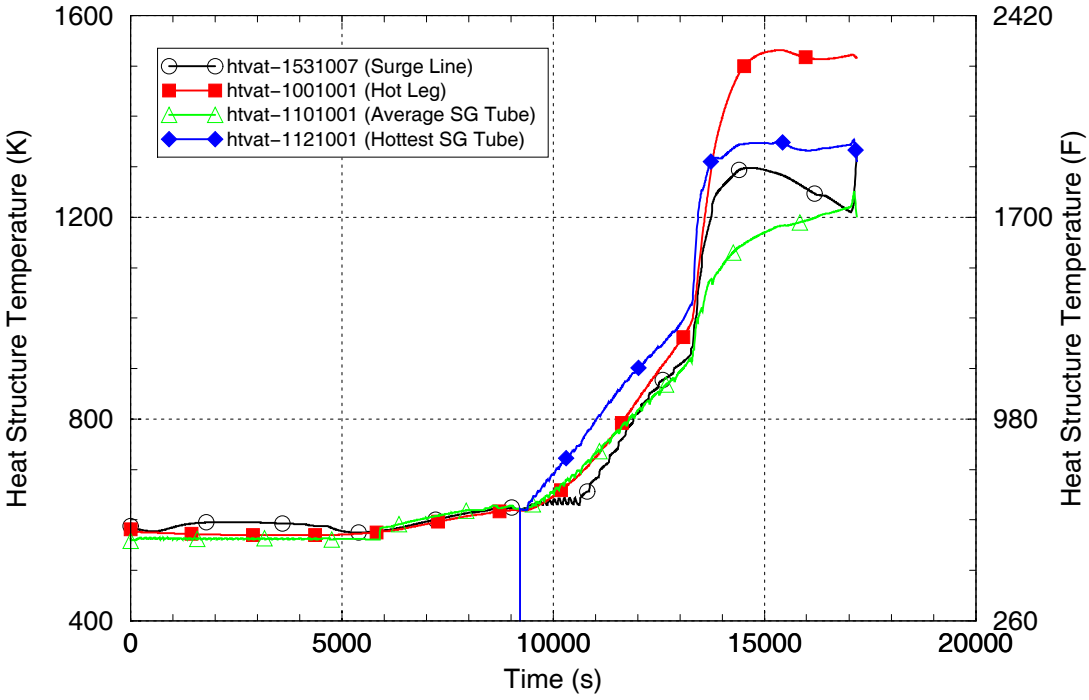

Figure 23. Loop 1 Structure Temperatures.

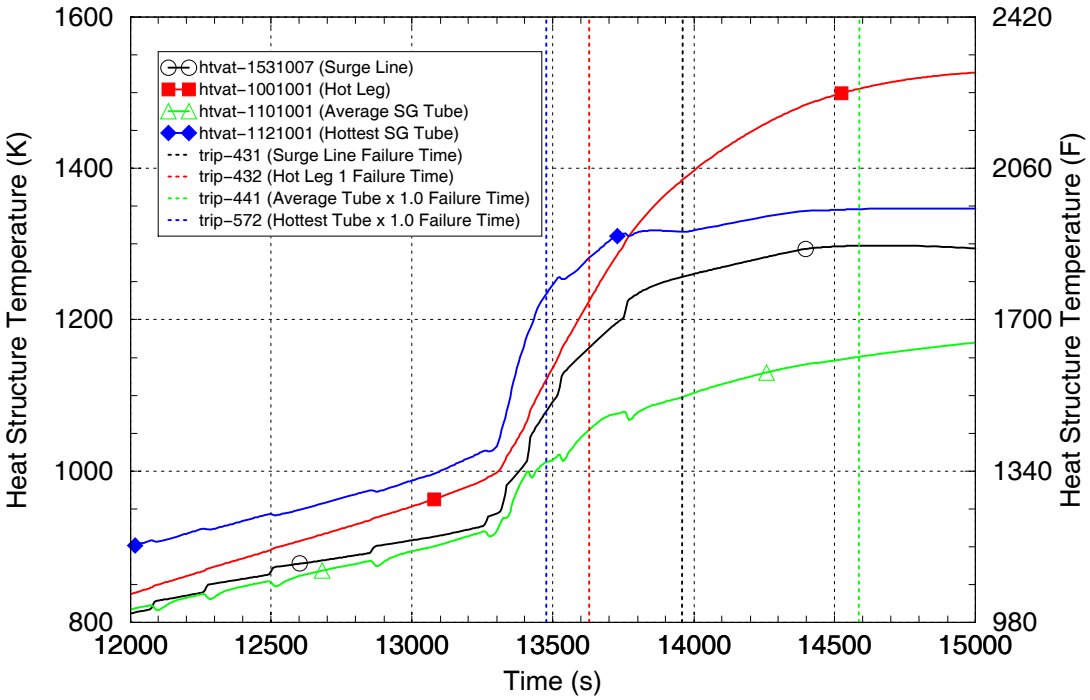

Figure 24. Correspondence Between Loop 1 Structure Temperatures and Failure Times.

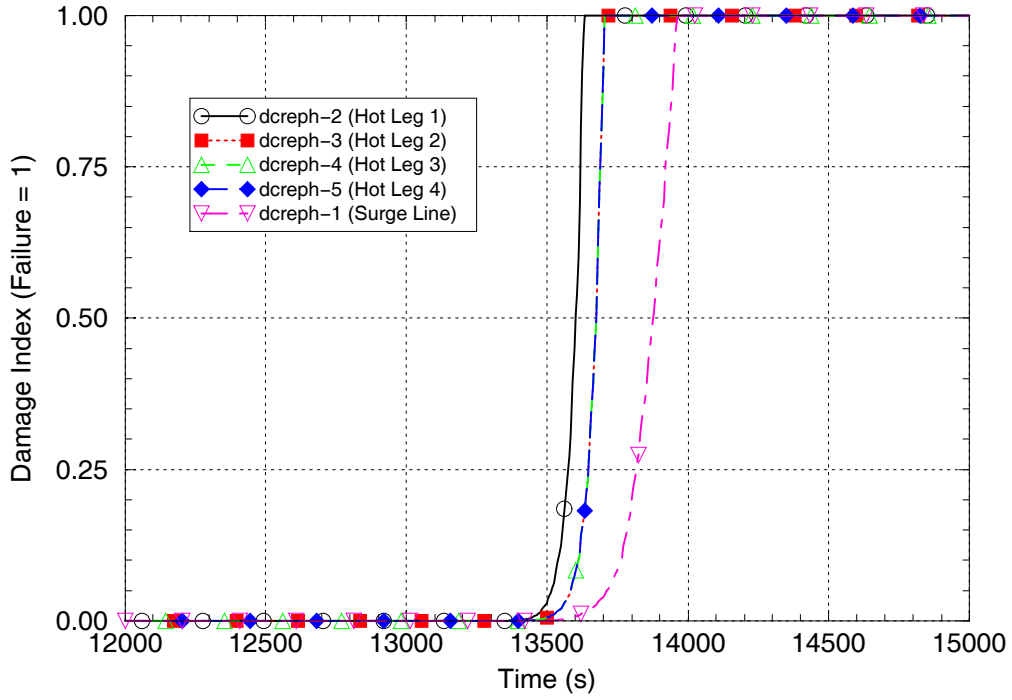

Figure 25. Hot Leg and Pressurizer Surge Line Creep Rupture Damage Indexes.

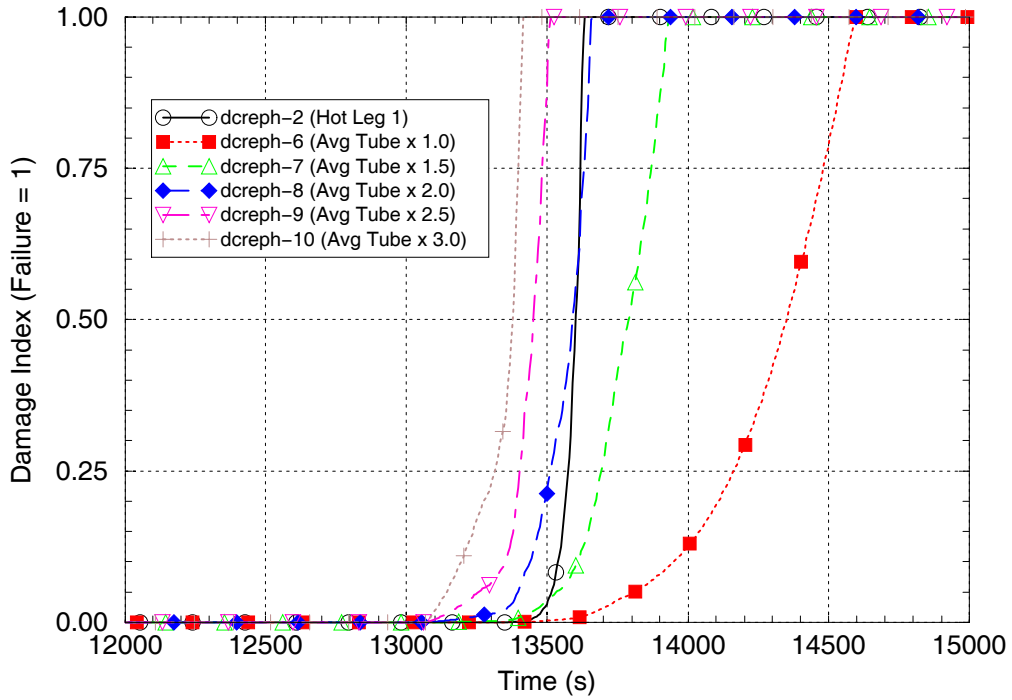

Figure 26. SG 1 Average Tube and Hot Leg 1 Creep Rupture Damage Indexes.

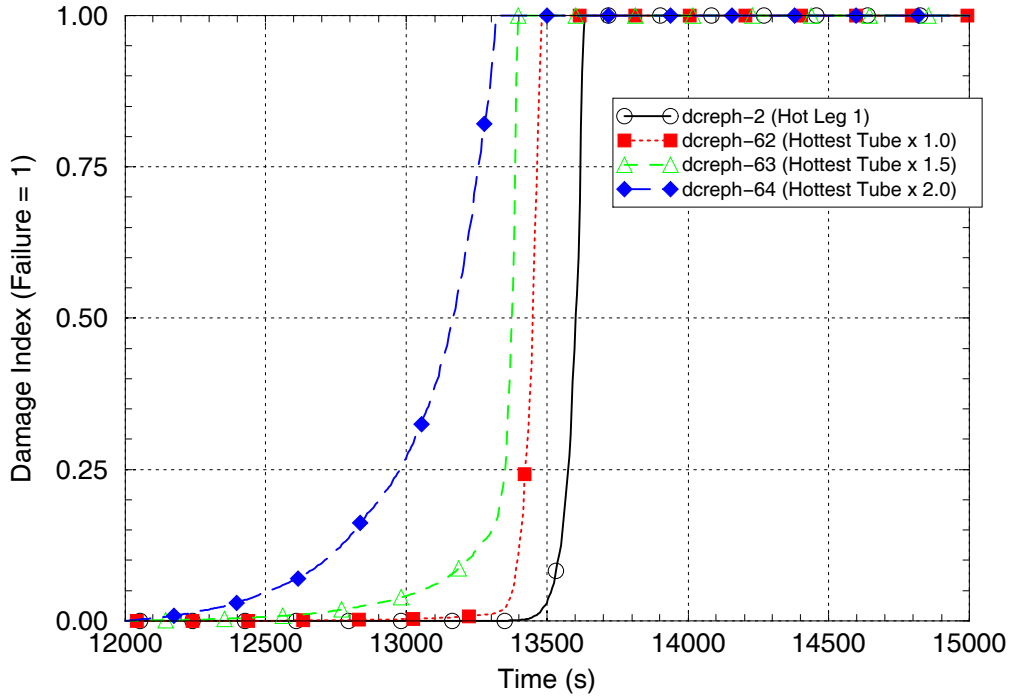

Figure 27. SG 1 Hottest Tube and Hot Leg 1 Creep Rupture Damage Indexes.

4.0 PHENOMENA IDENTIFICATION AND RANKING TABLE EVALUATION

A Phenomena Identification and Ranking Table (PIRT) exercise was conducted in Rockville, Maryland on September 28-29, 2005 to discuss the thermal-hydraulic behavior associated with the analysis of PWR containment bypass. Participants in the PIRT included:

USNRC-RES - Chris Boyd and David Bessette
USNRC-NRR – Steve Long, Len Ward and Walt Jensen
USNRC Consultants – Marino DiMarzo and Peter Griffith
ISL, Inc. – Don Fletcher, Bill Arcieri, Robert Beaton and Vesselin Palazov

The PIRT served first to provide an independent technical review of the SCDAP/RELAP5 modeling and analysis approaches and second to provide expert guidance regarding the dependent variables (figures of merit) and independent variables (important phenomena, processes and behavior) appropriate for an evaluation of the calculation uncertainties. Written minutes of the PIRT meeting were issued (Reference 12). Section 4.1 describes the major technical review issues discussed at the meeting that subsequently led to model upgrades. Sections 4.2 and 4.3, respectively, identify the parameters which the PIRT participants recommended be used for the uncertainty evaluation dependent and independent variables.

4.1 Independent Technical Review Issues

The PIRT discussions uncovered modeling questions and weaknesses that were subsequently investigated, leading to model upgrades in several areas. These upgrades included: (1) adding a representation of the pressurizer spray system to the model, (2) expanding the core region axial nodalization from 10 to 40 nodes, (3) employing finer axial nodalizations for the fluid cells and heat structures in the vicinity of the SG tubesheet and (4) replacing the target SG power fraction used in the SG inlet plenum flow-loss adjustment method with a target hot leg discharge coefficient. The latter of these modeling changes also addresses an earlier comment by the Advisory Committee on Reactor Safeguards (ACRS, Reference 13) regarding the unsuitability of using a target SG power fraction for that purpose. The change to a target hot leg discharge coefficient, which is based on experiments for flow through horizontal ducts connecting two reservoirs containing different fluids, Reference 14, provides a more physically-based target upon which to base the SCDAP/RELAP5 hot leg countercurrent flow behavior.

4.2 Identification of Dependent Variables for the Uncertainty Evaluation

The dependent variables are those for which it is desired to determine the uncertainties in the SCDAP/RELAP5-calculated results.

The PIRT recommended that the dependent variables include the SCDAP/RELAP5-calculated output parameters that the project stress analysts investigating hot leg, pressurizer surge line and SG tube structural failures are using as boundary conditions for their detailed analyses. These parameters are the: (1) **hot leg steam temperature**, (2) **hot leg piping wall inner-surface heat**

transfer coefficient, (3) **pressurizer surge line steam temperature**, (4) **pressurizer surge line piping wall inner-surface heat transfer coefficient**, and (5) **SG tube metal temperatures**.

The PIRT participants also acknowledged the importance for the regulatory decision-making process of the timing difference between the hot leg/surge line and SG tube structural failures and recommended that the **SG tube failure margins** also be included as dependent variables.

4.3 Identification of Independent Variables for the Uncertainty Evaluation

The independent variables are those judged to have the most influential impact on the dependent variables.

The PIRT participants discussed a variety of issues related to the thermal-hydraulic response of a Westinghouse PWR plant during station blackout severe accidents and to the containment bypass issue. During the discussions, a list of recommended independent variables for the uncertainty evaluation, and their relative rankings, was developed by consensus view of the PIRT participants.

Regarding the rankings, a prime consideration of the participants was that items seen to similarly affect structural failure times in all three locations (hot leg, surge line and SG tubes) should be considered to be of lower rank than those items seen to differently affect the three failure times. The latter set of items can logically be seen to have a greater effect on the SG tube failure margin because they have the potential to influence the relative failure times among the structures.

The group also decided to separate out those items that represent basic thermal-hydraulic processes from those items that instead represent event sequence assumptions or plant configuration differences.

Table 6 summarizes consensus opinions of the PIRT participants on the thermal-hydraulic phenomena, behavior, event sequence assumptions and plant configuration items that are expected to most significantly affect the dependent variables (temperatures, heat transfer coefficients and SG tube failure margins) for the uncertainty evaluation.

The table is separated into three sections (A, B, and C). Section A, which includes items that differently affect the behavior at the three locations, represents the high-ranked items. Section B, which includes items that similarly affect the behavior at the three locations, represents the medium-ranked items. Section C includes items that relate strictly to the event sequence assumptions or the plant configuration. The PIRT suggested that the uncertainty study may or may not need to consider the effects of the items listed in Section C, depending on the magnitudes and distributions of the variations in the event sequence and plant-to-plant configuration differences that may be uncovered during the study or prescribed by the probabilistic risk assessment (PRA) analysts. Within each table section, the relative ranking of the items is indicated by the assigned number (for example, within Section A Item A1 is considered the highest ranked item while Item A5 is considered the lowest ranked item).

Table 6. Ranking Table of Items Important for the Containment Bypass Issue During Station Blackout Severe Accident Scenarios in a Westinghouse PWR.

Rank	Phenomenon	Location(s) Affected			Reasons for Ranking, Other Pertinent Notes and Comments
		HL	SL	SG Tube	
A1	Full loop circulation (loop seal clearing and reactor vessel lower plenum clearing)			X	Top-level accident sequence assumption is that all cold leg loop seals remained water-filled. Cleared loop seals induce steam circulation throughout the loops, increasing potential for tube failure.
A2	Pressurizer Behavior (phase separation, PORV flow, CCFL & draining, spray nozzle venting)		X		Water draining from the pressurizer preferentially cools the SL and a small amount of water in the SL will prevent its failure. Timing of pressurizer draining relative to core heat up affects SL failure time and core degradation process. Pressurizer phase separation and relief valve flow inherently affects RCS pressure and RCS energy loss. Spray nozzle venting may affect pressurizer draining process.
A3	Mixing, SG inlet plenum			X	Critical to tube failure prediction. May be able to use scatter in the Westinghouse 1/7-scale test data to estimate uncertainty in this parameter. Need to address effects on both hot tubes and average tubes.
A4	SG tube outer wall heat transfer (SG secondary side heat transfer)			X	Strongest potential to change timing of SG tube failure relative to the HL failure. Provides mitigating effect for SG tubes by removing the tube heat to the SG secondary fluid. Include tube sheet modeling effects in a sensitivity study. P. Griffith suggested $\pm$30% as a best guess regarding the SG tube outer wall heat transfer coefficient.
A5	Buoyancy-driven flows in SG tubes (ratio of SG tube flow to hot leg flow)			X	The SG tube flow directly affects the tube temperatures but only indirectly affects the HL and SL temperatures. The tube flow determines the energy entering the tube. The tube fails just above the tube sheet. The recirculation ratio using the three-cell inlet plenum model is tuned to agree with the CFD analysis; its uncertainty is likely small. The hot leg flow model is being improved and will be more physically based.
B1	Core power, especially fuel rod cladding oxidation power	X	X	X	The hot gas generation due to oxidation drives the heat-up process. In a sensitivity calculation, a large variation in the oxidation model was not seen to significantly affect the SG tube failure margin results. The hydrogen generation from oxidation affects vessel mixing, buoyancy, and feeds back into the oxidation rate. The hydrogen generation also affects the transport of energy away from the core, the wall heat transfer processes and the SG inlet plenum fluid mixing processes. P. Griffith experiments indicate that hydrogen rapidly mixes with steam. Existing SCDAP/RELAP5 assessment cases may provide data regarding the expected uncertainties in the oxidation process.

Rank	Phenomenon	Location(s) Affected			Reasons for Ranking, Other Pertinent Notes and Comments
		HL	SL	SG Tube	
B2	Buoyancy-driven flow in vessel (includes effects of vessel internal flow resistances)	X	X	X	The vessel internal flows directly affect the temperatures at the core exit and at the vessel-to-hot leg connections. These flows also affect the oxidation rate and are considered to be of medium importance. The prediction capability for the vessel internal flows was judged to probably be within a factor of two, suggesting that a range between 0.5 and 2.0 be investigated in the uncertainty study.
B3	Buoyancy-driven flow in hot legs	X	X	X	The elevation change within the hot leg provides a buoyancy effect. However, buoyancy in the SG tubes, where the elevation change is much larger, is judged to be the driver for the flow circulation processes.
B4	RCS heat loss to containment	X	X	X	The prior sensitivity study indicated that the SG tube failure margin is affected by the assumed heat loss. Affects the heat transfer processes for all three locations, but to different extents.
B5	Mixing at the vessel-to-hot leg connection	X	X	X	Not much mixing occurs at this location. Test data (W 1/7-scale experiments) shows that hot leg and upper plenum temperatures are about the same, indicating that the hot-steam regions are well-mixed. The cooler steam returning through the lower hot leg sections falls into the periphery of the core as it enters the vessel, so there is little interaction with the hot steam exiting the vessel into the upper hot leg sections.
C1	Operator intervention (event sequence definition item)		X		Operator intervention includes depressurization of SGs and opening of the pressurizer PORVs. Prior sensitivity study indicated the success of this mitigation strategy if it is performed in a timely manner. Effect of the operator intervention on the SG tube failure margins was significant.
C2	RC pump seal leakage (event sequence definition item)	X	X	X	This phenomenon affects the primary system pressure and RCS energy balance. Prior sensitivity study indicated that the influence on the SG tube failure margin increases as the assumed leakage rate increases.
C3	SG tube leakage (event sequence definition item)			X	This phenomenon draws additional steam into the SG tubes, decreasing their failure margin. Prior sensitivity study indicated a moderate influence of the tube leakage on the tube failure margin.
C4	Surge line orientation (plant configuration item)		X		The surge line-to-hot leg connection configuration varies from plant to plant. In the Westinghouse plant under evaluation the connection is made on the side of the hot leg pipe while in the CE plant under evaluation the connection is made on the top of the hot leg pipe. Prior sensitivity calculations indicate a significantly earlier surge line failure when the surge line is connected on the top of the hot leg because much hotter steam is drawn into the surge line.

Rank	Phenomenon	Location(s) Affected			Reasons for Ranking, Other Pertinent Notes and Comments
		HL	SL	SG Tube	
C5	Distribution of metal mass in the plant (plant configuration item)	X	X	X	The distribution of the metal structures (vessel walls, vessel internals and piping walls) within the plant directly affects the spread of hot steam from the core into the RCS. Large structures near the core, where the steam is the hottest, tend to absorb much heat, reducing the steam temperatures and heat deposited into heat structures that are more distant from the core. The recent energy balance analysis for the Westinghouse plant demonstrates this effect.

5.0 SELECTION OF SENSITIVITY CASES

The PIRT identified the items listed in Table 6 as being important for predicting the behavior of the dependent variables (temperatures, heat transfer coefficients and SG tube failure margins) during simulations of the station blackout severe accident in a Westinghouse plant. These items are defined as the independent variables for the uncertainty evaluation. The items are separated into three groups, with Groups A and B representing the high-ranked and medium-ranked items, respectively and with Group C representing items that relate strictly to the event sequence assumptions or plant configuration.

In this section, SCDAP/RELAP5 sensitivity cases are identified in which model features representing the independent variables are varied around the nominal modeling for each feature, as present in the base case calculation. The SCDAP/RELAP5 sensitivity case calculations are then performed and the results of the sensitivity and base case calculations are compared in Section 6. In Section 7 the deviations in the dependent variables among the cases are calculated and used to estimate the uncertainties in the dependent variables.

Section 5.1 describes the specific forms (locations, evaluation times, smoothing processes, etc.) used for each of the dependent variables. Section 5.2 describes the selection of the sensitivity cases, including descriptions of the modeling feature revisions implemented and justifications for the ranges of the variations investigated.

5.1 Specific Forms of the Dependent Variables

The locations selected for evaluation of the dependent variable SCDAP/RELAP5 output are those where the fluid conditions important for structural failure considerations are the most limiting. For the hot legs, the most limiting location is in the upper section of Hot Leg 1, adjacent to the reactor vessel. For the pressurizer surge line, the most limiting location is at the end of the surge line, adjacent to Hot Leg 1. For the steam generator tubes, the most limiting locations are for the hot average tube and hottest tube, just above the tubesheet in SG 1.

Since the SCDAP/RELAP5-calculated output variables are functions of time, for the purpose of comparing results among many similar runs, it is necessary to smooth the output in time (to remove the oscillatory behavior related to opening and closing of the pressurizer relief valves) and use an evaluation-time selection criterion that can adjust for the effects of event sequence timing differences among the runs.

The analysis of the base case calculation in Section 3 indicates that failures of the hot leg, surge line and SG tube structures are tightly clustered within a short period (of about 500 seconds) following the time of the peak in the fuel rod oxidation rate. The general lack of adequate cooling for the core fission product decay heat results in a slow system heat up prior to the onset of fuel rod oxidation. But it is the core power spike resulting from fuel rod oxidation which dramatically increases the system heat up rate and causes the structural failures to be so tightly clustered.

The structural failures of the hot legs, surge line and SG tubes occur subsequent to the oxidation peak because time is required to transport the increasingly-hotter steam from the core through the hot legs and out into the surge line and SGs. Key aspects of the problem are therefore related to: (1) the core power and core heat up rate, (2) the rates at which heat is carried away from the core and through the various paths, (3) the proximity of the structures with respect to the core and (4) the structure geometries and materials which determine the temperatures needed to fail the structures. The essence of the problem is whether the effects of the rapidly-increasing steam temperatures are more critically felt in the hot leg and surge line structures before they are felt in the SG tube structures. Based on this discussion and results of the base case calculation, the specific forms of the dependent variables used for the uncertainty analysis were selected as follows.

Hottest SG Tube Failure Margin

For the majority of cases documented in this report, the hottest tube is predicted to fail prior to the time of hot leg or pressurizer surge line failure, even when a 1.0 tube stress multiplier is applied. For the uncertainty evaluation, the hottest tube failure margin is represented by the time interval in seconds by which the 1.0 multiplier hottest tube follows the hot leg or surge line failure. Therefore, a negative time interval indicates a situation where the hottest tube fails prior to the hot leg or surge line failure. This approach is consistent with the view that a negative SG tube failure margin exists in that situation.

Average SG Tube Failure Margin

The average SG tube failure margin is represented by the tube stress multiplier that results in SG tube failure coincident with the earliest RCS piping failure. The failure margin values are calculated by interpolating the failure time data for the hot leg and SG tube structures (Table 4 provides an example of this failure time data for stress-multiplier increments of 0.5 from the base case calculation).

Average and Hottest SG Tube Metal Temperatures

The average and hottest SG tube metal temperatures represent the smoothed (100-s lag) values for the average temperatures (across the tube wall thickness) at the time of the earliest RCS piping failure. The data are taken for the first axial SG tube wall heat structure above the top of the tubesheet in SG 1, where the tube temperatures are the highest. The time of earliest RCS piping failure was selected for the evaluation time because the SG tube failure margins are most affected by the relative relationships between the SG tube and RCS piping wall temperatures as the failure conditions for both structures are approached.

Hot Leg Steam Temperature and Wall Inside-Surface Heat Transfer Coefficient

The hot leg steam temperature and wall inside-surface heat transfer coefficient represent smoothed (100-s lag) values for those parameters 100 s after the time of the peak in the fuel rod oxidation rate. The data are taken for the first axial cell (adjacent to the reactor vessel) in the upper section of Hot Leg 1, where the hot leg temperature is the highest. The evaluation time

was selected because it is the time when the rate of increase in the smoothed steam temperature is the highest.

For the hot leg upper section, the wall inside surface heat transfer in the model represents a combination of convection from steam to the wall, radiation from steam to the wall and radiation from the wall to the opposing wall surfaces of the lower hot leg section (see Section 2.9 of Reference 8). Both the differential temperature and the direction of the heat flow for the wall-to-wall radiation heat transfer process are different from those for the two steam-to-wall heat transfer processes, and this complicates the calculation of a single, effective hot leg inside-wall heat transfer coefficient. For reference, the hot leg wall heat transfer processes at 13,517 s in the base case calculation (100 s after the time at which the fuel rod cladding oxidation process peaks) are summarized as follows. Of the heat transferred from the steam to the hot leg upper section wall, 62% is via convection and 38% is via steam-to-wall radiation. Of that total, 15% is radiated to the opposing hot leg lower-section inside wall surfaces.

For the purposes here, the effective total heat transfer coefficient is calculated by dividing the total wall heat flux (the net from all three of the heat transfer processes) by the differential temperature between the steam and hot leg upper section wall inside surface.

Pressurizer Surge Line Steam Temperature and Wall Inside-Surface Heat Transfer Coefficient

The pressurizer surge line steam temperature and wall inside-surface heat transfer coefficient represent smoothed (100-s lag) values for those parameters 100 s after the time of the peak in the fuel rod oxidation rate. The data are taken for the axial cell of the surge line adjacent to Hot Leg 1, where the surge line temperature is the highest. The evaluation time was selected because it is the time when the rate of increase in the smoothed steam temperature is the highest.

The SCDAP/RELAP5 model was modified to calculate the specific forms of the dependent variables described above. Table 5 in Section 3.3 identifies the SCDAP/RELAP5 output parameters that represent the dependent variables and lists the values for the dependent variables from the SCDAP/RELAP5 station blackout base case calculation. The values for the dependent variables in Table 5 are used as the nominal, reference-case output data against which the sensitivity case results are compared.

5.2 Selection and Implementation of the Independent Variable Modeling Revisions

Table 7 identifies the sensitivity cases needed to evaluate variations in the independent variables for the uncertainty study as suggested by the PIRT, and summarizes the model feature revisions that implement those variations into the model. Table 8 provides a concise list of all sensitivity cases run, including those cases used in the uncertainty study and additional cases which were run to address various other issues.

Additional information regarding the selection of the cases, the exclusion of others, the modeling revisions and the justifications for the ranges of variables evaluated is described as follows. The discussion is organized by the PIRT item identifiers from Table 6.

A1 Full loop circulation (loop seal clearing and reactor vessel lower plenum clearing)

An important underlying assumption of the analysis is that the loop seals in all coolant loops remain plugged with water. If this is not the case, then superheated steam flow in the normal direction around the coolant loops will cause the SG tubes to fail before the hot leg or surge line. The PIRT considered this a binary parameter: either all loop seals remain water plugged or they do not. Prior analysis for the Westinghouse plant has indicated that the margin to loop seal clearing is very large; therefore, no sensitivity runs are identified.

A2 Pressurizer Behavior (phase separation, PORV flow, CCFL & draining, spray nozzle venting)

Spray Nozzle Venting Effects

Based on PIRT recommendation, representations of the spray lines and valves were added to the base case model. This model revision was found to result in slightly faster pressurizer draining but no other significant effects. The base case model now better represents the plant configuration and no sensitivity runs related to spray nozzle venting are identified.

CCFL and Draining

The PIRT recommended that the effects of countercurrent flow limiting (CCFL) behavior on the pressurizer draining process be evaluated. A previous study investigated variations in CCFL parameters at the tank-to-surge line connection and found that the effects of those variations were small (Reference 9). The PIRT also recommended that the possibility for CCFL limiting as a result of hydraulic jump conditions forming at elbows between vertical and horizontal sections of the surge line be evaluated. Papers describing this situation were obtained and the SCDAP/RELAP5 calculated surge line conditions were evaluated. It was found that the calculated steam flow from the hot leg into the surge line is so highly superheated that significant flow of liquid from the tank into the hot leg is prevented. Liquid that enters the surge line from the bottom of the tank is vaporized as it drains into the surge line, creating single-phase steam and droplet flow regimes inside the surge line, depending on whether pressurizer relief valves are open or closed. The vaporization of liquid cools the steam inside the surge line and thereby delays the start of the heat-up of the surge line wall until after the completion of pressurizer draining. These evaluations indicated that pressurizer draining is controlled by CCFL at the tank-to-surge line connection and that the conditions that could result in hydraulic- jump effects within the surge line are not present. No sensitivity runs related to surge line CCFL effects are identified.

Phase Separation in the Tank

The upward flow of steam through the pressurizer and out the relief valves can support a frothy mixture inside the pressurizer tank. If the froth level is at the top of the tank, then the relief valve flow is a two-phase mixture of water and steam. When the froth level has dropped below the top of the tank, then the relief valve flow is single-phase steam, potentially with entrained liquid droplets. The SCDAP/RELAP5 interphase drag models determine the distribution of steam in

the tank and the mixture level. The pressurizer fluid conditions during the pressurizer draining period in the base case calculation were evaluated in order to determine the interphase drag models that are most important for this event sequence. For periods when the pressurizer relief valves are open, slug flow is seen in the bottom of the tank and mist flow is seen in the upper regions of the tank. For periods when the relief valves are closed, vertically-stratified and bubbly flows are seen in the bottom of the tank and mist flow is seen in the upper regions of the tank. Therefore, interphase drag models for the bubbly and slug flow regimes are of most interest for simulating the tank mixture level.

To evaluate the sensitivity of results to variations in the interphase drag models, a check run was made in which the hydraulic diameter for the pressurizer tank was reduced by a factor of 5.0 from the actual tank diameter. For large-diameter vertical tanks, SCDAP/RELAP5 uses the Zuber-Findlay (Reference 15) and Kataoka and Ishii (Reference 16) correlations for churn-turbulent bubbly and slug flows. The slip between the phases with the Zuber-Findlay correlation is proportional to the square root of the hydraulic diameter while for the Kataoka and Ishii correlation it is directly proportional to the hydraulic diameter. Therefore, the run with reduced hydraulic diameter effectively implements a reduction in the slip ratio by a factor of between 2.24 and 5.0 and corresponding increases in the interphase drag and the tank mixture level. Compared with the base case, the check run with the reduced tank hydraulic diameter indicated only a small difference in the pressurizer draining process and event sequence timing and no effect on the calculated SG tube failure margins. As a result of this finding, no sensitivity runs related to phase separation in the tank are identified.

Relief Valve Flow

Because the pressurizer pressure remains high in this event sequence, the flow of fluid through the pressurizer PORVs and SRVs is controlled by critical flow processes. The relief valves pass liquid, two-phase fluid and steam over the course of the event sequence. The calculation of critical flow through the valves is subject to uncertainties related to modeling of the critical flow process in general and to uncertainties related to correctly simulating the fluid conditions at the valve inlets. Since the flow of mass and energy out of the primary coolant system by fluid exiting through the pressurizer relief valves is large, it is appropriate to evaluate the sensitivity of calculation results to variations in the relief valve critical flow.

A survey was made of prior assessments of RELAP5 capabilities (Reference 17) for representing valve and break flows in experiments in the Marviken (References 18 and 19), LOFT (References 20, 21 and 22), ROSA-IV (Reference 23) and MIST (References 24 and 25) test facilities. These assessments cover uncertainties related both to critical flow modeling and to adequately representing the fluid conditions upstream of the choking location. Five high-pressure experiments were evaluated, one of which (MIST Test 360499) featured the behavior for flow through a stuck-open pressurizer PORV. These assessments included a large range of upstream fluid conditions and indicated that RELAP5 overpredicted and underpredicted the critical flow by up to 27% and 25%, respectively. Based on these assessment findings, sensitivity runs with the pressurizer PORV and SRV valve flow areas varied by $\pm$30% are identified to account for the uncertainties in the relief valve flow.

A3 Mixing, SG Inlet Plenum

Sensitivity calculations are identified for variations in the hot leg discharge coefficient, recirculation ratio and hot/cold mixing fraction, all of which affect mixing behavior in the SG inlet plenum region. A sensitivity calculation with the assumed hot/cold tube split altered is also identified. The ranges of the variations selected for the sensitivity runs are based on observations of the Westinghouse 1/7-scale experimental data (Reference 7) and recent CFD analyses. In these sensitivity runs, the SG inlet plenum flow coefficients are adjusted so as to attain the revised target value for the parameter that is varied while maintaining the base-case target values for the other mixing parameters.

A4 SG tube outer wall heat transfer (SG secondary side heat transfer)

The base case model uses the maximum heat transfer coefficient among forced, free and laminar convection correlations. The base case model includes a 1.284 multiplier on the heat transfer coefficient (which is needed in order for the model to achieve a satisfactory concurrent match with plant data for the SG secondary pressure, SG secondary fluid mass and the SG heat removal rate during full-power steady state operation). The base case model also includes a physically-based multiplier (which is only applied on the heat transfer coefficient calculated using the Dittus-Boelter forced convection correlation, Reference 26) that accounts for the effects of flow passing through a tube bundle parallel to the tube axis. However, it is expected that substantial portions of the swirling flows within the actual SG tube bundle will be across the tubes, not in parallel with them. Such crossflows result in still-higher heat transfer coefficients and the extent of this enhancement is not known. During the period when the SG boiler is steam filled, the calculated heat transfer coefficient is very small (~10 W/m^2-K).

Sensitivity runs are identified to evaluate +400% and -50% variations in the SG tube outer wall heat transfer coefficient to bound the potential effects of the heat transfer variations described in the previous paragraph.

A5 Buoyancy-driven flows in SG tubes (ratio of SG tube flow to hot leg flow)

The ratio of the SG tube and hot leg flows is represented in the model by the calculated recirculation ratio. Sensitivity runs evaluating the effect of variations in the target recirculation ratio are proposed (see PIRT Parameter A3 above).

B1 Core power, especially fuel rod cladding oxidation power

In the model, the core power is calculated as the sum of fission product decay power and the fuel rod metal-water reaction oxidation power. The fission decay power is based on the nominal ANS1979 standard, Reference 27. The fission decay power response is relatively stable in time and its uncertainty is relatively small (~10%); placing a multiplier on the fission decay power to represent this uncertainty is expected to only significantly affect the timing of the sequence events (SG dry out, core uncovering, etc.). No sensitivity studies related to fission decay power are identified. The oxidation power is, however, of particular interest because its response is

transient, the peak oxidation power is relatively high (11.2 times the fission decay power) and the structural failures of reactor coolant piping and SG tubes occur during the period when the oxidation power is peaking. Therefore, sensitivity runs related to the oxidation process are identified.

In a prior sensitivity study, Reference 9, Section 3.14, the impact of varying the oxidation process modeling was evaluated using a run in which the peak fuel rod linear oxidation heat was limited to 1,000 W/m. That model change limited the peak oxidation rate to 57% of that seen in the base case run and significantly extended the length of the oxidation period. That study indicated only a small reduction in the SG tube failure margin resulted from the change in oxidation modeling. The modeling approach used in the prior study only allows for modeling decreases in the oxidation power (and not increases) so an alternate modeling approach for evaluating variations in the oxidation power is used here.

Sensitivity studies are identified where both increases and decreases in the oxidation power are evaluated by installing artificial heat structures in the core region of the model to add and subtract heat from the core fluid at a rate that is a specified multiple of the oxidation power. Results from a check run made with the artificial structures included in the model but with zero power were compared against the base case calculation to assure that just the presence of the artificial structures does not significantly alter the results. The comparison indicated only slight biases between the output of the two runs, and the sensitivity run results used in the uncertainty calculations are adjusted for those biases.

Volume 5 of the SCDAP/RELAP5 code manual (Reference 1) describes assessments of the code for predicting reactor core behavior during severe accidents. The code performance for predicting fuel rod oxidation behavior was evaluated against test data from nine experiments. Some of the experiments included measurements for oxidation rate while for other experiments only cumulative hydrogen production data are available. The summary finding of the assessment for hydrogen production due to fuel rod oxidation from the nine different experiments (Reference 1, Volume 5, Table 3-1) is that the predicted hydrogen production from fuel rod oxidation ranged from 50% above to 15% below the measured hydrogen production. An additional assessment of the code capabilities for predicting fuel rod oxidation processes against measured/inferred data for the Three Mile Island accident (Reference 1, Volume 5, Table 4-4) indicates that the code overpredicted oxidation by 22%. Sensitivity runs are identified for +20% and -50% variations in the calculated oxidation power (to bound the +18% to -33% range of code predictive capabilities evidenced in these assessments).

B2 Buoyancy-driven flow in vessel (includes effects of vessel internal flow resistances)

The PIRT committee suggested that the SCDAP/RELAP5-calculated predictions of vessel circulation rates are “likely within a factor of two” of the physical circulation rates and two sensitivity runs were identified to evaluate the effects of this variation. Modeling uncertainties that could affect the reactor vessel internal flow rates were evaluated and it was found that the current model may be understating the friction losses associated with flows that decline into the laminar range. Based on this evaluation, a sensitivity run is identified in which the friction losses are increased so as to reduce the flow rates by 50%. A survey of prior RELAP5 assessments

(Reference 17) for predicting buoyancy-driven flows in vessels uncovered a UPTF assessment case (Reference 28) in which the code underpredicted the circulating flows by 50%. Therefore, a second sensitivity run is identified in which the friction losses are decreased such that the vessel circulating flow rates are increased by 100%.

B3 Buoyancy-driven flow in hot legs

This parameter is represented in the model by the calculated hot leg discharge coefficient, C_D, which relates the hot leg flow rate to the densities of the hot and cold fluid streams. Sensitivity runs evaluating the effect of variations in the target hot leg discharge coefficient are identified (see PIRT parameter A3 above).

B4 RCS heat loss to containment

A nominal 4 MW full power operation total heat loss from the outer surfaces of the RCS to containment is included in the base case model. This heat loss rate is based on the capacities of the containment fan coolers, which remove the heat load during normal plant operation. The heat loss is implemented in the model by applying a constant heat transfer coefficient on the outer wall surfaces of the RCS piping, SG and reactor vessel structures. A prior sensitivity study (Reference 9, Section 3.8) indicated that the SG tube failure margins are moderately affected by variation in the RCS heat loss. Sensitivity studies are identified with the heat loss reduced to 2 MW and increased to 8 MW. This factor-of-two variation is based on an EPRI report (Reference 29) that evaluated the causes for plant operating containment temperatures generally exceeding their design values. The report found that many insulating materials did not meet the specified heat-loss requirement and that heat losses from vertical components were greater than previously analyzed. To implement the changes into the model, the constant heat transfer coefficient that results in the 4 MW heat loss is halved and doubled.

B5 Mixing at the vessel-to-hot leg connection

The PIRT committee discussed that mixing at the connection between the reactor vessel and hot leg is expected to be much less robust than mixing in the SG inlet plenum region. The cool steam returning to the vessel tends to fall downward into the peripheral regions of the core and does not mix with the hot steam that flows into the upper hot leg sections. Buoyancy effects therefore tend to keep the hot and cold streams apart at the location of this connection.

The SCDAP/RELAP5 base case model is set up to well represent the fluid buoyancy behavior at the vessel-to-hot leg connections and the calculated response is plausible. Within the vessel upper plenum region, the code predicts a radially-outward flow of hot steam toward the hot legs through the uppermost region of the upper plenum. The flow exiting the vessel into the upper hot leg sections represents only a portion (~30%) of the hot steam carried by that flow. The remainder of the flow turns downward, where it is mixed with the returning cooler steam from the lower hot leg section, and then turns radially-inward toward the vessel centerline. The SCDAP/RELAP5-calculated behavior in the hot leg nozzle region results in limited local mixing between the cooler steam entering the vessel from the lower hot leg sections and the hotter steam that flows out of the vessel into the upper hot leg sections.

NRC CFD simulations also display this buoyancy behavior and show only minimal mixing of the hot and cool streams at the vessel-to-hot leg connection. Therefore no SCDAP/RELAP5 sensitivity runs related to fluid mixing at the vessel to hot leg connection are identified.

C1 Operator intervention (event sequence definition item)

Operator intervention to mitigate the accident was investigated in a prior sensitivity study (Reference 9, Section 3.9.2). The intervention involves recognizing the event sequence signature and depressurizing the primary and secondary systems according to procedures. The prior studies demonstrated the effectiveness of the operator intervention for mitigating the accident and the event sequence timing limitations involved. No new sensitivity runs are proposed.

C2 RC pump seal leakage (event sequence definition item)

Evaluations of reactor coolant pump shaft seal leakage for station blackout event sequences have been performed by Brookhaven National Laboratory (Reference 30). Those evaluations indicate that a leak rate of 21 gpm/pump is likely over the early portion of a station blackout accident event sequence. Later during the event sequence a variety of other leak rates are possible, depending on failures of pump seal components.

Sensitivity calculations are identified for a variety of pump seal leakage situations, with the leak rate changing from the 21 gpm/pump rate after two hours. Calculations investigating a decrease to 1 gpm and increases to 61 gpm, 90 gpm, 120 gpm, 182 gpm and 300 gpm in all four pumps after two hours are identified. Calculations investigating increases to 300 gpm in only one pump are also identified. Most of these calculations are performed to address issues relating to the effects of pump seal leakage variations and, as described below, not for the purpose of the uncertainty evaluation.

Previous sensitivity studies (Reference 9, Section 3.2) were performed with the SCDAP/RELAP5 model to evaluate the effects of various increases in the leak rate after two hours. Those studies indicated that an increase in the leak rate to 61 gpm/pump at two hours moderately decreased the SG tube failure margins and that larger increases in the leak rate led to early core melt and greatly increased SG tube failure margins.

For the purposes of the uncertainty study it is assumed that the event sequence under investigation specifies a 21 gpm/pump leakage rate throughout the event, consistent with the pump seal leak assumption used in the base case calculation. Considerations of lower and higher leak rates are judged to represent separate, distinct event sequences from a probabilistic risk assessment view. However, it is acknowledged that (in addition to those considerations) there are uncertainties related simply to the ability of SCDAP/RELAP5 to simulate a 21 gpm/pump leak. Those uncertainties relate to the simulation of the fluid conditions upstream of the leak, the configuration of the leak geometry as well as the ability to predict the critical flow. The uncertainty study assumes that the uncertainty in the SCDAP/RELAP5 simulation for the 21 gpm/pump leak rate is $\pm$20 gpm. A SCDAP/RELAP5 sensitivity run is made for the 1 gpm assumed leak rate case. For the 41 gpm leak rate assumption, results are obtained by

interpolating between the 21-gpm leakage in the SCDAP/RELAP5 base case calculation and a SCDAP/RELAP5 sensitivity case calculation which assumes 61 gpm leakage.

C3 SG tube leakage (event sequence definition item)

The effects of introducing preexisting SG tube leakage conditions into the event sequence description were evaluated in a prior sensitivity study (Reference 9, Section 3.10). No new sensitivity runs are identified to address uncertainties in this parameter. However, an additional SG leakage sensitivity run (Case 8C), unrelated to the uncertainty study, is discussed in Section 6.2.

C4 Surge line orientation (plant configuration item)

The configuration of the surge line and the location of its hot leg connection are fixed (the connection is made on the side of hot leg). No sensitivity runs are identified to address uncertainties in this parameter. However, an additional surge line configuration sensitivity run (Case 8A), unrelated to the uncertainty study, is discussed in Section 6.2.

C5 Distribution of metal mass in the plant (plant configuration item)

The distributions of metal mass and materials among the piping and vessels are fixed. No sensitivity runs are identified.

Table 7. Summary of Sensitivity Runs Implementing Variations in the Uncertainty Study Independent Variables.

Independent Variable	Notes Regarding Implementing Variations into the Model	Sensitivity Runs Identified to Support the Uncertainty Study
A1 Full loop circulation (loop seal clearing and reactor vessel lower plenum clearing)	An underlying assumption of the analysis is that the loop seals in all four loops will remain plugged with water, setting up circulating flow patterns in the hot leg and SG tube regions. Prior analysis indicates that significant margin to loop seal clearing exists. The uncertainty that the loop seals will not remain plugged is very small.	None
A2 Pressurizer Behavior (phase separation, PORV flow, CCFL & draining, spray nozzle venting)	Spray nozzle venting effects CCFL and draining Phase separation in the tank Relief valve critical flow In the base case run, the pressurizer PORVs and safety relief valves are modeled with flow areas that are sized to deliver the rated flow at the rated upstream pressure condition. Variations in valve flow area account for uncertainties in modeling the critical flow process and in simulating the fluid conditions at the valve inlets.	None None None Run 1A +30% Valve Flow Area Run 1B -30% Valve Flow Area
A3 Mixing, SG inlet plenum	Variations in the target values for the hot leg discharge coefficient, recirculation ratio and hot/cold mixing fraction will be evaluated. The nominal values for the mixing parameters in the SCDAP/RELAP5 base case run are: Hot Leg C_D = 0.12 Recirculation Ratio = 2.0 Hot and Cold Mixing Fraction = 0.85 Hot/Cold Tube Split = 41%/59% The SG inlet plenum flow coefficients will be readjusted so as to attain the desired target value for the parameter that is varied while maintaining the base case target values for the other parameters.	Run 2A Hot Leg C_D = 0.138 Run 2B Hot Leg C_D = 0.102 Run 2C Recirculation Ratio = 2.3 Run 2D Recirculation Ratio = 1.7 Run 2E Mixing Fraction = 0.95 Run 2F Mixing Fraction = 0.75 Run 2G Hot/Cold Tube Split = 50%/50%
A4 SG tube outer wall heat transfer (SG secondary side heat transfer)	In the sensitivity runs, multipliers are applied to the SG tube outer wall heat transfer coefficient.	Run 3A Tube Outer Wall HTC x 5.0 Run 3B Tube Outer Wall HTC x 0.5

Independent Variable	Notes Regarding Implementing Variations into the Model	Sensitivity Runs Identified to Support the Uncertainty Study
A5 Buoyancy-driven flows in SG tubes (ratio of SG tube flow to hot leg flow)	In the model, the calculated recirculation ratio represents the relationship between the SG tube and hot leg flows.	Variations in the target recirculation ratio are evaluated in Sensitivity Runs 2C and 2D (see PIRT Parameter A3 above).
B1 Core power, especially fuel rod cladding oxidation power	Fission product decay power Oxidation power Implement into model by adding or subtracting heat from the core fluid at rates that are fixed percentages of the code-calculated oxidation power	None Run 4A Oxidation power x 1.2 Run 4B Oxidation power x 0.5
B2 Buoyancy-driven flow in vessel (includes effects of vessel internal flow resistances)	Artificial increases and decreases in the input flow losses are made in the axial and crossflow vessel internal junctions to account for uncertainties related to predicting buoyancy-driven flows and friction losses at very low flow rates.	Run 5A 50% decrease in internal vessel flow Run 5B 100% increase in internal vessel flow
B3 Buoyancy-driven flow in hot legs	This parameter is represented in the model by the calculated hot leg discharge coefficient, C_D, which relates the hot leg flow to the densities of the hot and cold fluids.	Variations in the target hot leg discharge coefficient are evaluated in Sensitivity Runs 2A and 2B (see PIRT Parameter A3 above).
B4 RCS heat loss to containment	The base case model assumes a nominal 4 MW heat loss from the RCS to containment at full-power normal operating conditions. The heat loss is implemented by applying a constant heat transfer coefficient on the outer surfaces of the RCS piping and vessel heat structures. For the sensitivity cases the base case heat transfer coefficient is multiplied by 0.5 and 2.0.	Run 6A 2 MW total RCS heat loss at full power conditions Run 6B 8 MW total RCS heat loss at full power conditions
B5 Mixing at the vessel-to-hot leg connection	SCDAP/RELAP5-calculated flow patterns in the region of this connection are physical and consistent with NRC CFD simulations. Therefore, no sensitivity runs are identified.	None
C1 Operator intervention (event sequence definition item)	Operator intervention involves recognizing the event sequence signature and depressurizing the primary and secondary systems according to procedures. Sensitivity studies evaluating operator intervention were previously performed; no new sensitivity runs are identified.	None

Independent Variable	Notes Regarding Implementing Variations into the Model	Sensitivity Runs Identified to Support the Uncertainty Study
C2 RC pump seal leakage (event sequence definition item)	The base case model includes flow areas for the pump shaft seals that initially pass 21 gpm/pump into the containment. For the sensitivity run, the flow areas are scaled up for the higher assumed leak rate. The uncertainty study assumes a ±20 gpm simulation uncertainty for pump shaft seal leakage and only a 61 gpm/pump sensitivity case is needed for the generation of statistics for the uncertainty study. Note that sensitivity runs not used for the uncertainty study are identified to investigate other higher pump shaft seal leakage rates, See Table 8.	Run 7A Leak rate increases to 61 gpm/pump at 2 hours (Interpolation between this run and the base case is used to provide results for a 41 gpm/pump leak rate assumption). Run 7G Leak rate decreases to 1 gpm/pump at 2 hours (Note that discussions of additional pump seal leakage sensitivity runs, unrelated to the uncertainty study, are included in Section 6.1, see Cases 7B, 7C, 7D, 7E, 7F and 7F2.)
C3 SG tube leakage (event sequence definition item)	Preexisting SG tube leakage conditions were evaluated in a prior sensitivity study. No sensitivity runs are needed to support the uncertainty study. However a tube leakage sensitivity run not used for the uncertainty study is identified, see Table 8.	None (Note that discussion of an additional SG tube leakage sensitivity run, unrelated to the uncertainty study, is included in Section 6.2, see Case 8C.)
C4 Surge line orientation (plant configuration item)	The configuration of the surge line and the location of its hot leg connection are fixed (the connection is made on the side of hot leg). No sensitivity runs are identified to support the uncertainty study. However a sensitivity run, not used for the uncertainty study, which evaluates the effects of relocating the surge line connection to the top of the hot leg is identified, see Table 8.	None (Note that discussion of an additional surge line configuration sensitivity run, unrelated to the uncertainty study, is included in Section 6.2, see Case 8A.)
C5 Distribution of metal mass in the plant (plant configuration item)	The distribution of metal mass in a plant is fixed. No sensitivity runs are identified.	None

Table 8. List of Sensitivity Calculations.

Case Number*	Sensitivity Calculation Description
Base Case	Nominal: pressurizer relief valve areas, oxidation model, hot leg and surge line inside wall HTCs, SG tube outer wall HTC, vessel internal circulation. No stuck-open SG relief valves or tube leakage. Surge line connects to side of Hot Leg 1. Hot Leg C_D=0.120, recirculation ratio=2.0, hot/cold mixing fractions=0.85, hot/cold tube split=41%/59%, RCP seal leakage=21 gpm/pump, steam leak area per SG=0.5 in^2, total RCS heat loss=4 MW.
1A	Pressurizer PORV and SRV valve flow areas increased by 30%
1B	Pressurizer PORV and SRV valve flow areas decreased by 30%
2A	Hot Leg C_D increased to 0.138
2B	Hot Leg C_D decreased to 0.102
2C	Recirculation ratio increased to 2.3
2D	Recirculation ratio decreased to 1.7
2E	Hot and cold mixing fractions increased to 0.95
2F	Hot and cold mixing fractions decreased to 0.75
2G	Hot/cold tube split ratio changed to 50%/50%
3A	SG tube outer wall HTC x 5.0
3B	SG tube outer wall HTC x 0.5
4A	Oxidation power x 1.2
4B	Oxidation power x 0.5
5A	50% decrease in reactor vessel internal circulation flow rates
5B	100% increase in reactor vessel internal circulation flow rates
6A	2 MW total RCS heat loss
6B	8 MW total RCS heat loss
7A	RCP shaft seal leak rate increases to 61 gpm/pump at 2 hours
7B*	RCP shaft seal leak rate increases to 300 gpm/pump at 2 hours
7C*	RCP shaft seal leak rate increases to 182 gpm/pump at 2 hours
7D*	RCP shaft seal leak rate increases to 120 gpm/pump at 2 hours
7E*	RCP shaft seal leak rate increases to 90 gpm/pump at 2 hours
7F*	RCP shaft seal leak rate increases to 300 gpm in Loop 1 pump at 2 hours
7F2*	RCP shaft seal leak rate increases to 300 gpm in Loop 2 pump at 2 hours
7G	RCP shaft seal leak rate decreases to 1 gpm/pump at 2 hours
8A*	Pressurizer surge line connection moved to top of hot leg
8B*	Stuck open PORV on SG 1, no leakage from SG secondary in the other 3 SGs
8C*	100 gpm assumed tube leakage in SG 1, Coolant Loop 1 flow parameters adjusted to attain 0.14 hot leg C_D, 1.75 recirculation ratio and 0.75 mixing fractions
8D*	Surge line and hot leg upper section inside wall HTCs x 2.0
8E*	Tubesheet HTC x 2.0
8G*	SG steam leakage flow areas of 0.4, 0.3, 0.2 and 0.1 in^2 (one run with different leak area in each SG to determine minimum leak rate needed to depressurize SGs by the time of hot leg failure)

* Runs marked with an asterisk are not used for the statistical evaluation of uncertainties, only for evaluating various other issues.

6.0 SENSITIVITY RUN RESULTS

The selection of the SCDAP/RELAP5 SBO sensitivity cases is described in Section 5. As described there, the sensitivity runs are segregated into two groups: those runs related to important phenomena identified by the PIRT and used for the statistical evaluations of uncertainty, and additional runs performed to evaluate various other modeling, sequence event assumption and plant configuration issues. The results for sensitivity runs which fall into those two groups are discussed in Sections 6.1 and 6.2, respectively. To facilitate analyses performed by others in the project, standard SCDAP/RELAP5 input, output and plot files and data for selected output channels from the SCDAP/RELAP5 sensitivity case calculations are provided on DVDs which are available to others in the project. The selected additional data channels are identified in Appendix A.

6.1 Sensitivity Runs Used for the Statistical Evaluations of Uncertainty

Nineteen sensitivity runs identified in Table 8 are used to generate the data needed for the statistical evaluations of uncertainty.

With the exception of runs made specifically to evaluate the effect of variations in the SG inlet plenum mixing and flow parameters, the sensitivity runs were generally performed with the SG inlet plenum region flow coefficients readjusted to retain agreement between the calculated and target mixing and flow parameters specified for the base case. Table 9 compares the SCDAP/RELAP5-calculated results for the mixing and flow parameters from the 19 runs with the base case calculation and the target values for the mixing and flow parameters. (Note that this table includes data from additional reactor coolant pump shaft seal leakage sensitivity Cases 7B, 7C, 7D, 7E, 7F and 7F2, which were not used for uncertainty evaluation. These cases are included here only for consistency with the discussion of Cases 7A and 7G, which were used for that purpose.) The output data from the calculations for the dependent variables, which is used for the development of the uncertainty estimates, is shown in Tables 10 and 11. Other results from the sensitivity runs are summarized as follows:

Pressurizer PORV and SRV Flow Area Variations

The nominal pressurizer PORV and SRV flow areas used in the base case calculation are those needed to provide the rated valve flows at the rated pressures. Two sensitivity runs were performed, Case 1A (with nominal PORV and SRV flow areas increased by 30%) and Case 1B (with nominal PORV and SRV flow areas decreased by 30%).

The mass flow rates through one of the two pressurizer PORVs in the base case, Case 1A and Case 1B are compared in Figure 28. As expected, during periods when the valve is open the flow rates for Cases 1A and 1B are respectively greater and less than the corresponding base case flow rate. Because the relief valves open as often and as long as needed to control the RCS pressure, the overall results from the three runs are generally not very different, as shown by the comparison of the RCS pressure responses for the three runs in Figure 29. For the case with the larger valve area the valve opens for shorter periods than in the base case; the opposite is true for the case with the smaller valve area. The SG tube failure margins are only very slightly affected

by the variations in the pressurizer relief valve flow areas. Note that the PORVs are not functional after the station batteries are assumed to be depleted at four hours (14,400 s). Afterward, the pressurization of the RCS is limited only by the opening of the pressurizer SRVs.

Hot Leg Discharge Coefficient Variations

The nominal target hot leg discharge coefficient used in the base case calculation is 0.12. Two sensitivity runs were performed, Case 2A (with the discharge coefficient increased by 15% to 0.138) and Case 2B (with the discharge coefficient decreased by 15% to 0.102).

The responses of the Hot Leg 1 discharge coefficients for the base case, Case 2A and Case 2B are compared in Figure 30. The calculated discharge coefficients are in good agreement with the desired target values for all three runs.

Figure 31 compares the flow rates in the upper section of Hot Leg 1, near the reactor vessel, among the three runs. As expected, the hot leg flow rate is higher when the higher discharge coefficient is used and lower when the lower discharge coefficient is used. Figure 32 compares the integrated SG 1 power fractions among the three runs. Figures 31 and 32 show the close correlation between the hot leg flow and the portion of the core heat that is removed to the SGs. The difference in SG heat removal is seen to have a moderate effect on the SG average tube failure margins. Stress multipliers of 1.92, 2.10 and 2.39, respectively are needed for average tube failure to occur coincident with the hot leg using the increased, nominal and reduced hot leg discharge coefficients. The comparisons also show a small event sequence timing effect, with the lower hot leg discharge coefficient leading to an acceleration of events and the higher discharge coefficient leading to a deceleration of events. This effect results because the reduced SG heat removal associated with a lower hot leg discharge coefficient leads to more frequent and longer opening periods for the pressurizer PORVs, which tends to reduce the RCS fluid inventory more rapidly and accelerate the system heat up process.

Subsequent to performing Cases 2A and 2B, it was uncovered that the $\pm$15% hot leg discharge coefficient variations assumed in these runs may not fully bound the expected range in the parameter. For that reason, the results from these two runs are extrapolated to effectively incorporate a $\pm$30% hot leg discharge coefficient variation in the uncertainty analysis presented in Section 7.

Recirculation Ratio Variations

The nominal target recirculation ratio used in the base case calculation is 2.0. Two sensitivity runs were performed, Case 2C (with the recirculation ratio increased to 2.3) and Case 2D (with the recirculation ratio decreased to 1.7).

The responses of the Loop 1 recirculation ratios for the base case, Case 2C and Case 2D are compared in Figure 33. The calculated recirculation ratios are in good agreement with the desired target values for all three runs.

Figure 34 compares the integrated SG 1 power fractions among the three runs. With the other flow and mixing target parameters held constant, an increase in recirculation ratio is seen to increase the SG heat removal. The difference in SG heat removal is seen to have a small effect on the average tube failure margins. Stress multipliers of 2.02, 2.10 and 2.18, respectively are needed for average tube failure to occur coincident with the hot leg using the reduced, nominal and increased recirculation ratios. The average tube failure margin increases as the recirculation ratio increases because (with a cold mixing fraction of 0.85) most of the increased cold return tube flow is directed to the mixing plenum, where it lowers the inlet temperature for the hot average tube.

Unlike the average tube failure margin, the hottest tube failure margin is seen (in Table 10) to decline as the recirculation ratio increases. The reason for this difference is that the modeling which determines the inlet temperatures for the average and hottest tubes is different. For the average tube, the inlet temperature is based on the temperatures in the upper hot leg section and mixing plenum and on the flow rates from those two into the SG tube. However, for the hottest tube the inlet temperature is based only on the hot leg upper section temperature and cold tube return temperature (and a constant which defines the hottest tube inlet temperature within the range between the two). So, for an increased recirculation ratio, the average tube benefits, but the hottest tube does not, from the cooling effects of the higher cold return flow rate that passes to the mixing plenum.

The comparisons also show a small event sequence timing effect, with a lower recirculation ratio leading to an acceleration of events and a higher recirculation ratio leading to a deceleration of events. This effect results because the reduced SG heat removal associated with a lower recirculation ratio leads to more frequent and longer opening periods for the pressurizer PORVs, which tends to reduce the RCS fluid inventory more rapidly and accelerate the system heat up process.

Mixing Fraction Variations

The nominal target hot and cold mixing fractions used in the base case calculation are 0.85. Two sensitivity runs were performed, Case 2E (with the mixing fractions increased to 0.95) and Case 2F (with the mixing fractions decreased to 0.75).

The responses of the Loop 1 hot and cold mixing fractions for the base case, Case 2C and Case 2D are compared in Figures 35 and 36. The calculated hot and cold mixing fractions are in good agreement with the desired target values for all three runs.

Figure 37 compares the integrated SG 1 power fractions among the three runs. With the other flow and mixing target parameters held constant, a decrease in the mixing fractions is seen to increase the SG heat removal. This is the result because less flow is directed to the SG mixing inlet plenum and more flow is directed to the hot inlet plenum and cold inlet plenum. The difference in SG heat removal is seen to have a moderate effect on the SG average tube failure margins. Stress multipliers of 1.81, 2.10 and 2.50, respectively are needed for average tube failure to occur coincident with the hot leg using the decreased, nominal and increased mixing fractions.

Hot/Cold Tube Split Variation

The nominal hot/cold tube split assumed in the base case calculation is 41%/59%. A sensitivity run, Case 2G, was performed with the assumed tube split ratio changed to 50%/50%.

The mass flow rates in the SG 1 hot average tube for Case 2G and the base case are virtually the same, as shown in Figure 38. The changing of the partitioning of tubes into the hot and cold sections changes the flow areas of those sections, but the conservation of mass consideration requires that the mass flows through the two sections be the same, regardless of their relative sizes. However, the cross sectional flow area of the hot average tube section is larger (50% of the total) in Case 2G than it is in the base case (where it is 41% of the total). So, although the mass flow rates are the same, the hot average tube fluid velocities are lower in Case 2G than they are in the base case, as shown in Figure 39.

Lower velocities lead to lower heat transfer coefficients on the inside surfaces of the SG tubes. Figure 40 shows that the fluid-to-wall heat transfer coefficient for the SG 1 hot average tube section (just above the tubesheet) is lower in Case 2G than in the base case. And the lower wall heat transfer coefficients are seen to result in lower SG 1 tube metal temperatures at that location in Case 2G than in the base case, as shown in Figure 41.

These differences result in moderately higher SG tube failure margins for Case 2G than for the base case. The SG average tube requires a stress multiplier of 2.21 to fail coincident with the hot leg in Case 2G, whereas in the base case a stress multiplier of 2.10 is required.

SG Tube Outer-Wall Heat Transfer Coefficient Variations

The base case calculation employs the standard SCDAP/RELAP5 routines for wall heat transfer on the outside surfaces of the SG tubes. Two sensitivity runs were performed, Case 3A (with a 5.0 multiplier applied to the tube outside-surface heat transfer coefficient) and Case 3B (with a 0.5 multiplier applied to the tube outside-surface heat transfer coefficient).

The responses of the SG 1 hot average tube outside wall heat transfer coefficients for the base case, Case 3A and Case 3B are compared in Figure 42. The calculated heat transfer coefficients are in good agreement with their expected relative values. Note that the heat transfer coefficient multipliers in the sensitivity case runs were implemented at the time when the core uncovers and the temperature of the steam entering the hot legs becomes superheated. The runs were made in this manner because: (1) it is the behavior as the system heats up which is of interest and (2) implementing the multipliers earlier (for example, when the SGs still contain water) would have resulted in significant event sequence timing differences among the runs that would have obscured the desired comparisons.

The difference in the tube outer wall heat transfer coefficients is seen to have a moderate effect on the SG average tube failure margins. Stress multipliers of 2.07, 2.10 and 2.35, respectively are needed for average tube failure to occur coincident with the hot leg using the reduced, nominal and increased heat transfer coefficients.

The behavior differences among these runs are complex and include many competing effects regarding the temperatures and flow rates among the regions of the primary and secondary coolant systems. The fluid temperatures and velocities in the SG tube primary and SG secondary boiler regions are strong functions of the assumed tube outer-wall heat transfer coefficient. Figure 43 compares the SG 1 hot average tube wall temperatures (just above the tubesheet) among the three runs for a short time period which includes the hot leg failure times in all runs (that occur between 13,550 s and 13,650 s). The figure shows that the base case and Case 3B exhibit a similar behavior, but the much higher heat transfer coefficient in Case 3A causes the behavior to be different from the others. That, coupled with the 100-s difference in the hot leg failure time, leads to the SG tube failure margin differences among the cases. The competing effects associated with this sensitivity evaluation are discussed in more detail in a 2004 report documenting station blackout sensitivity studies (see Reference 9, Section 3.4).

Fuel Rod Cladding Oxidation Variations

The base case calculation employs the standard SCDAP/RELAP5 models for the fuel rod cladding oxidation process. Two sensitivity runs were performed, Case 4A (with an additional 20% of the calculated oxidation power added to the fluid in the core region) and Case 4B (with 50% of the calculated oxidation power removed from the fluid in the core region).

The oxidation powers from the base case, Case 4A and Case 4B are compared in Figure 44. The calculated oxidation power responses are in good agreement with their expected relative values among the cases. It is noted that the sequence event timing and peak oxidation power are significantly affected by the oxidation modeling revisions. In Case 4A, for which supplemental power is added, the peak oxidation power is higher and it occurs earlier than in the base case. In Case 4B, for which supplemental power is removed, the oxidation power peak is much lower and later than in the base case. These differences are as expected because of the positive feedback between the oxidation rate and temperature. For example, the added power causes the heat up to become more rapid, and the feedback effect causes the oxidation rate to be higher, which leads to still higher powers and temperatures.

The difference in the oxidation modeling is seen to have a small effect on the SG average tube failure margins. Stress multipliers of 1.91, 2.10 and 2.16, respectively are needed for average tube failure to occur coincident with the hot leg using the reduced, nominal and increased oxidation rates. This relationship between the oxidation power and average SG tube failure margin is created mainly because a higher oxidation rate leads to a faster system heat-up and the hot legs are located in closer proximity to the reactor core (where the steam is the hottest) than are the SG tubes.

Figure 45 compares the Hot Leg 1 upper section fluid temperatures near the reactor vessel among the three runs. The system heat up rate for the +20% oxidation case is higher than for the base case and much higher than for the -50% oxidation case. The average tube failure margin for the +20% oxidation case is higher than for the base case because the heat-up rate is faster and the time delay required for the increasingly-hotter steam to migrate out into the SG tubes becomes a more important factor. Conversely, the average tube failure margin for the -50% oxidation case

is lower than for the base case because the heat up rate is slower and the migration time delay is no longer as important. In other words, for faster heat ups the proximity to the core becomes more important, causing the hot legs to reach failure temperature preferentially sooner than the SG tubes and for slower heat ups the proximity to the core becomes less important, causing the SG tubes to reach to reach failure temperature preferentially sooner than the hot legs.

Unlike the average tube failure margin, the hottest tube failure margin is seen (in Table 10) to decline as the oxidation rate increases. The reason for this difference is that the modeling which determines the inlet temperatures for the average and hottest tubes is different. For the average tube, the inlet temperature is based on the temperatures in the upper hot leg section and mixing plenum and on the flow rates from those two into the SG tube. However, for the hottest tube the inlet temperature is based only on the hot leg upper section temperature and cold tube return temperature (and a constant which defines the hottest tube inlet temperature within the range between the two). So, for the increased tube flow rate that results from a faster system heat-up, the average tube benefits, but the hottest tube does not, from the cooling effects of the higher cold return flow rate that passes to the mixing plenum.

Reactor Vessel Internal Circulation Rate Variations

The SCDAP/RELAP5 base case flow circulations within the reactor vessel are based on the configuration of the reactor vessel fluid regions and internal structures, the fluid conditions and the flow loss coefficients specified in the input model. Two sensitivity runs were performed, Case 5A (with flow loss coefficients increased so as to reduce the vessel internal circulation flow rates by 50%) and Case 5B (with flow loss coefficients decreased so as to increase the vessel internal circulation flow rates by 100%).

The flow rates at the top of the central core channel for the base case, Case 5A and Case 5B are compared in Figure 46. The relative flow rates among the three calculations are as desired at this representative location. The flow comparisons at other locations within the reactor vessel show similar relative behavior among the three cases.

The changes in the reactor vessel internal flow loss modeling are seen to have a small effect on the average tube failure margins. Stress multipliers of 2.28, 2.10 and 1.97, respectively are needed for average tube failure to occur coincident with the hot leg for the cases representing the reduced, nominal and increased vessel circulation flow rates.

These margin differences were found to result primarily because the vessel internal circulation rate affects the fuel rod oxidation process. Figure 47 compares the total fuel rod oxidation power responses for the three cases. The reduced vessel circulation case resulted in a lower and earlier peak oxidation power than the base case. The increased vessel circulation case resulted in a higher and later peak oxidation power than the base case. This difference in oxidation behavior results because, although the vessel internal circulation rates differ widely among the runs, the hot leg flow rates in all three runs are for the most part the same. Therefore, in the reduced vessel circulation case the cooling afforded by the flow leaving and returning to the vessel becomes a more significant factor, leading to lower core temperatures and lower fuel rod oxidation rates.

The cases with higher vessel internal flow rates and oxidation powers are seen to lead to lower average tube failure margins, which is the reverse of the results discussed for the oxidation modeling sensitivity above. This difference appears to result because the peak temperatures achieved were similar in all three of the oxidation power sensitivity runs (see Figure 45, which shows the Hot Leg 1 upper section fluid temperature) but the peak temperatures achieved in the three vessel-circulation sensitivity runs are quite different, as shown in Figure 48 for the same parameter.

The fluid temperature differences between the three vessel circulation sensitivity cases are important because they affect the peak hot leg wall temperatures (shown in Figure 49) which directly affect the prediction of the hot leg structural failure. A spread of 395 K (711^{o}F) is seen among the peak hot leg wall temperatures achieved for the three cases.

Unlike the average tube failure margin, the hottest tube failure margin is seen (in Table 10) to increase as the vessel internal circulation rate increases. The reason for this difference is that the modeling which determines the inlet temperatures for the average and hottest tubes is different. For the average tube, the inlet temperature is based on the temperatures in the upper hot leg section and mixing plenum and on the flow rates from those two into the SG tube. However, for the hottest tube the inlet temperature is based only on the hot leg upper section temperature and cold tube return temperature (and a constant which defines the hottest tube inlet temperature within the range between the two). The hot leg failure time varied significantly among the three runs (13,355 s for the reduced vessel flow case, 13,630 s for the base case and 14,125 s for the increased vessel flow case) and the coolant loop and SG recirculation flows at those times varied from case to case. These flow differences directly affected the average tube failure margins but not the hottest tube failure margins.

Reactor Coolant System Heat Loss Variations

The base case calculation assumes a 4 MW total heat loss from the outer surfaces of the primary and secondary reactor coolant systems to the containment. Two sensitivity runs were performed, Case 6A (with the assumed total heat loss reduced to 2 MW) and Case 6B (with the assumed total heat loss increased to 8 MW).

The heat fluxes from the outside surface of the reactor vessel cylindrical wall (at an elevation near the center of the core) for the base case, Case 6A and Case 6B are compared in Figure 50. The relative heat fluxes among the three calculations are as desired at this representative location. The heat flux comparisons at other locations within the reactor vessel show similar relative behavior among the three cases.

The different heat loss modeling is seen to have a small effect on the SG average tube failure margins. Stress multipliers of 2.12, 2.10 and 1.92, respectively are needed for average tube failure to occur coincident with the hot leg for the cases representing the reduced, nominal and increased reactor coolant system heat losses.

These SG tube failure margin differences were found to result primarily from sequence of events timing differences induced by the different heat loss assumptions. Lower heat losses tend to accelerate the timing of events while higher heat losses tend to decelerate it. This effect is illustrated in Figure 51, which shows the pressurizer level comparison among the three cases. The timing differences were found to result from competing effects that differentially affect the heat-up of the hot leg and surge line relative to the heat-up of the SG tubes. The competing effects associated with this sensitivity evaluation are discussed in more detail in a 2004 report documenting station blackout sensitivity studies (see Reference 9, Section 3.8).

Reactor Coolant Pump Shaft Seal Leakage Variations

The base case calculation simulates shaft seal leakage in all four reactor coolant pumps based on an initial 21 gpm per pump leak rate at the start of the station blackout event sequence. Eight sensitivity runs listed in Table 8 were performed assuming that changes in the leak rate occur two hours following the start of the station blackout sequence. Case 7A assumes that the leak rate in all pumps increases to 61 gpm. Case 7B assumes that the leak rate in all pumps increases to 300 gpm. Case 7C assumes that the leak rate in all pumps increases to 182 gpm. Case 7D assumes that the leak rate in all pumps increases to 120 gpm. Case 7E assumes that the leak rate in all pumps increases to 90 gpm. Case 7F assumes that the leak rate in only the Loop 1 pump increases to 300 gpm. Case 7F2 assumes that the leak rate in only the Loop 2 pump increases to 300 gpm. Case 7G assumes that the leak rate in all pumps decreases to 1 gpm.

Of these sensitivity runs, only output data from Case 7A (61 gpm) and Case 7G (1 gpm) is used for the purposes of evaluating uncertainties. The uncertainty study considers $\pm$20 gpm variations around the 21 gpm nominal leak rate after two hours. The output data from Cases 7A and 7G is used to estimate the effects of those variations, see discussion for PIRT Parameter C2 in Section 5.2.

The discussion of results for the pump seal leakage sensitivity runs is grouped into symmetric cases (where the same leakage assumption is used in all four pumps) and unsymmetrical cases (where an increased leakage is assumed to occur in only one pump):

Symmetric Cases (Same Leakage in All Four Pumps)

The symmetric cases investigate changes in the leakage rates to 1 gpm, 61 gpm, 90 gpm, 120 gpm, 182 gpm and 300 gpm per pump. These are Cases 7G, 7A, 7E, 7D, 7C and 7B, respectively.

Figure 52 compares the Pump 1 leak rates from these six sensitivity cases with that in the base case. The figure shows that the calculated relative leakage rates among the seven cases are as expected.

Figure 53 compares the RCS pressure responses among the seven cases. Prior to 10,637 s, when the pressurizer drains, the pressure responses in all runs are virtually the same. While pump leakage provides some added capabilities for reducing RCS pressurization, prior to this time the pressurization load is high and the pump leakage only results in less frequent opening of the

pressurizer relief valves. However after the pressurizer drains the RCS steam production rate declines, the pressurization load is reduced and the added pump leakage can succeed in reducing the RCS pressures. The larger the assumed pump shaft seal leakage rate, the greater the RCS pressure relief that is provided and the lower the RCS pressures.

Figure 54 compares the Hot Leg 1 upper section fluid temperatures among the seven cases. Looking at the period when the heat-up rates are the highest (from about 12,500 s to 13,200 s), the figure shows that the heat-up rate is generally proportional to the assumed pump shaft seal leakage rate. The exception is for the largest assumed leakage rate, 300 gpm in Case 7B, which shows a reduced heat-up rate relative to the next-largest leakage run, Case 7C.

The pump shaft seal leakage modeling is seen to have a large effect on the SG average tube failure margins. For the seven cases (1 gpm, 21 gpm, 61 gpm, 90 gpm, 120 gpm, 182 gpm and 300 gpm), stress multipliers of 2.08, 2.10, 2.33, 2.50, 3.30, 4.58 and 7.01 respectively are needed for average tube failure to occur coincident with the hot leg failure. As indicated above, lower RCS pressures and faster RCS heat-ups are seen as the assumed leakage rate increases. Both of these effects promote increased SG tube failure margins. Lower RCS pressures reduce the differential pressure across the SG tubes, reducing the potential for their failure. Higher RCS heat up rates preferentially favor earlier hot leg failure relative to SG tube failure (see the discussion under "Fuel Rod Cladding Oxidation Variations" above). For 300-gpm Case 7B, the heat-up rate is slower than for 182-gpm Case 7C, but the RCS depressurization effects are much larger, which leads to the very large calculated SG tube failure margin for Run 7B.

Unsymmetrical Cases (Increased Leakage in Only One Pump)

The unsymmetrical cases investigate increased leakage rates of 300 gpm in only one of the four reactor coolant pumps. In Case 7F, the increased leakage is assumed to be in Pump 1 and in Case 7F2 the increased leakage is assumed to be in Pump 2.

Figure 55 compares the leak rates from these two cases for the pumps which experience the increased leakage. For comparison purposes, the leak rates for these two unsymmetrical cases are compared with the leak rate for the 90-gpm symmetric leakage Case 7E. Note that the leakage shown for Case 7E is only for Pump 1 and that the total pump leakage in Case 7E is 360 gpm. The figure shows that the relative leakage rates among these three cases are as expected.

Figure 56 compares the RCS pressure responses among the three cases. As expected, because the total leak rates are the same for all three cases, their pressure responses are also similar. SCDAP/RELAP5 did not predict loop seal clearing in any coolant loop in any of the calculations described in this report.

Figure 57 compares the Hot Leg 1 upper section fluid temperatures among the three cases. Looking at the period when the heat-up rates are the highest (from about 12,600 s to 13,000 s), the figure shows that the heat-up rates among the three runs also are similar.

The pump shaft seal leakage assumptions for the unsymmetrical cases are seen to have only a small effect on the SG average tube failure margins. For the four cases (the 21-gpm in four pumps base case, the 90-gpm in four pumps Case 7E, the 300-gpm in Pump 1 Case 7F and the 300-gpm in Pump 2 Case 7F2) stress multipliers of 2.10, 2.50, 2.00 and 2.15 respectively are needed for average tube failure to occur coincident with the hot leg. Therefore the average tube failure margins for these four cases are quite similar. Note that in Case 7F (with the increased leakage in Pump 1) Hot Leg 2 is the first to fail and the same minimum average tube failure margin is calculated in SGs 2, 3 and 4. And, in Case 7F2 (with the increased leakage in Pump 2) note that Hot Leg 1 is the first to fail and that the minimum average tube failure margin is calculated in SG 3.

The average tube failure margins calculated for the unsymmetrical pump seal leakage cases (7F and 7F2) are moderately lower than that calculated for the symmetrical pump seal leakage case with roughly the same total leakage rate (7E). The average tube failure margins for the two unsymmetrical cases show only a small effect of moving the leakage from the pressurizer loop to a non-pressurizer loop. However, as shown in Table 10, large differences in the hottest tube failure margins are observed among these three cases.

The pump shaft seal leakage sensitivity cases included in this uncertainty evaluation report necessarily represent only a first look into the issue of symmetrical versus unsymmetrical leakage assumptions. A more extensive investigation into this issue would likely require many more runs evaluating various combinations of leak rates and opening times for the four reactor coolant pumps. Should additional runs be needed for this purpose, the model should be upgraded to include representations for a hottest tube in all SGs and detailed analyses performed for the average-tubes and hottest-tubes in all four SGs.

Table 9. Comparison of Target and SCDAP/RELAP5-Calculated SG Inlet Plenum Mixing and Flow Parameters for the Cases Used in the Uncertainty Analysis.

Case Number* and Time Evaluated	Loop 1 Hot Leg C_D	SG 1 Recirculation Ratio	SG 1 Hot Mixing Fraction	SG 1 Cold Mixing Fraction	SG 1 Power Fraction
Base Case, Target	0.12	2.0	0.85	0.85	None
Base Case, 13,000 s	0.120	1.990	0.853	0.848	0.07143
Case 1A, 13,000 s	0.120	1.981	0.852	0.848	0.07000
Case 1B, 13,000 s	0.121	2.000	0.853	0.849	0.07052
Case 2A, 13,000 s	0.137	1.969	0.857	0.848	0.07491
Case 2B, 13,000 s	0.103	2.011	0.847	0.847	0.06716
Case 2C, 13,000 s	0.120	2.261	0.851	0.871	0.07222
Case 2D, 13,000 s	0.118	1.725	0.853	0.831	0.06958
Case 2E, 13,000 s	0.122	2.053	0.930	0.943	0.06723
Case 2F, 13,000 s	0.118	1.948	0.741	0.770	0.07472
Case 2G, 13,000 s	0.120	2.042	0.853	0.853	0.07188
Case 3A, 13,000 s	0.120	1.975	0.853	0.847	0.06872
Case 3B, 13,000 s	0.120	1.994	0.853	0.849	0.07196
Case 4A, 13,000 s	0.120	1.991	0.853	0.848	0.07135
Case 4B, 13,000 s	0.120	1.983	0.853	0.847	0.07064
Case 5A, 12,300 s	0.121	1.998	0.853	0.850	0.06534
Case 5B, 13,000 s	0.120	1.991	0.853	0.848	0.07357
Case 6A, 12,500 s	0.121	1.991	0.853	0.848	0.07003
Case 6B, 13,000 s	0.121	2.021	0.853	0.850	0.07254
Case 7A, 13,000 s	0.117	1.981	0.852	0.848	0.06656
Case 7B*, 12,000 s	0.104	1.974	0.838	0.851	0.04122
Case 7C*, 12,000 s	0.111	2.007	0.843	0.852	0.05031
Case 7D*, 12,000 s	0.114	2.017	0.847	0.852	0.05602
Case 7E*, 12,500 s	0.114	1.977	0.850	0.849	0.06087
Case 7F*, 12,500 s	0.116	2.023	0.850	0.851	0.06694
Case 7F2*, 12,500 s	0.116	2.019	0.850	0.851	0.06510
Case 7G, 13,000 s	0.122	1.971	0.854	0.847	0.07018

* Runs marked with an asterisk are not used for the statistical evaluation of uncertainties, only for evaluating various other issues.

Table 10. Comparison of SCDAP/RELAP5-Calculated Results for Failure Times and Margins for the Cases Used in the Uncertainty Analysis.

Case Number*	First Primary Failure Component	First Primary Failure Time (s)	SG 1 Hottest Tube with 1.0 Multiplier Failure Time – First Primary Failure Time (s)	SG 1 Average Tube Stress Multiplier for Tube Failure Coincident with First Primary Failure
Base Case	Hot Leg 1	13,630	-155	2.10
Case 1A	Hot Leg 1	13,660	-155	2.07
Case 1B	Hot Leg 1	13,685	-150	2.11
Case 2A	Hot Leg 1	13,775	-155	1.92
Case 2B	Hot Leg 1	13,470	-135	2.39
Case 2C	Hot Leg 1	13,765	-170	2.18
Case 2D	Hot Leg 1	13,615	-135	2.02
Case 2E	Hot Leg 1	13,605	-145	2.50
Case 2F	Hot Leg 1	13,740	-160	1.81
Case 2G	Hot Leg 1	13,750	-140	2.21
Case 3A	Hot Leg 1	13,550	-35	2.35
Case 3B	Hot Leg 1	13,650	-160	2.07
Case 4A	Hot Leg 1	13,435	-170	2.16
Case 4B	Hot Leg 1	14,535	-90	1.91
Case 5A	Hot Leg 1	13,355	-260	2.28
Case 5B	Hot Leg 1	14,125	-90	1.97
Case 6A	Hot Leg 1	13,295	-140	2.12
Case 6B	Hot Leg 1	14,385	-255	1.92
Case 7A	Hot Leg 1	13,465	-210	2.33
Case 7B*	Hot Leg 2	14,320	Did Not Fail	7.01
Case 7C*	Hot Leg 2	14,475	Did Not Fail	4.58
Case 7D*	Hot Leg 2	14,300	Did Not Fail	3.30
Case 7E*	Hot Leg 2	13,450	10	2.50
Case 7F*	Hot Leg 2	13,380	Did Not Fail	2.00
Case 7F2*	Hot Leg 1	13,460	-275	2.15**
Case 7G	Hot Leg 1	13,395	-140	2.08

* Runs marked with a single asterisk are not used for the statistical evaluation of uncertainties, only for evaluating various other issues.

** For Case 7F2, the minimum average-tube failure margin shown is calculated in SG 3.

Table 11. Comparison of SCDAP/RELAP5-Calculated Results for Temperatures and Wall Heat Transfer Coefficients for the Cases Used in the Uncertainty Analysis.

Case Number*	SG 1 Average Tube Structure Temperature (K)	SG 1 Hottest Tube Structure Temperature (K)	Hot Leg 1 Steam Temperature (K)	Hot Leg 1 Wall HTC (W/m^2-K)	Surge Line Steam Temperature (K)	Surge Line Wall HTC (W/m^2-K)
Base Case	1021.7	1239.6	1776.0	423.13	1373.0	490.86
Case 1A	1023.0	1239.6	1771.9	434.52	1378.3	562.30
Case 1B	1020.9	1238.7	1773.8	412.90	1370.6	454.83
Case 2A	1039.3	1254.1	1744.7	428.99	1360.6	501.09
Case 2B	999.80	1218.4	1744.5	399.42	1346.6	475.78
Case 2C	1014.6	1247.7	1729.4	424.26	1349.2	561.65
Case 2D	1028.6	1217.1	1729.8	404.27	1348.8	470.96
Case 2E	986.70	1226.0	1725.1	407.90	1352.2	517.18
Case 2F	1053.0	1247.1	1780.3	438.17	1369.0	542.98
Case 2G	1013.8	1217.3	1788.3	407.35	1377.0	442.90
Case 3A	1000.7	1173.0	1737.9	413.83	1353.7	499.80
Case 3B	1023.8	1248.5	1751.0	413.18	1355.0	463.99
Case 4A	1018.8	1240.1	1776.8	438.84	1368.1	548.26
Case 4B	1030.9	1189.6	1677.7	297.93	1274.6	243.77
Case 5A	999.20	1157.5	1603.3	380.91	1248.7	468.74
Case 5B	1031.8	1231.3	1800.5	422.80	1405.7	527.39
Case 6A	1017.9	1235.0	1764.1	415.13	1364.8	462.60
Case 6B	1040.7	1250.6	1739.8	419.04	1325.5	490.39
Case 7A	997.80	1180.2	1731.2	364.63	1127.6	279.77
Case 7B*	918.10	949.70	1558.3	234.15	623.20	133.41
Case 7C*	952.80	989.90	1481.8	247.84	720.10	180.11
Case 7D*	960.00	1010.6	1489.1	269.00	741.00	181.79
Case 7E*	984.20	1139.9	1719.2	332.79	745.00	284.46
Case 7F*	950.10	1049.8	1668.0	334.26	848.20	234.29
Case 7F2*	1007.3	1186.1	1668.1	340.33	1004.9	251.34
Case 7G	1023.0	1234.6	1735.3	421.27	1360.7	562.50

* Runs marked with an asterisk are not used for the statistical evaluation of uncertainties, only for evaluating various other issues.

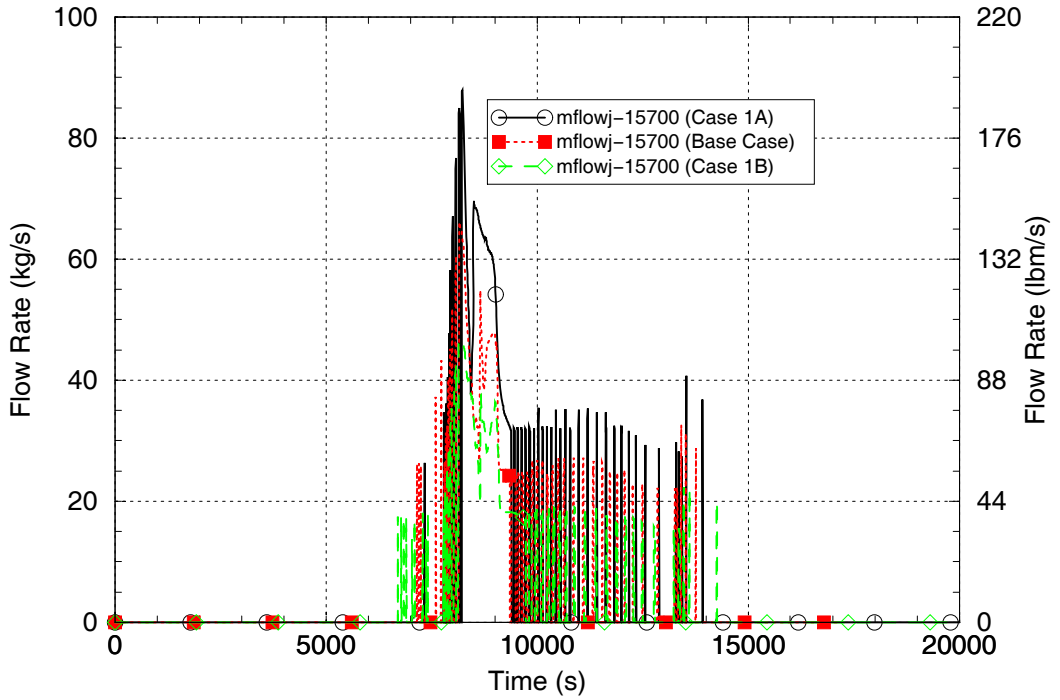

Figure 28. Mass Flow Rates Through One of the Two Pressurizer PORVs for the Relief Valve Flow Area Sensitivity Cases.

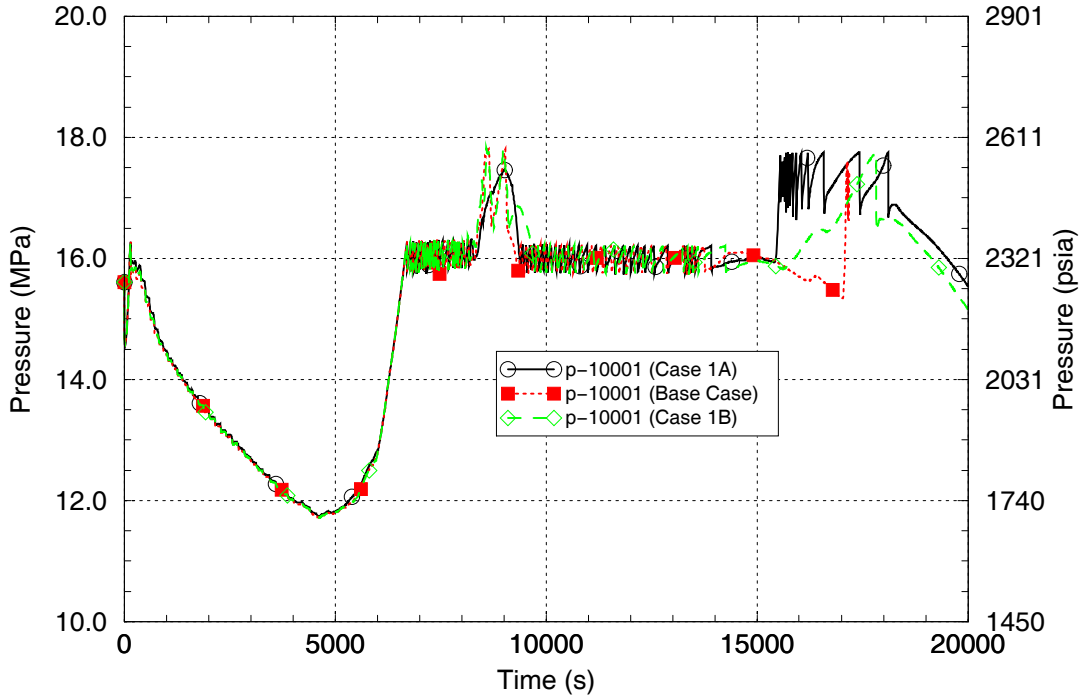

Figure 29. RCS Pressures for the Relief Valve Flow Area Sensitivity Cases.

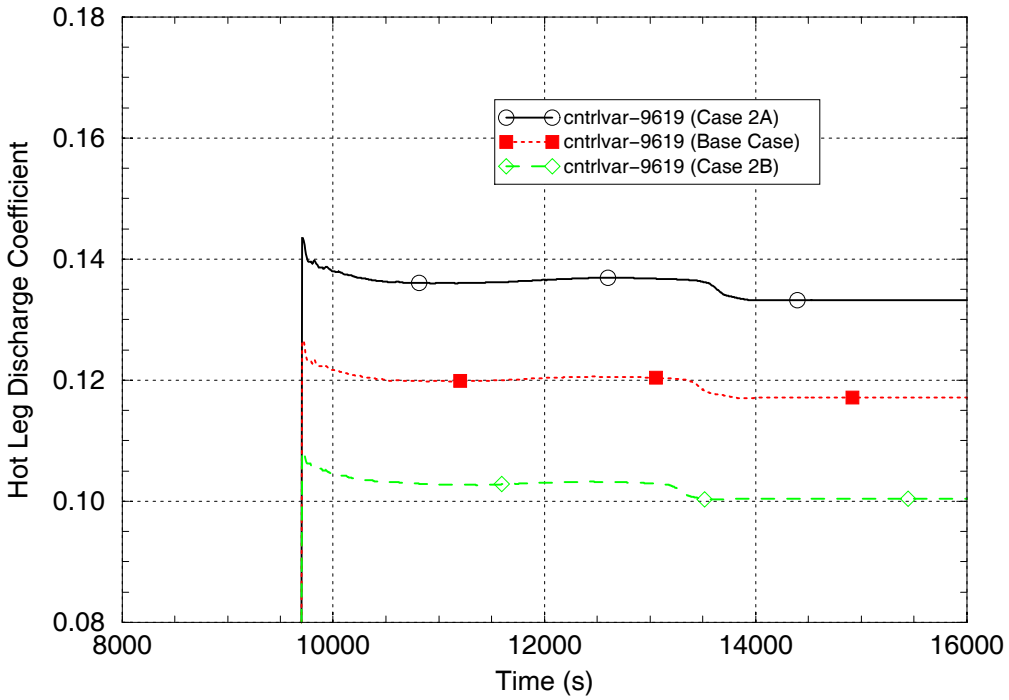

Figure 30. Hot Leg 1 Discharge Coefficient Responses for the Hot Leg Discharge Coefficient Sensitivity Cases.

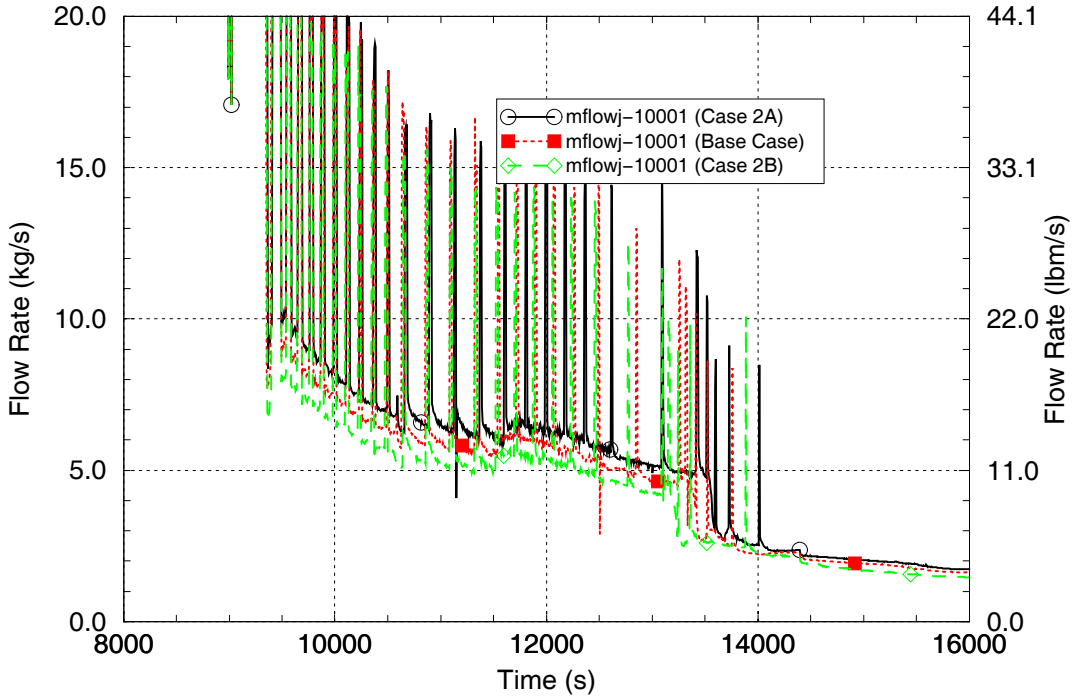

Figure 31. Hot Leg 1 Upper Section Flow Rates for the Hot Leg Discharge Coefficient Sensitivity Cases.

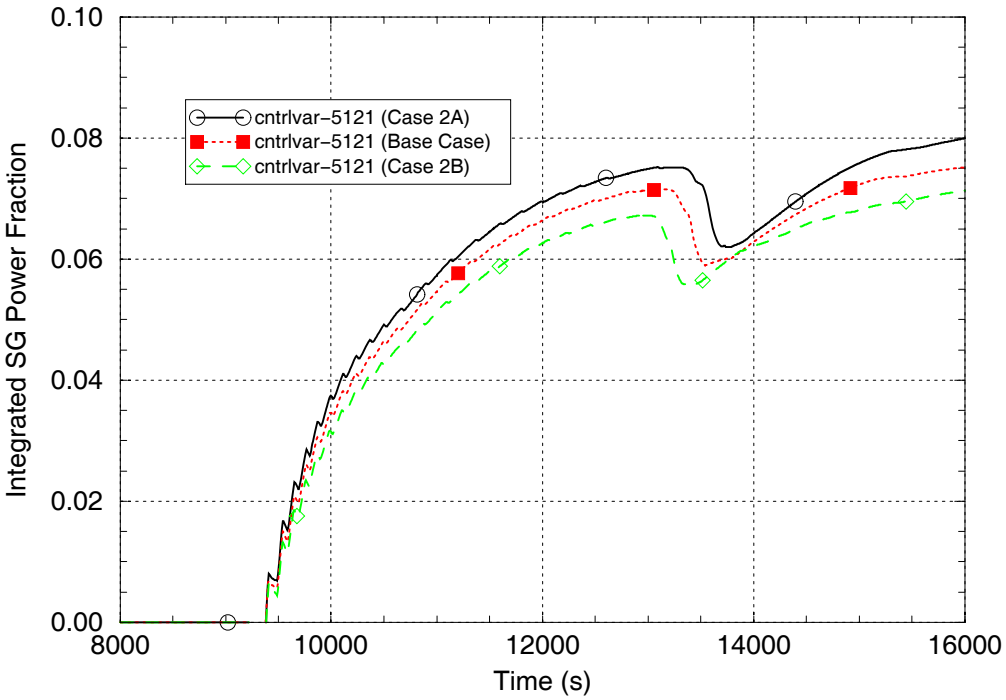

Figure 32. Integrated SG Power Fractions for the Hot Leg Discharge Coefficient Sensitivity Cases.

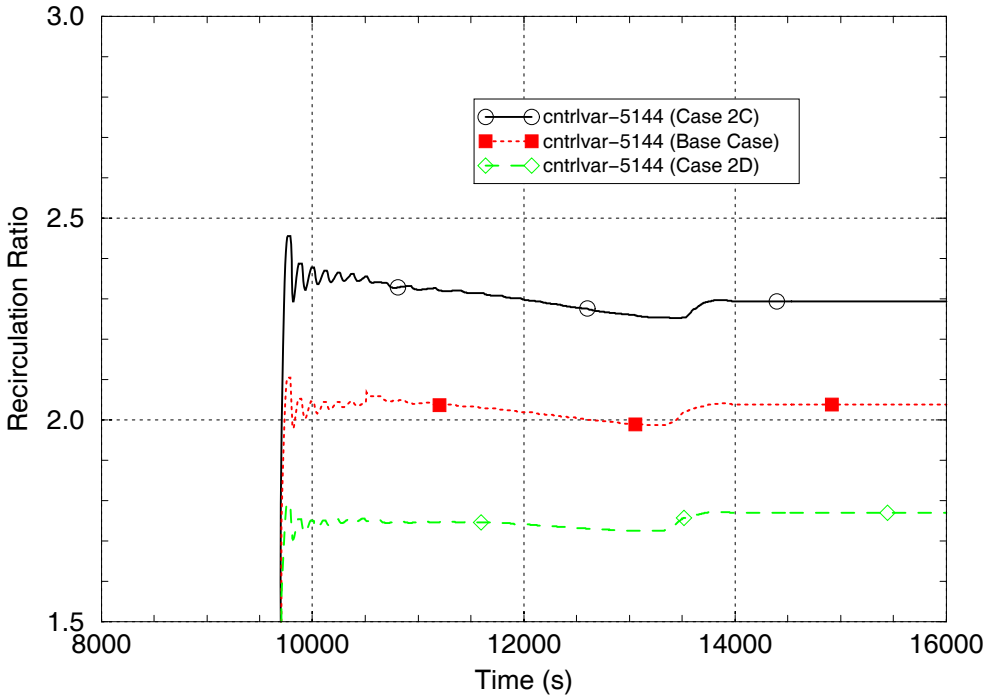

Figure 33. Loop 1 Recirculation Ratio Responses for the Recirculation Ratio Sensitivity Cases.

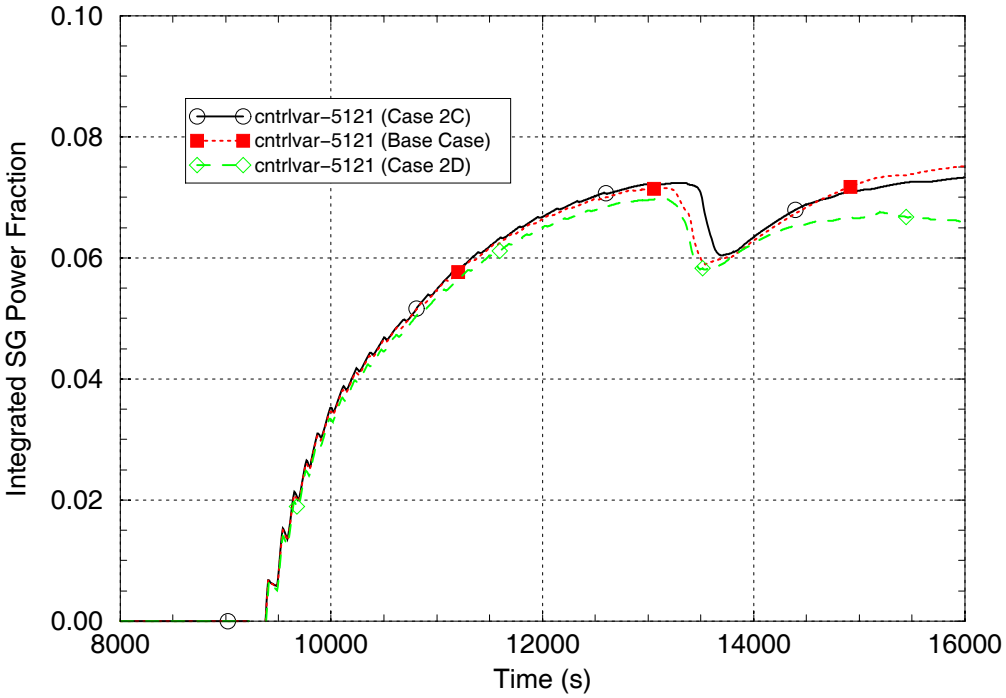

Figure 34. Loop 1 Integrated SG Power Fractions for the Recirculation Ratio Sensitivity Cases.

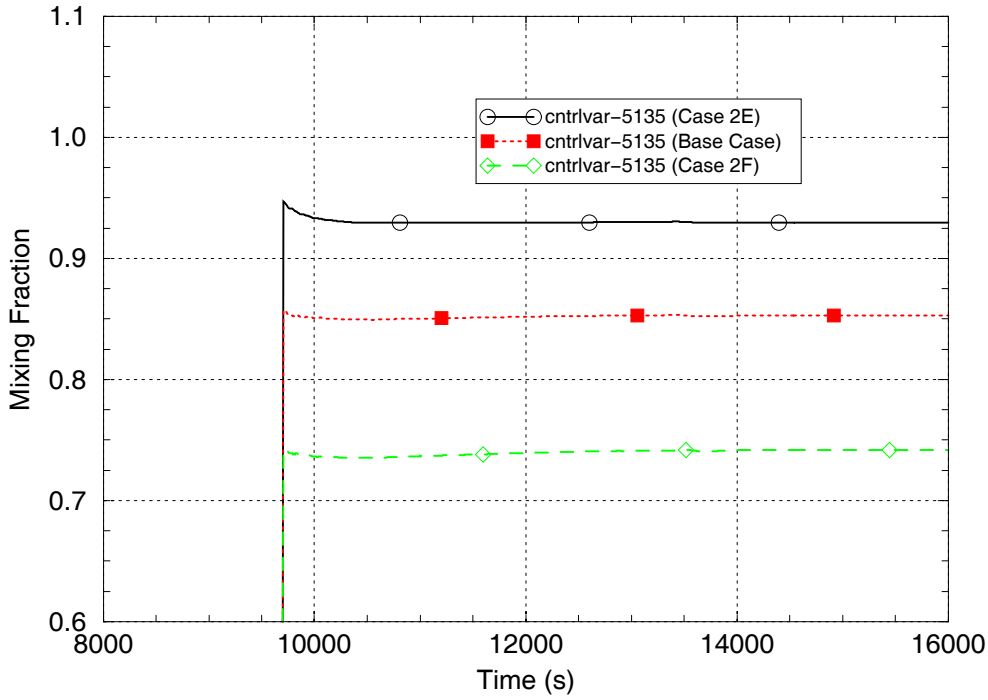

Figure 35. Loop 1 Hot Mixing Fraction Responses for the Mixing Fraction Sensitivity Cases.

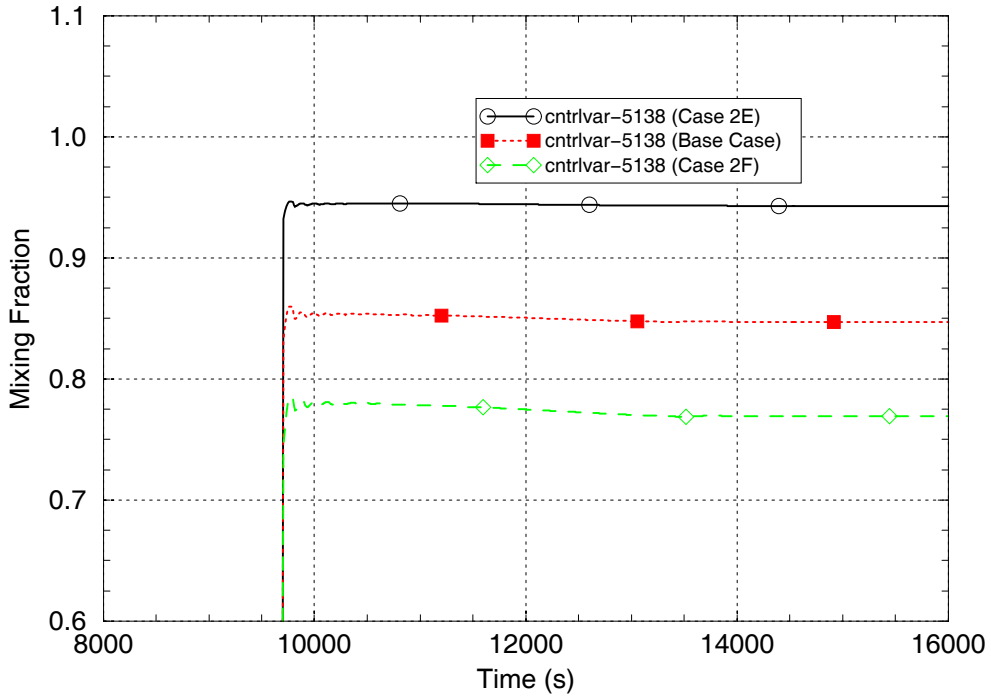

Figure 36. Loop 1 Cold Mixing Fraction Responses for the Mixing Fraction Sensitivity Cases.

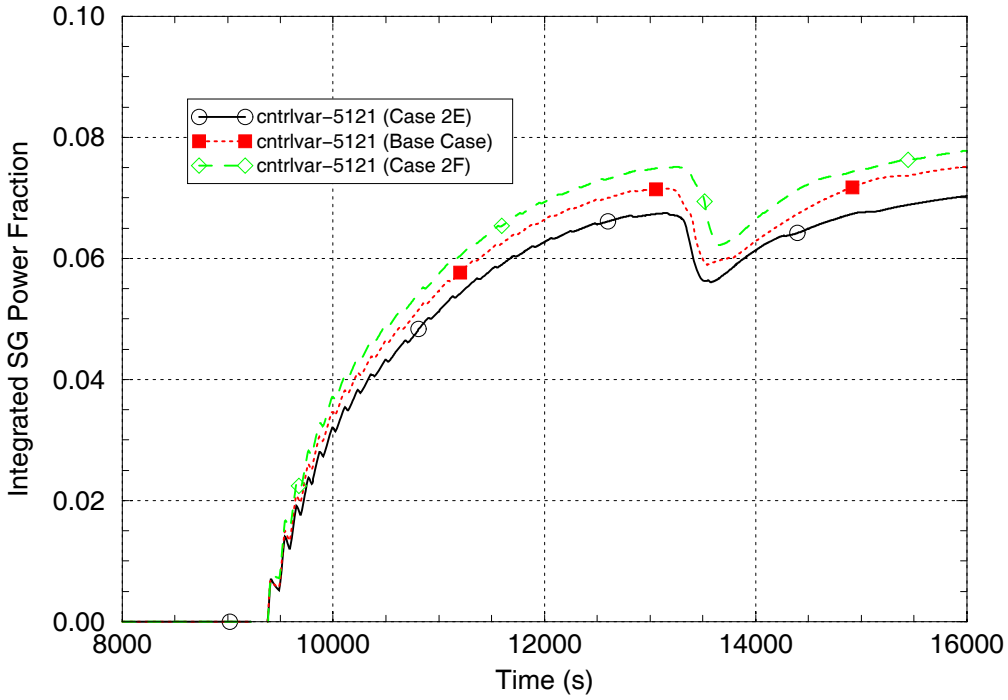

Figure 37. Integrated SG 1 Power Fractions for the Mixing Fraction Sensitivity Cases.

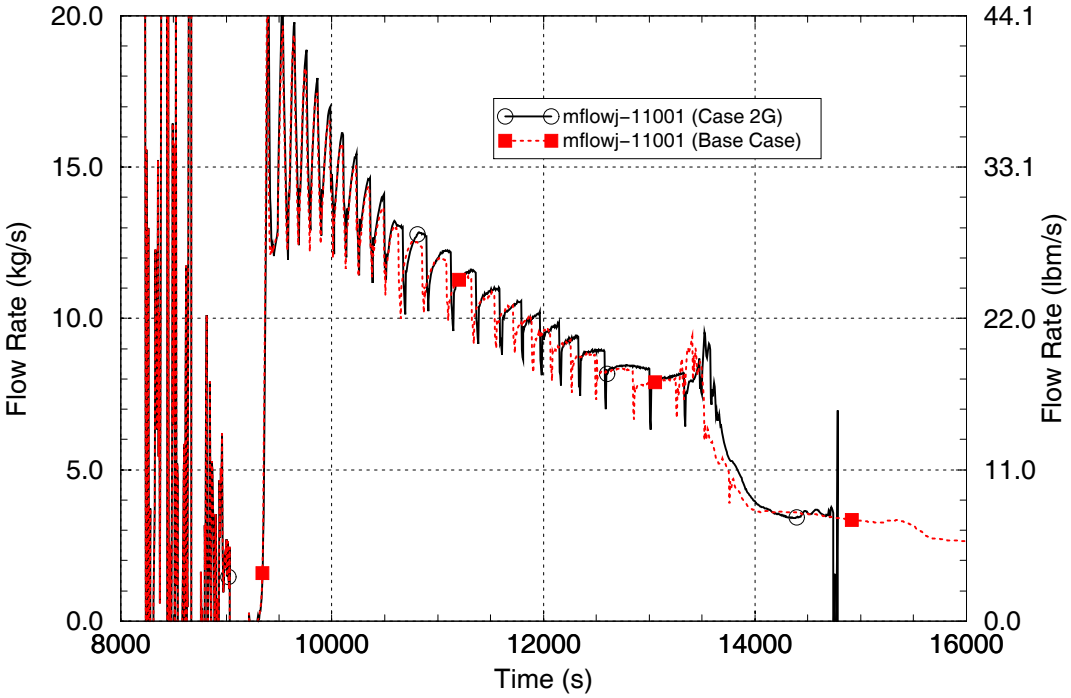

Figure 38. Mass Flow Rates in SG 1 Hot Average Tube for the Tube Split Sensitivity Cases.

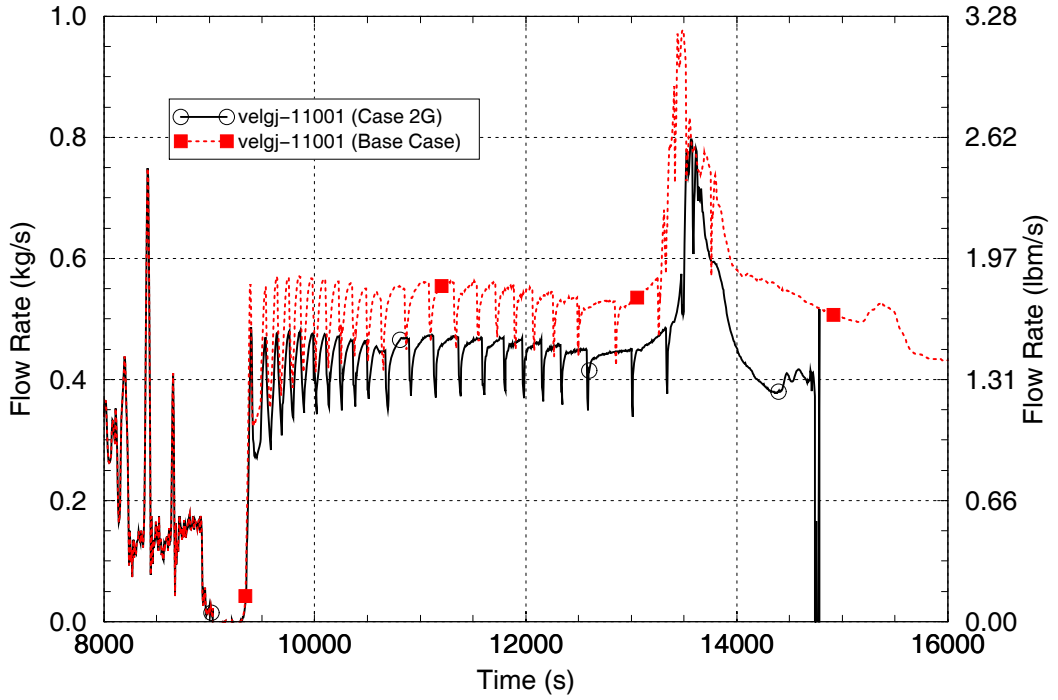

Figure 39. Fluid velocities in SG 1 Hot Average Tube for the Tube Split Sensitivity Cases.

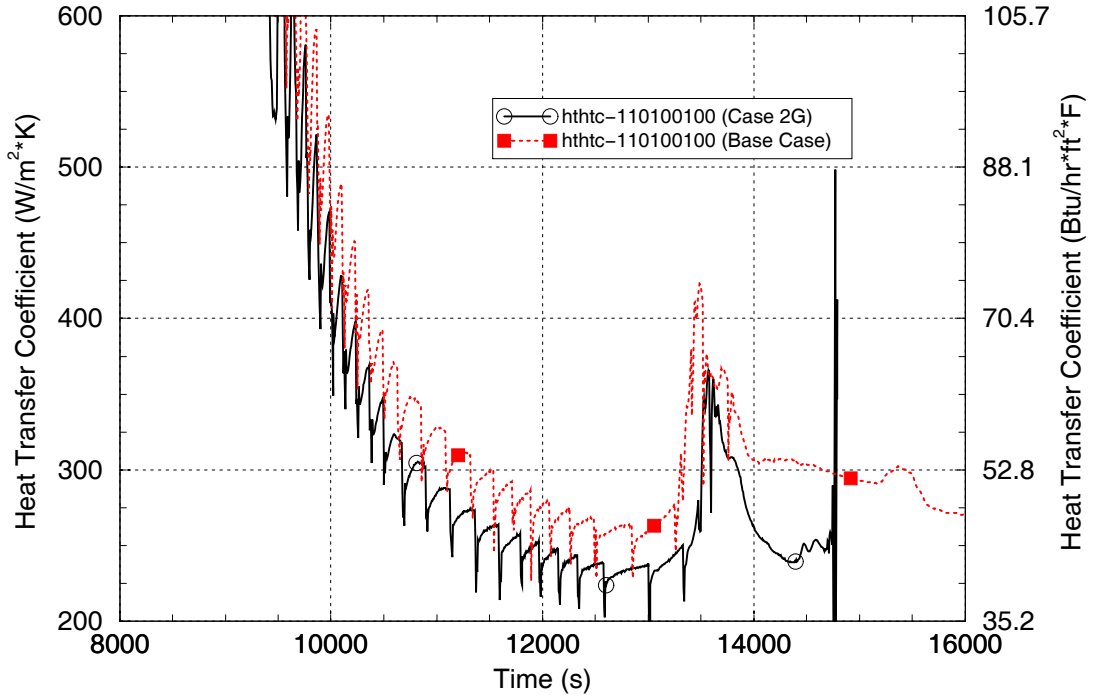

Figure 40. SG 1 Hot Average Tube Wall Inside Surface Heat Transfer Coefficients for the Tube Split Sensitivity Cases.

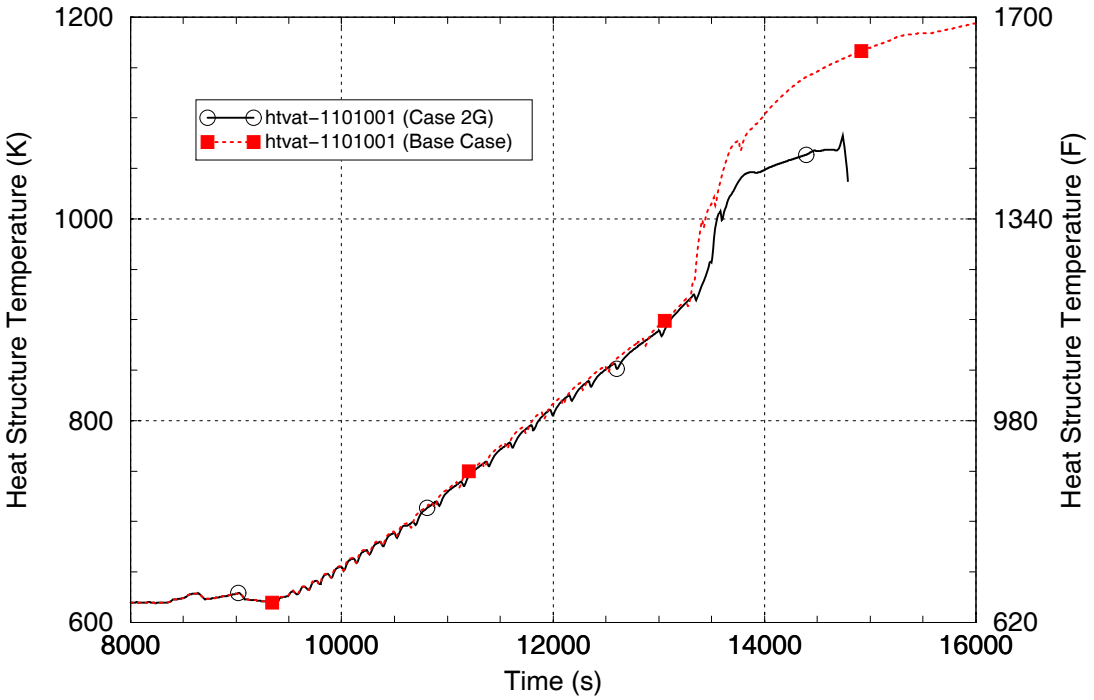

Figure 41. Tube Wall Temperatures in SG 1 Hot Average Tube for the Tube Split Sensitivity Cases.

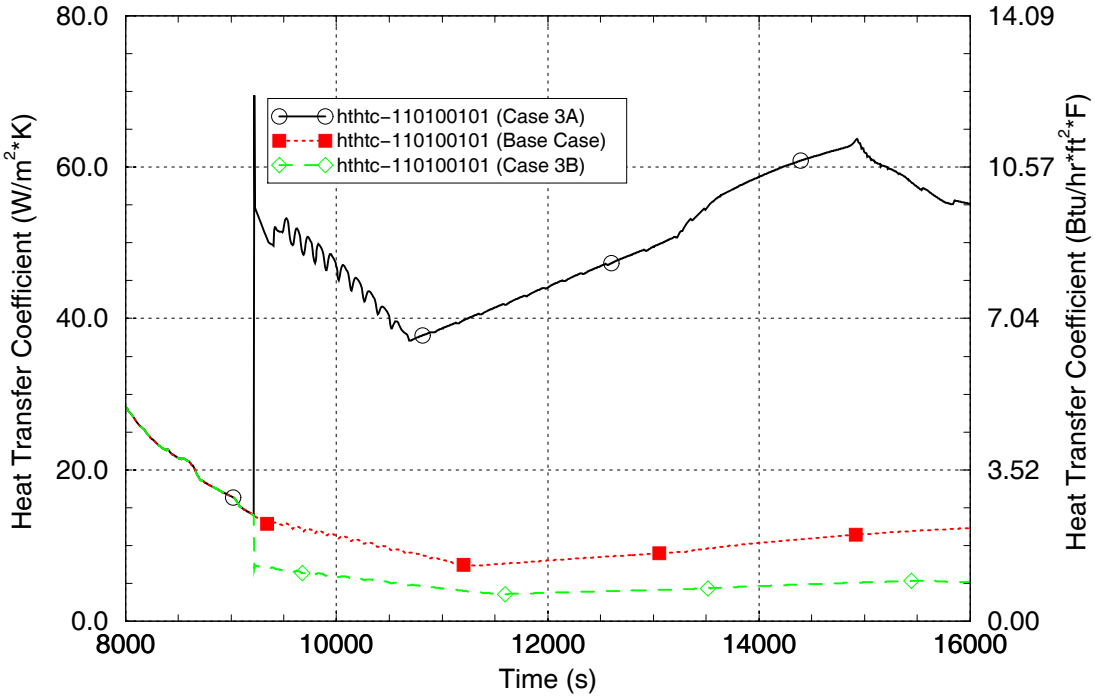

Figure 42. SG 1 Hot Average Tube Outer Surface Heat Transfer Coefficients for the Tube Outer Wall Heat Transfer Sensitivity Cases.

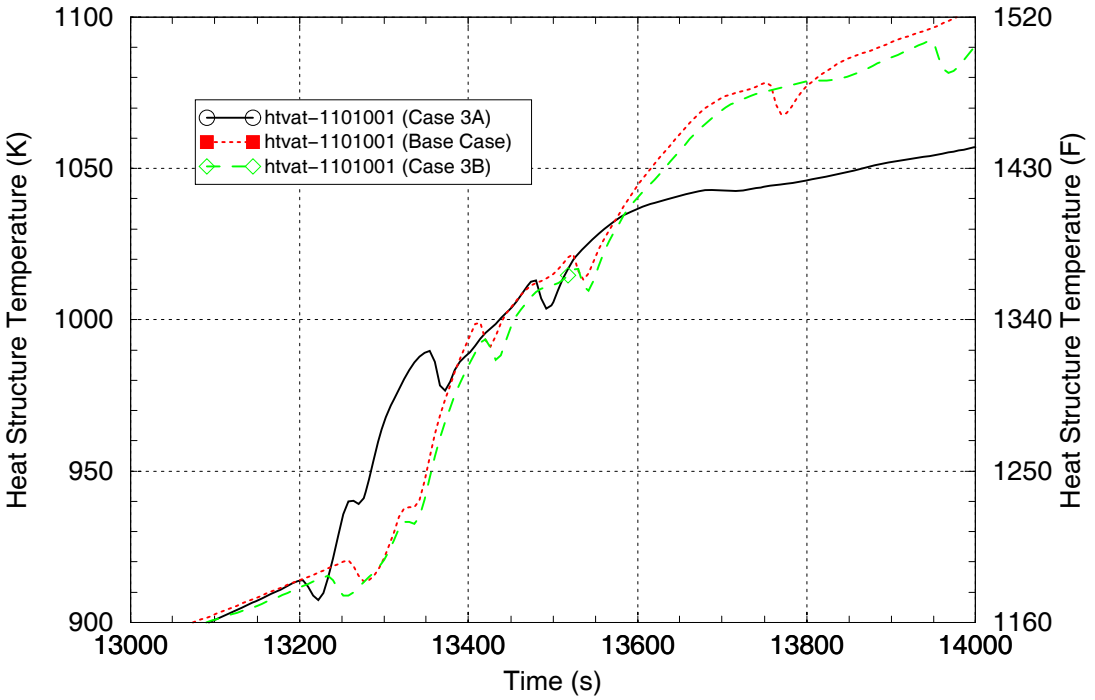

Figure 43. SG 1 Hot Average Tube Wall Temperatures for the Tube Outer Wall Heat Transfer Sensitivity Cases.

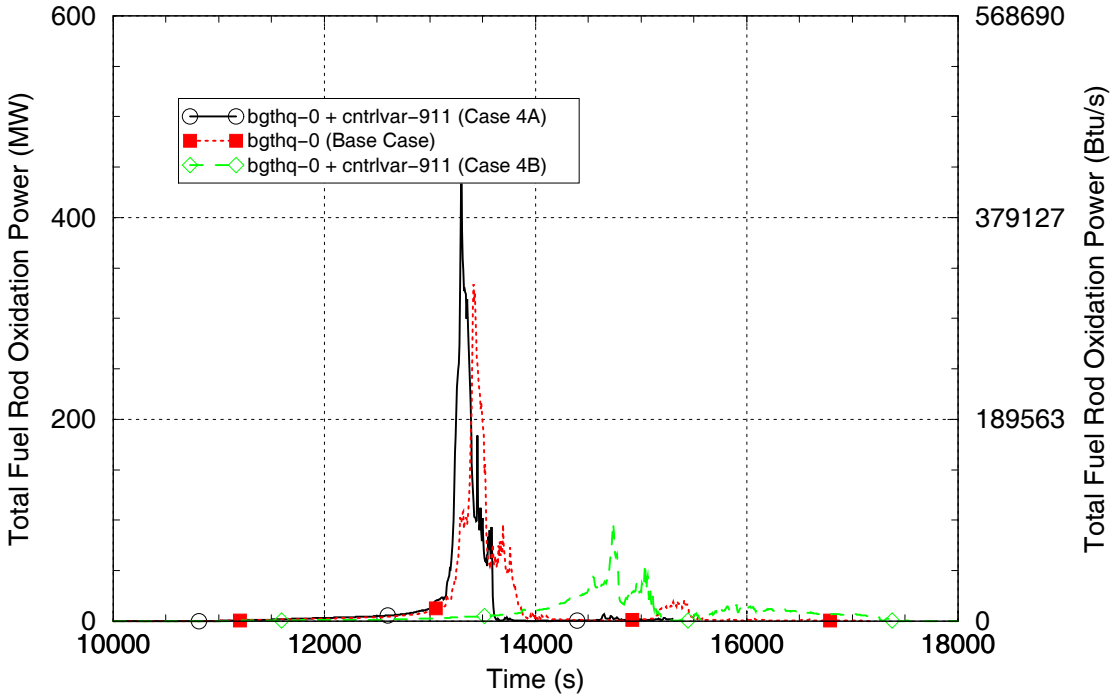

Figure 44. Fuel Rod Cladding Oxidation Powers for the Oxidation Sensitivity Cases.

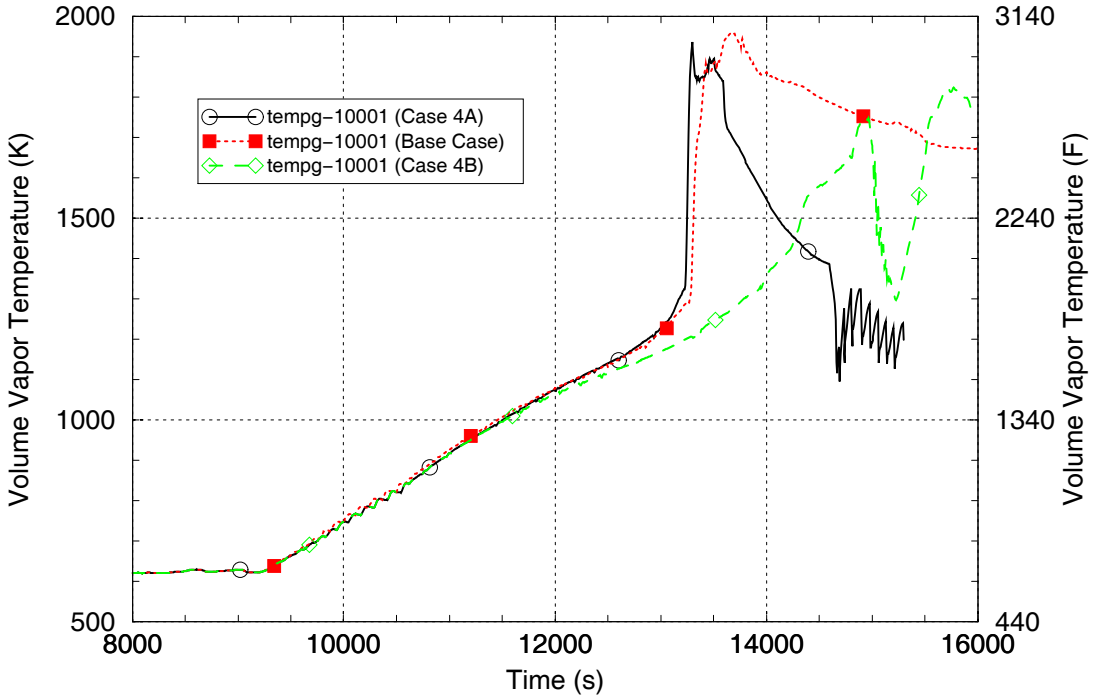

Figure 45. Hot Leg 1 Upper Section Fluid Temperatures for the Oxidation Sensitivity Cases.

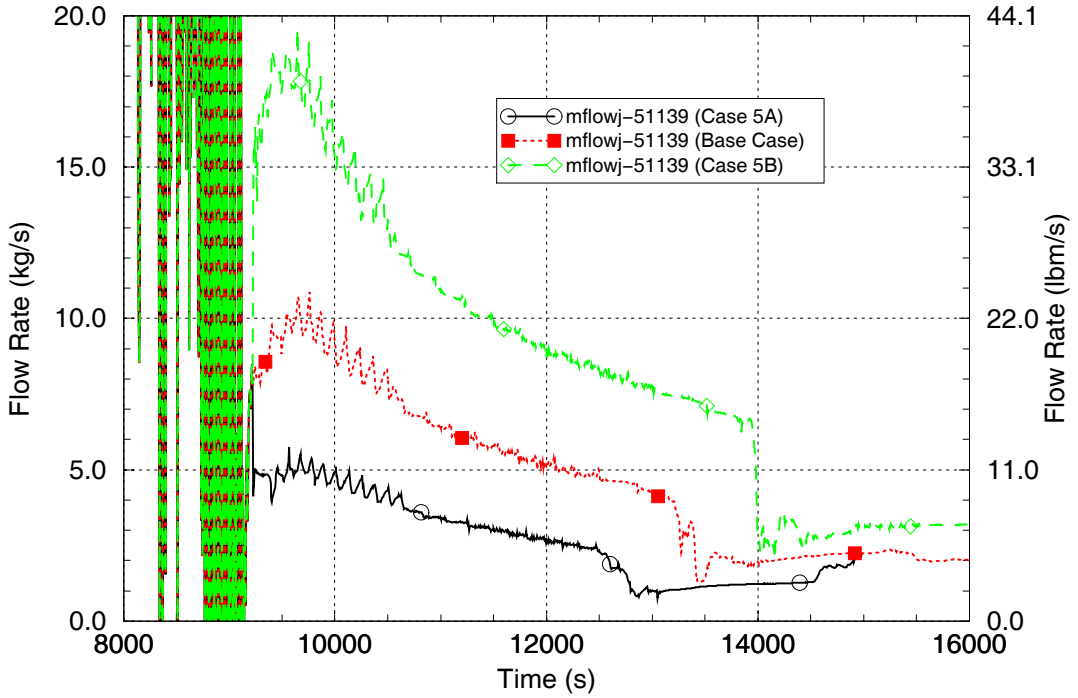

Figure 46. Flow Rates at Top of Central Core Region for the Vessel Circulation Sensitivity Cases.

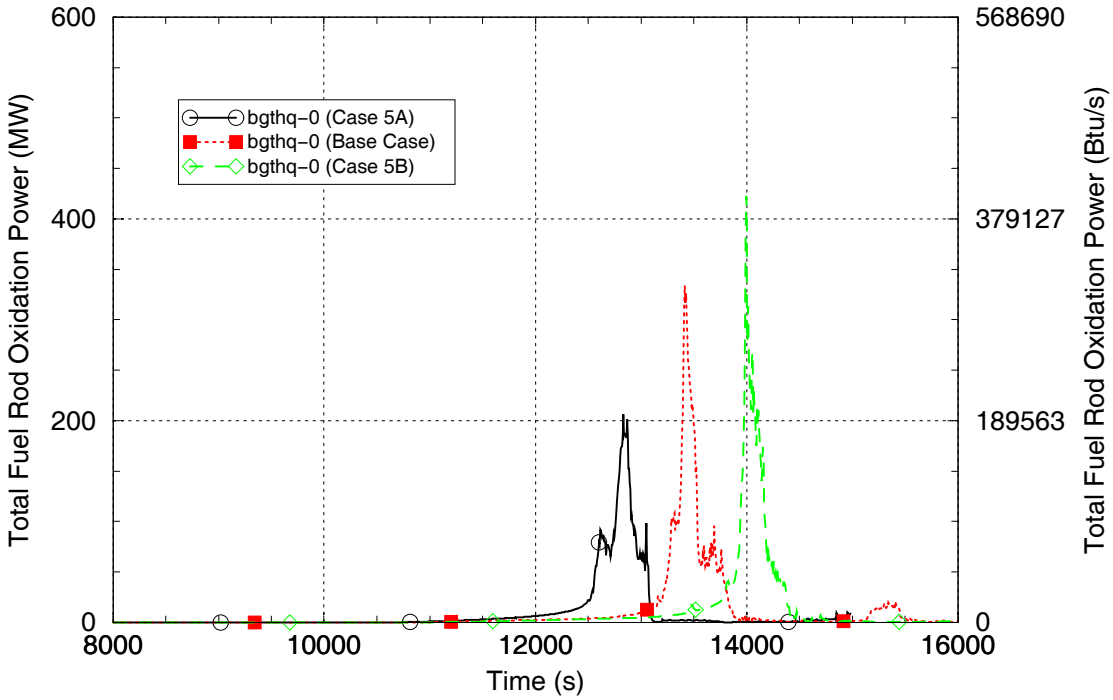

Figure 47. Total Fuel Rod Cladding Oxidation Power for the Vessel Circulation Sensitivity Cases.

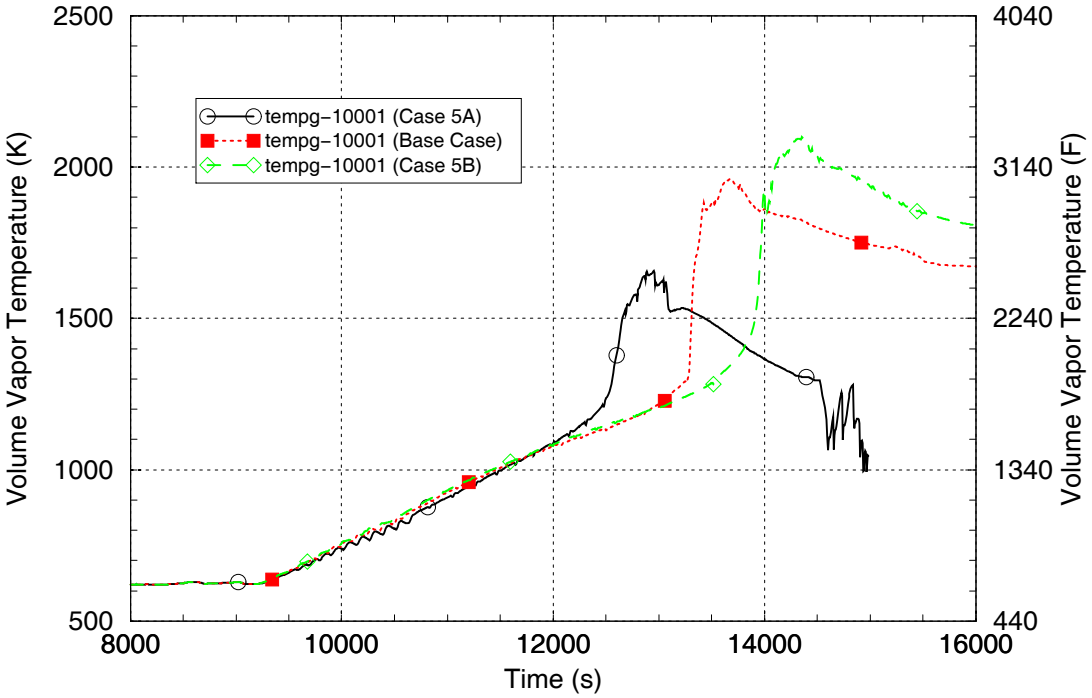

Figure 48. Hot Leg 1 Upper Section Fluid Temperatures for the Vessel Circulation Sensitivity Cases.

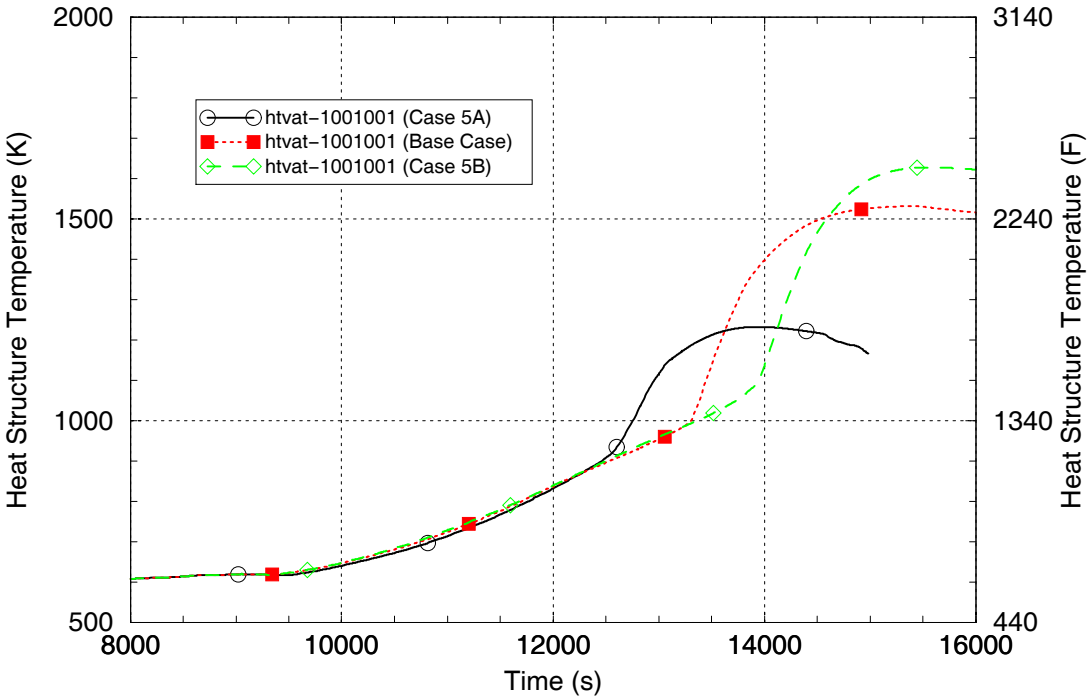

Figure 49. Hot Leg 1 Upper Section Average Wall Temperatures for the Vessel Circulation Sensitivity Cases.

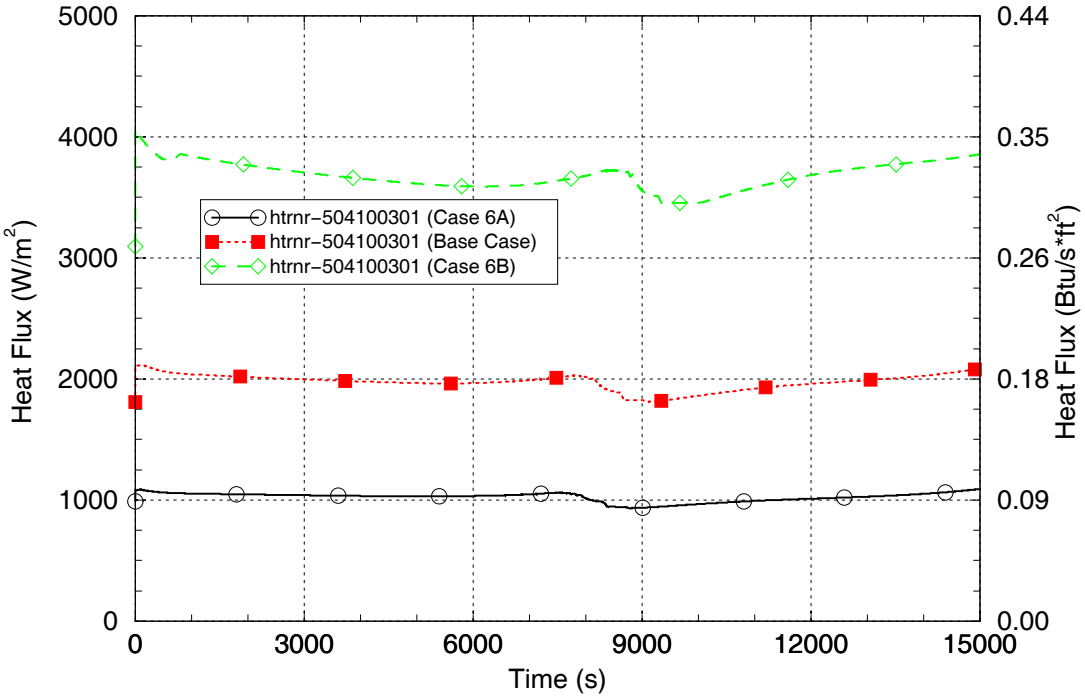

Figure 50. Heat Fluxes from Outer Surface of Reactor Vessel to Containment for the RCS Heat Loss Sensitivity Cases.

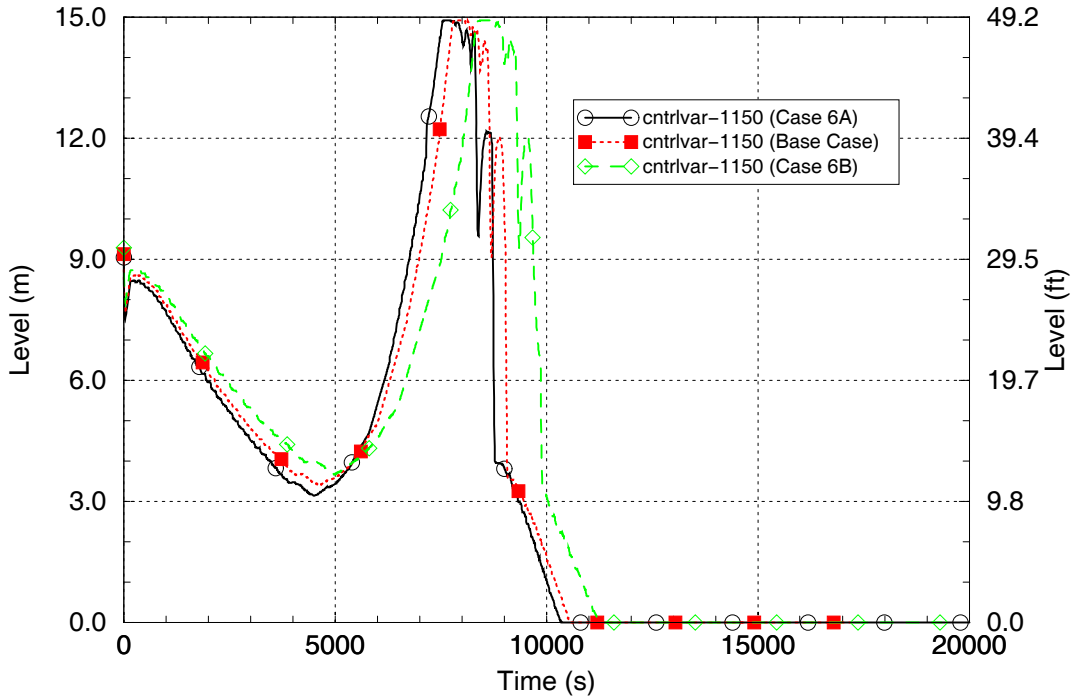

Figure 51. Pressurizer Level Responses for the RCS Heat Loss Sensitivity Cases.

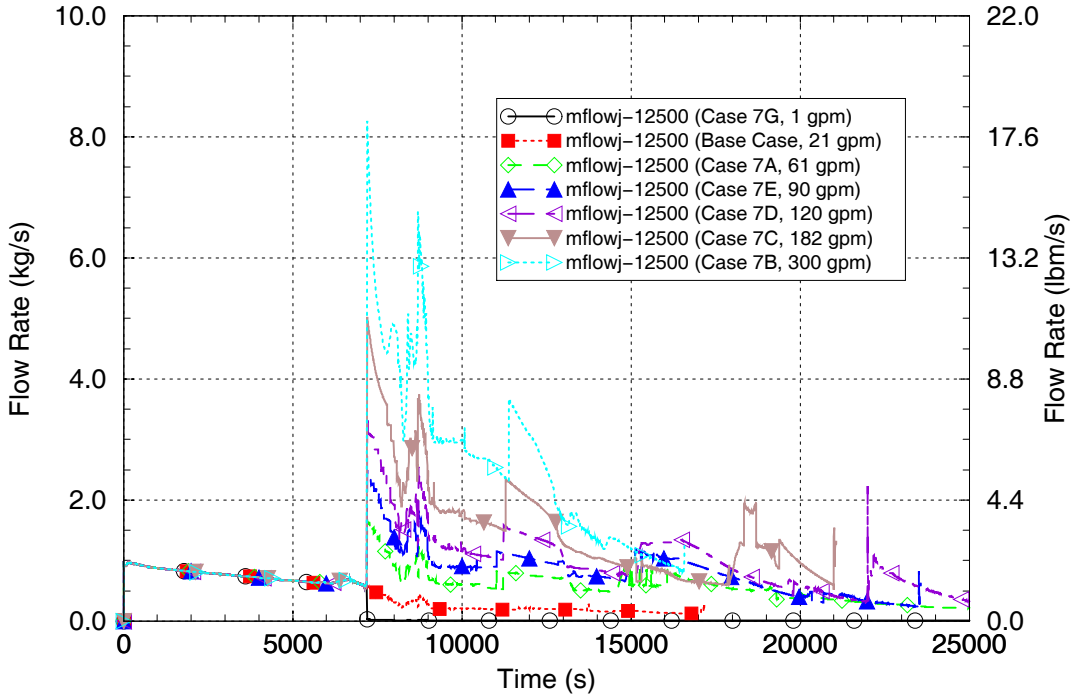

Figure 52. Pump 1 Leakage Rates for the Symmetric Pump Shaft Seal Leak Sensitivity Cases.

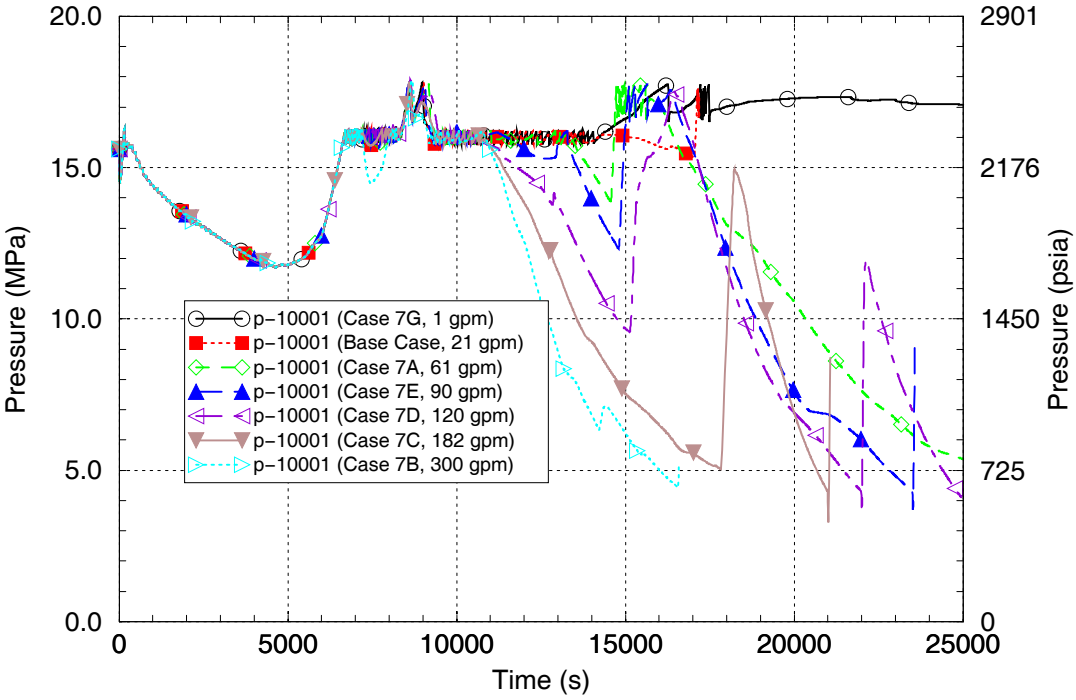

Figure 53. RCS Pressures for the Symmetric Pump Shaft Seal Leak Sensitivity Cases.

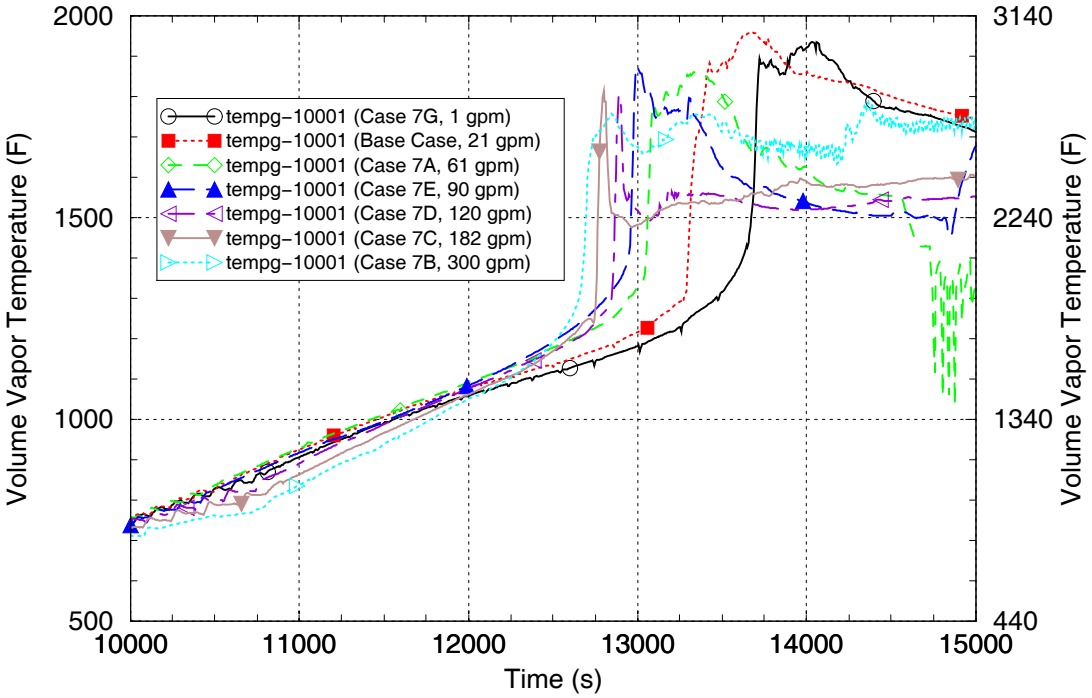

Figure 54. Hot Leg 1 Fluid Temperatures for the Symmetric Pump Shaft Seal Leak Sensitivity Cases.

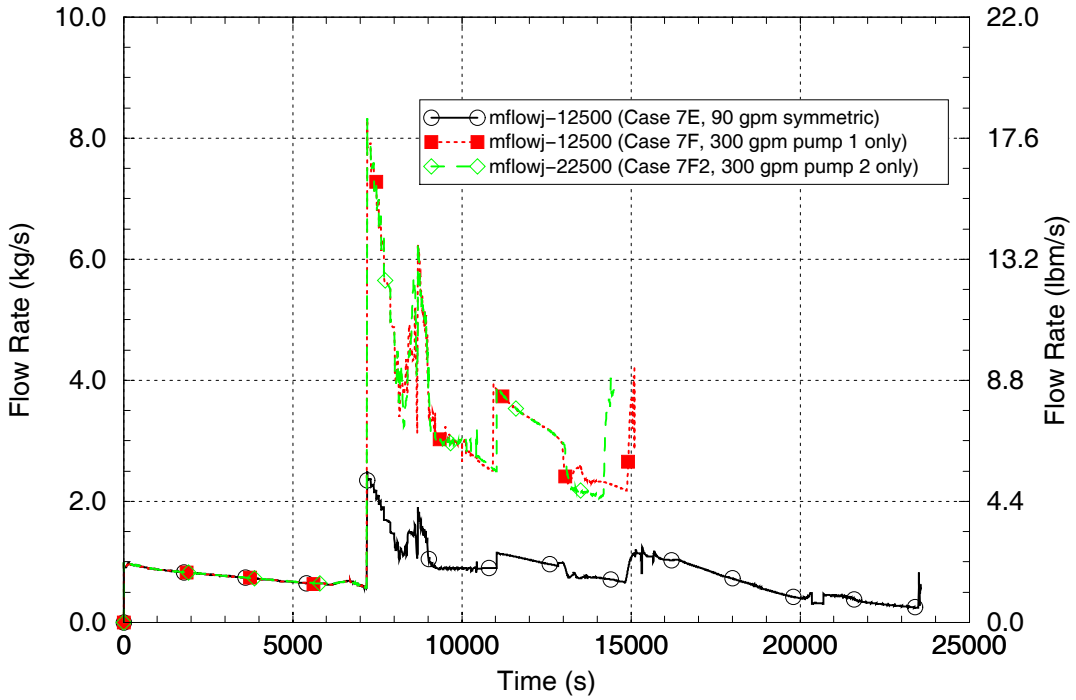

Figure 55. Single-Pump Leakage Rates for the Unsymmetrical Pump Shaft Seal Leak Sensitivity Cases.

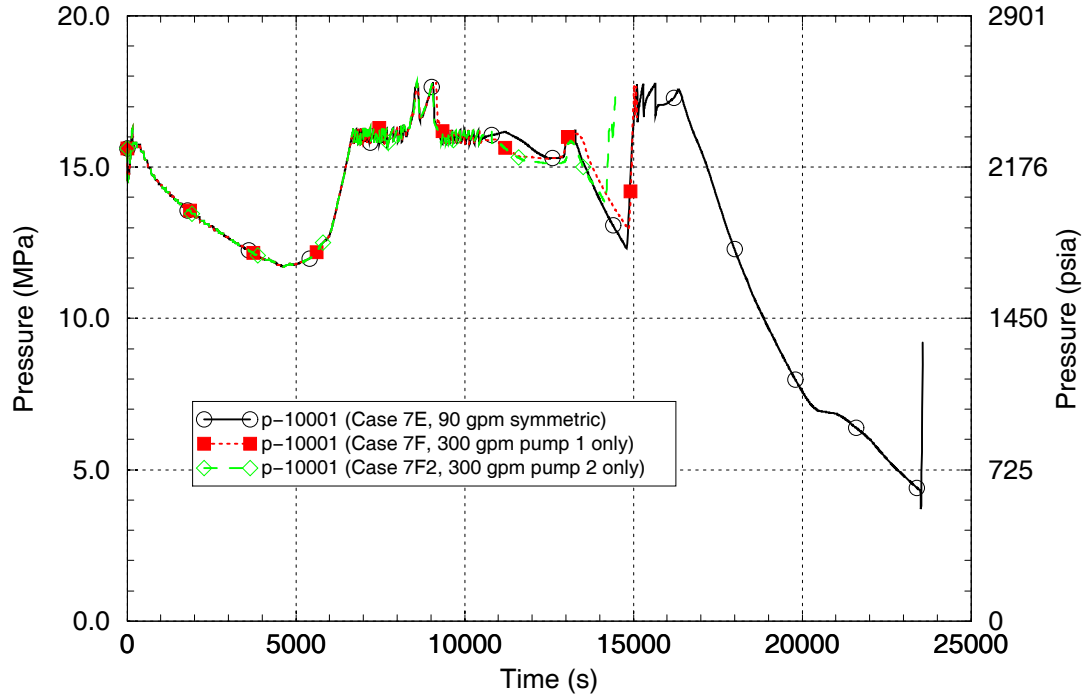

Figure 56. RCS Pressures for the Unsymmetrical Pump Shaft Seal Leak Sensitivity Cases.

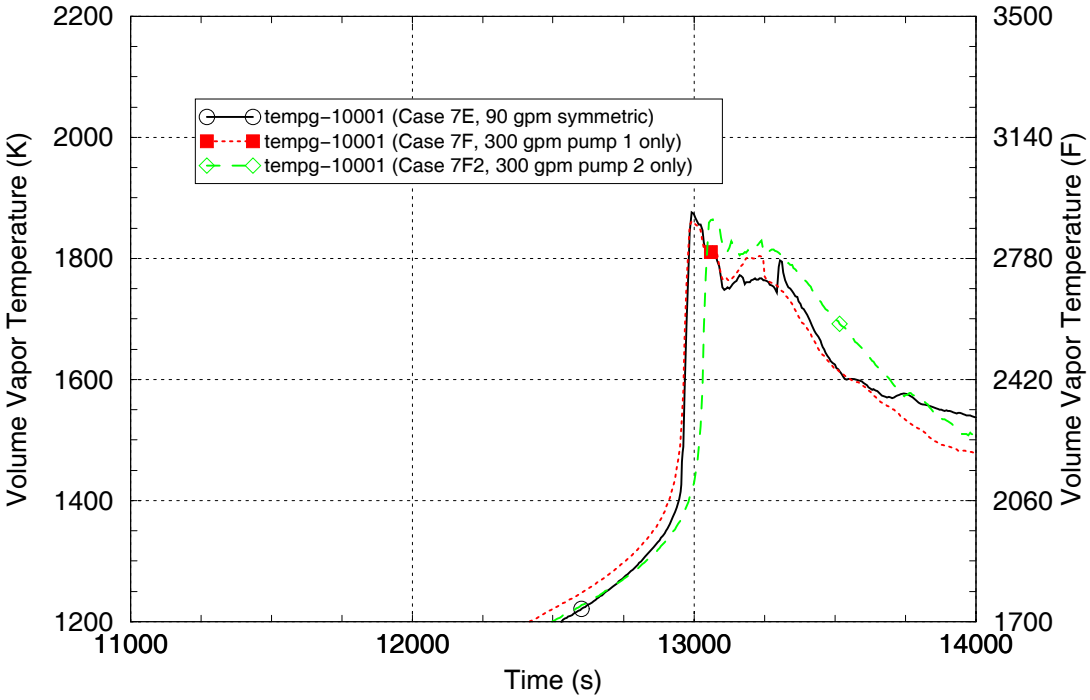

Figure 57. Hot Leg 1 Fluid Temperatures for the Unsymmetrical Pump Shaft Seal Leak Sensitivity Cases.

6.2 Additional Sensitivity Runs

Twelve additional sensitivity runs identified in Table 8 are used to investigate various modeling, plant configuration and sequence event assumption issues unrelated to the uncertainty analysis.

With the exception of runs made specifically to evaluate the effect of variations in the SG inlet plenum mixing and flow parameters, the sensitivity runs were generally performed with the SG inlet plenum region flow coefficients readjusted to retain agreement between the calculated and target mixing and flow parameters specified for the base case. Table 12 compares the SCDAP/RELAP5-calculated mixing and flow parameters for six of the additional sensitivity runs with the base case calculation and target values (Table 9 shows the calculated data for the other six additional sensitivity calculations which are related to pump seal leakage).

For comparison purposes only, the output from the additional twelve sensitivity calculations that would be used for development of uncertainty estimates (if these runs were used for that purpose) is shown in Tables 10, 11, 13 and 14.

The results for the six additional sensitivity runs related to pump seal leakage are summarized in Section 6.1; the results for the remaining six sensitivity runs are summarized as follows:

Effect of Configuration of the Hot Leg-to-Surge Line Connection

The base case calculation models the surge line connection on the side of the Loop 1 hot leg, consistent with an actual Westinghouse plant configuration. A sensitivity run, Case 8A, was performed with the surge line connection moved from the side to the top of the Loop 1 hot leg. This run was made to evaluate the behavior for a top-mounted surge line, which is the configuration in some plants of Westinghouse design.

Figure 58 compares the pressurizer surge line fluid temperatures (near the hot leg connection) from Case 8A (with the top-mounted surge line) and the base case (with the side mounted surge line). The figure shows that, as expected, the surge line temperatures are higher when the surge line is connected on the top of the hot leg.

In the base case the hot leg failed first, at 13,630 s, followed by the surge line at 13,960 s. In Case 8A, the surge line failed first, at 13,660 s, followed by the hot leg at 13,720 s. Although the time of the first primary piping component is about the same in the two runs, the extra energy removed from the RCS through the pressurizer relief valves as a result of the hotter surge line flow in Case 8A reduced the heat up rate of the rest of the system, including the SGs. As a result, the average SG tube failure margin increased slightly from a stress multiplier of 2.10 in the base case run to 2.33 in Case 8A. Therefore, the consideration of the surge line connection location on the circumference of the hot leg has an effect on the SG tube failure margin, but it is not large.

Effect of Stuck-Open Steam Generator Relief Valve

The base case calculation models nominal steam leakage from the secondary systems of all four SGs but no stuck-open relief valve on any SG. A sensitivity run, Case 8B, was performed assuming a secondary system PORV in SG 1 sticks open (at the time of its first opening) but that no steam leakage exists from the other three SGs. This case was run for historical comparison purposes, as its assumptions are consistent with those in prior analyses of SBO in Westinghouse plants (as reported in References 3 through 6, Reference 8 and Reference 9).

The SG secondary pressure responses for Case 8B and the base case are compared in Figure 59 for SG 1 and Figure 60 for SG 2. The SG 1 pressures experienced at the time when the hot leg failure occurs (14,060 s in Case 8B and 13,630 s in the base case) are not significantly different between the two runs.

Figure 61 compares the Hot Leg 1 upper section fluid temperatures (near the reactor vessel) for Case 8B and the base case. The different SG secondary pressure responses lead to a event timing difference between the two runs, however the heat up rates at the time when hot leg failure is encountered are very similar.

Since the temperature and pressure responses of the two runs are similar, little difference is noted in the average SG 1 tube failure margins. The failure margin decreased only slightly from a stress multiplier of 2.10 in the base case to 2.05 in Case 8A. This result occurs because the SG 1 steam leakage rate seen in the base case is sufficient to fully depressurize all of the SGs before the maximum system heat up rate is experienced. See "Effect of Varying SG Secondary Leakage Rate" below for considerations related to the assumed size of the steam leakage path.

Effect of Varying the Assumed SG Secondary Leakage

A sensitivity run, Case 8G, was performed to evaluate behavior using different assumptions on the steam leakage rate. For this run, a different steam leakage flow area was used in each of the four SGs. Flow areas representing 80%, 60%, 40% and 20% of the 0.5 in^2 per SG leak flow area assumed in the base case calculation were used in SGs 1 through 4, respectively.

Figure 62 compares the SG secondary pressure responses for the SGs from Case 8G with 0.1, 0.2, 0.3, and 0.4 in^2 leak flow areas in their secondary systems with the base case SG 1 pressure, which was calculated using the 0.5-in^2 leak flow area. As expected the SG depressurization rate is proportional to the size of the assumed leak flow area.

The average SG tube failure margin in the base case indicated that a 2.10 stress multiplier is needed for the tube to fail coincident with the hot leg. That indication is based on the response in SG 1 and a 0.5 in^2 leak flow area. The tube failure margins indicated by the behavior of the other SGs with 0.5 in^2 leak flow areas in the base case were slightly different. The tube failure margins indicated by the results from Case 8G and the base case are summarized in Table 15. The results indicate that the SG tube failure margins increase gradually as the leak flow area is decreased from 0.5 in^2 to 0.3 in^2, and then increase significantly faster as the flow area falls below 0.3 in^2.

Surge Line and Hot Leg Wall Inside Surface Heat Transfer Coefficient Variation

A sensitivity run, Case 8D, was performed to simulate increased heat transfer from the fluid to the inside surfaces of the surge line and hot leg upper section walls. A multiplier of 2.0 was placed on the heat transfer coefficients employed in the base case for the combination of convection and steam-to-wall radiation heat transfer. No change was made in the hot leg wall-to-wall radiation heat transfer modeling.

Figure 63 compares the heat transfer coefficient on the inside surface of the upper section of Hot Leg 1 (near the reactor vessel) for Case 8D and the base case. The increase in the heat transfer coefficient in Case 8D is as expected at this representative location. The heat transfer coefficient comparisons at other locations within the upper hot leg sections and the pressurizer surge line are similar.

The heat transfer modeling revisions in Case 8D are seen to result in a moderate increase in the SG average tube failure margins. Stress multipliers of 2.96 and 2.10, respectively, are needed for average tube failure to occur coincident with the hot leg using the increased and nominal hot leg and pressurizer surge line heat transfer coefficients.

This margin improvement results because the increased heat transfer coefficient leads to faster heat up of the hot leg wall (and earlier hot leg failure) and slower heat up of the SG tubes (and later SG tube failure). Figure 64 compares the Hot Leg 1 upper section wall temperatures for the two cases and Figure 65 compares the SG 1 hot average tube wall temperatures for the two cases.

Tubesheet Wall Inside Surface Heat Transfer Coefficient Variation

A sensitivity run, Case 8E, was performed to simulate increased heat transfer from the fluid to the SG tubesheet structures. A multiplier of 2.0 was placed on the heat transfer coefficients employed in the base case for the combination of convection and steam-to-wall radiation heat transfer.

Figure 66 compares the heat transfer coefficient on the SG 1 tubesheet (near the SG inlet plenum) for Case 8E and the base case. The increase in the heat transfer coefficient in Case 8E is as expected at this representative location. The heat transfer coefficient comparisons at other tubesheet locations are similar.

The heat transfer modeling revisions in Case 8E are seen to result in a small increase in the SG average tube failure margins. Stress multipliers of 2.20 and 2.10, respectively, are needed for average tube failure to occur coincident with the hot leg using the increased and nominal tubesheet heat transfer coefficients.

This margin improvement results because the increased heat transfer coefficient leads to a faster heat up of the tubesheet wall and a slower heat up of the SG tubes (and later SG tube failure). Figure 67 compares the SG 1 tubesheet wall temperatures for the two cases and Figure 68 compares the SG 1 hot average tube wall temperatures for the two cases.

Effect of Pre-Existing Steam Generator Tube Leakage

The base case calculation assumes no SG tube leakage exists. A sensitivity run, Case 8C, is performed assuming that a tube leakage path with an initial flow rate of 100 gpm in SG 1 exists at the start of the station blackout event sequence. The leak is assumed to be located midway between the tubesheet and the top of the U-bend, in the hot average tube. To implement the tube leakage into the model, Valve 140 with a flow area of 0.0006428 ft^2 is added to the model at the start of the transient event sequence calculation. This flow area represents a circular hole with a diameter of 0.343 in; therefore the leak flow area is less than the equivalent flow area through one SG tube.

The SG 1 inlet plenum flow losses were adjusted to attain the following revised set of target values for the mixing and flow parameters: hot leg discharge coefficient 0.14 (versus 0.12 in the base case), recirculation ratio 1.75 (versus 2.0 in the base case) and hot and cold mixing fractions 0.75 (versus 0.85 in the base case). These revised target values resulted from CFD evaluations of the fluid conditions expected in a coolant loop with a leaking SG tube. No changes were made to the SG inlet plenum flow losses in the other three SGs.

The results from Case 8C are compared with the base case results in Tables 12 through 14 and Figures 69 through 73.

The tube leakage mass flow rate is shown in Figure 69. The flow rate generally declines as the leakage changes from water at the beginning of the event sequence to saturated steam and then to superheated steam. Table 12 shows that the agreements between the calculated and revised Case 8C target values for the SG 1 mixing and flow parameters described above are acceptable.

Table 13 shows that, relative to the base case, the results for Case 8C indicate improved SG tube failure margins for both the hottest tube in SG 1 and the average tube in SG 1. The hottest SG 1 tube fails 2,235 s after the hot leg fails in Case 8C, while in the base case it failed 155 s earlier than the hot leg. The SG 1 average tube stress multiplier required for tube failure coincident with hot leg failure rose from 2.10 in the base case to 2.94 in Case 8C as a result of the relative changes in the hot leg and SG 1 average tube failure times.

Figures 70 and 71, respectively, compare the Hot Leg 1 upper section and SG 1 average tube wall temperatures from the two runs. From the base case calculation to the Case 8C calculation, comparable changes are seen in the times when the hot leg and tube temperatures rise rapidly. Therefore, the improved SG tube failure margins in Case 8C do not result from changes in the relative timing of structure heat-up.

Figures 72 and 73, respectively, compare the Hot Leg 1 and SG 1 secondary pressures from the two runs. On the primary side, the tube leakage leads to moderately more depressurization than seen in the base case. Less frequent pressurizer PORV opening is seen in Case 8C, however the peak RCS pressures and the behavior of the RCS pressure during the period when structure failures occur are nearly the same for the two cases. On the SG 1 secondary side, the tube leakage causes the pressure to be significantly higher in Case 8C than in the base case. The

differential pressure from primary to secondary in Case 8C is therefore much less than seen in the base case, and this is the explanation for the increased SG 1 failure margins for the hottest and average tubes.

The tube failure margin improvements for the SG 1 tubes are not shared by the tubes in the other three SGs. The tube leakage in SG 1 does not affect the secondary pressures in SGs 2, 3 and 4 and no readjustments of SG inlet plenum flow losses are made in SGs 2, 3 and 4. As a result, for Case 8C the limiting tube failure moves from SG 1 to SG 3. The data in Table 16 show that the increase in the SG 3, 2.0-multiplier average tube failure time from the base case to Case 8C is virtually identical to that seen for the hot leg failure time. Only a small improvement is seen in the limiting average tube failure margin (a stress multiplier for tube failure coincident with hot leg failure of 2.21 for the SG-3 tube in Case 8C, versus 2.10 for the SG-1 tube in the base case). The conclusion is therefore that the effect of pre-existing SG tube leakage in a single SG does not significantly affect the overall outcome of the analysis.

It is noted, however, that the Case 8C event sequence evaluated here does not include rapid depressurization of the SG secondary systems that could result, for example, from a stuck-open relief valve or main steam line break. The analysis results may be different for a case where the pre-existing SG tube leakage resides in a rapidly-depressurizing SG.

Table 12. Comparison of Target and SCDAP/RELAP5-Calculated SG Inlet Plenum Mixing and Flow Parameters for Sensitivity Cases Addressing Issues Other than Uncertainty Analysis.

Case Number and Time Evaluated	Loop 1 Hot Leg C_D	SG 1 Recirculation Ratio	SG 1 Hot Mixing Fraction	SG 1 Cold Mixing Fraction	SG 1 Power Fraction
Base Case, Target	0.12	2.0	0.85	0.85	None
Base Case, 13,000 s	0.120	1.990	0.853	0.848	0.07143
Case 8A, 13,000 s	0.120	1.985	0.853	0.848	0.07107
Case 8B, 13,000 s	0.120	1.961	0.852	0.847	0.06730
Case 8C, 12,000 s*	0.142	1.742	0.744	0.731	0.08278
Case 8D, 13,000 s	0.120	1.977	0.853	0.848	0.06986
Case 8E, 13,000 s	0.120	1.977	0.853	0.847	0.07204
Case 8G 13,000 s	0.120	1.980	0.854	0.848	0.07141

* Note that different target values are used for this case, see text.

Table 13. Comparison of SCDAP/RELAP5-Calculated Results for Failure Times and Margins for Sensitivity Cases Addressing Issues Other than Uncertainty Analysis.

Case Number	First Primary Failure Component	First Primary Failure Time (s)	SG 1 Hottest Tube with 1.0 Multiplier Failure Time – First Primary Failure Time (s)	SG 1 Average Tube Stress Multiplier for Tube Failure Coincident with First Primary Failure
Base Case	Hot Leg 1	13,630	-155	2.10
Case 8A	Hot Leg 1	13,660	-75	2.33
Case 8B	Hot Leg 1	14,060	-145	2.05
Case 8C	Hot Leg 1	15,395	2,235*	2.94*
Case 8D	Hot Leg 1	13,495	60	2.96
Case 8E	Hot Leg 1	13,660	-155	2.20
Case 8G	Hot Leg 1	14,090	-155	See Text

* Note that the limiting tube failures for this case are in SG 3, see text.

Table 14. Comparison of SCDAP/RELAP5-Calculated Results for Temperatures and Wall Heat Transfer Coefficients for Sensitivity Cases Addressing Issues Other than Uncertainty Analysis.

Case Number	SG 1 Average Tube Structure Temperature (K)	SG 1 Hottest Tube Structure Temperature (K)	Hot Leg 1 Steam Temperature (K)	Hot Leg 1 Wall HTC (W/m^2-K)	Surge Line Steam Temperature (K)	Surge Line Wall HTC (W/m^2-K)
Base Case	1021.7	1239.6	1776.0	423.13	1373.0	490.86
Case 8A	1000.3	1203.7	1772.2	439.43	1622.7	576.96
Case 8B	1025.5	1237.9	1763.1	430.77	1377.3	564.35
Case 8C	1030.9	1112.4	1728.5	399.37	1097.6	248.54
Case 8D	956.40	1111.2	1759.0	890.63	1347.4	1169.5
Case 8E	1013.9	1240.6	1774.5	423.94	1374.9	507.88
Case 8G	1023.6	1232.2	1737.7	418.36	1354.7	526.31

Table 15. SCDAP/RELAP5-Calculated Results for Case 8G, Evaluating Sensitivity to SG Secondary Steam Leak Flow Area Assumptions.

SG Number	Case	Leak Flow Area (in^2)	Average SG Tube Failure Margin (Stress Multiplier for Tube Failure Coincident with Hot Leg Failure
1	Base	0.5	2.100
1	8G	0.4	2.076
2	Base	0.5	2.150
2	8G	0.3	2.303
3	Base	0.5	2.133
3	8G	0.2	2.679
4	Base	0.5	2.150
4	8G	0.1	2.909

Table 16. Comparison of Failure Time Data from the Case 8C and Base Case Runs.

Component	Failure Time in the Base Case (s)	Failure Time in Case 8C (s)	Change in Failure Time from the Base Case to Case 8C (s)
Hot Leg 1	13,630	15,395	1,765
Surge Line	13,960	18,875	4,915
SG 1 Hottest Tube, 1.0 Multiplier	13,475	17,630	4,155
SG 1 Average Tube, 2.0 Multiplier	13,660	16,140	2,480
SG 3 Average Tube, 2.0 Multiplier	13,670	15,420	1,760

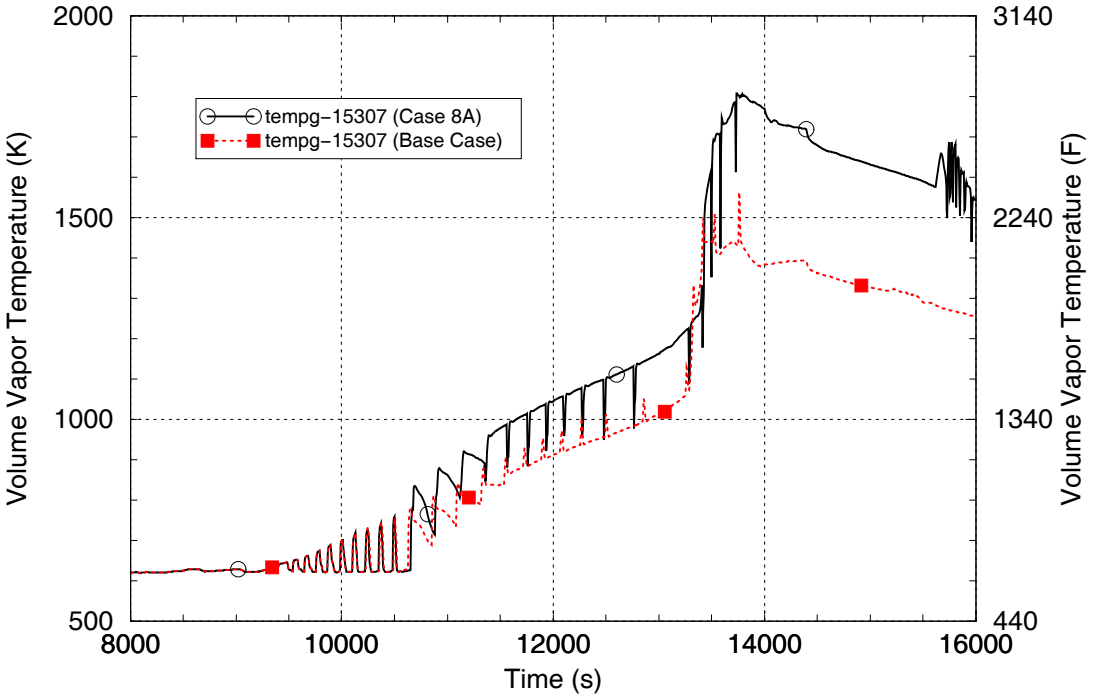

Figure 58. Pressurizer Surge Line Fluid Temperature for the Top Mounted Surge Line Sensitivity Case.

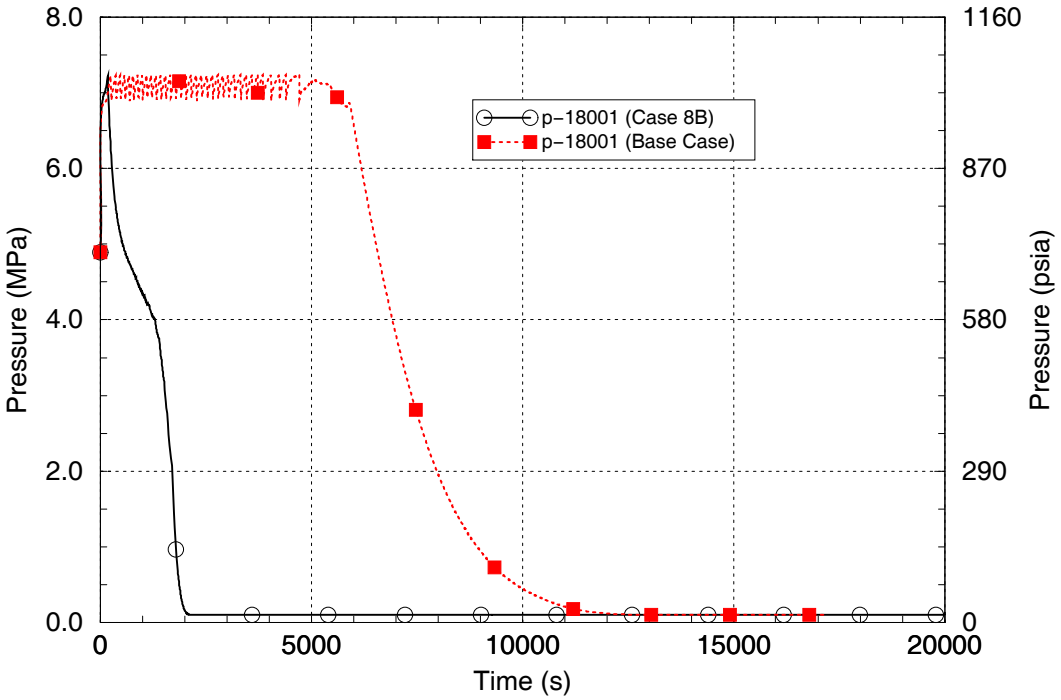

Figure 59. SG 1 Pressure for the Stuck-Open SG Safety Relief Valve Sensitivity Case.

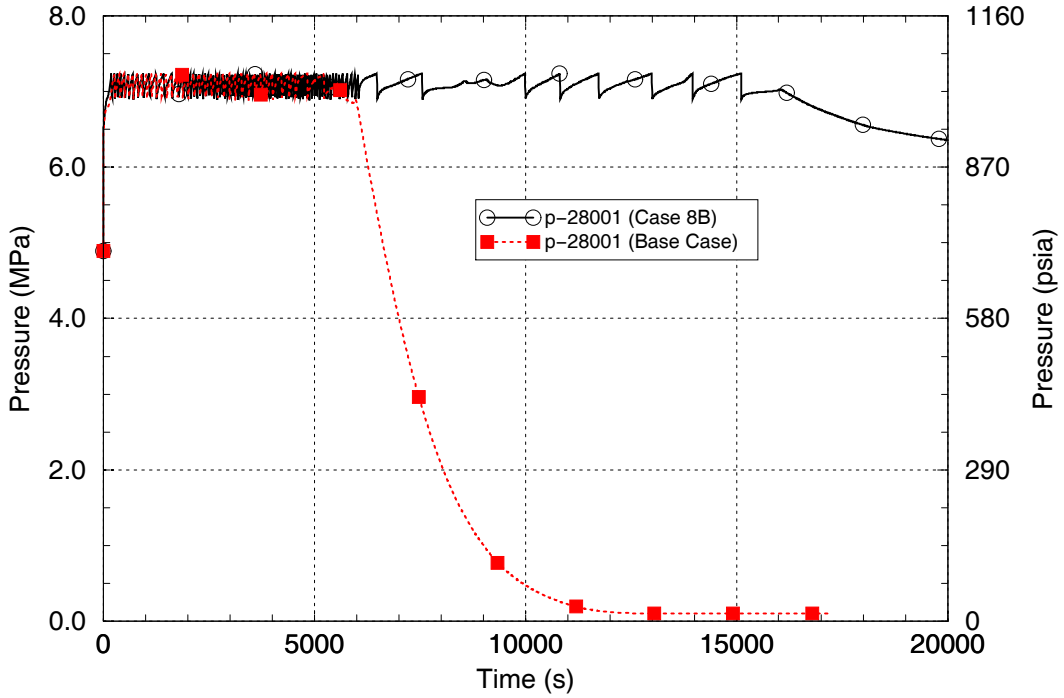

Figure 60. SG 2 Pressure for the Stuck-Open SG Safety Relief Valve Sensitivity Case.

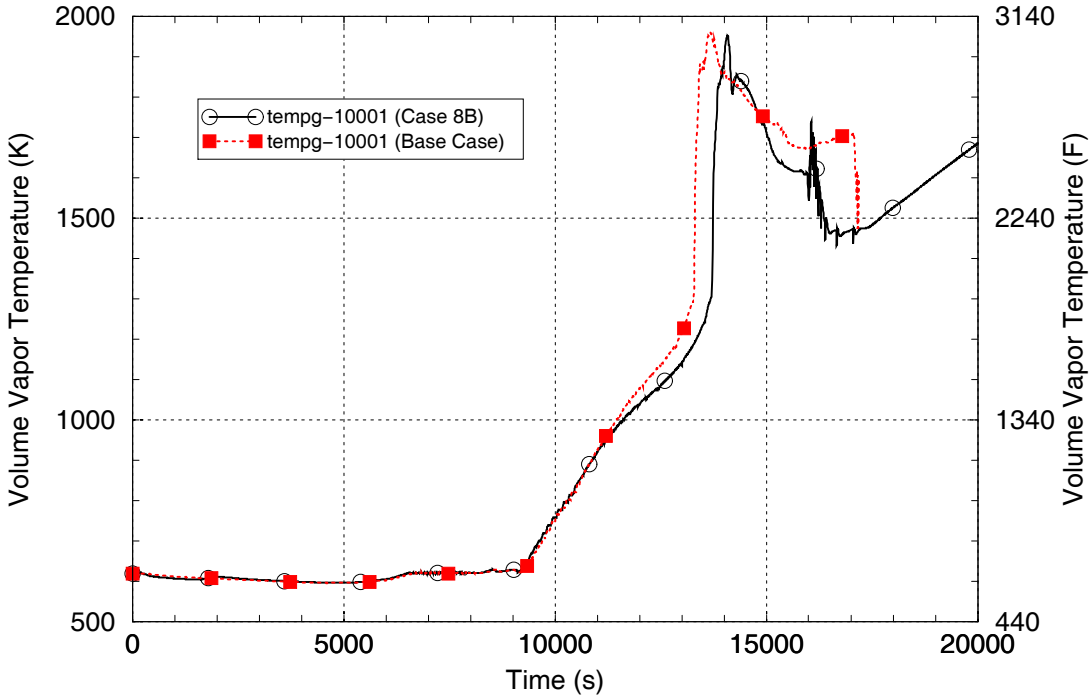

Figure 61. Hot Leg 1 Fluid Temperature for the Stuck-Open SG Safety Relief Valve Sensitivity Case.

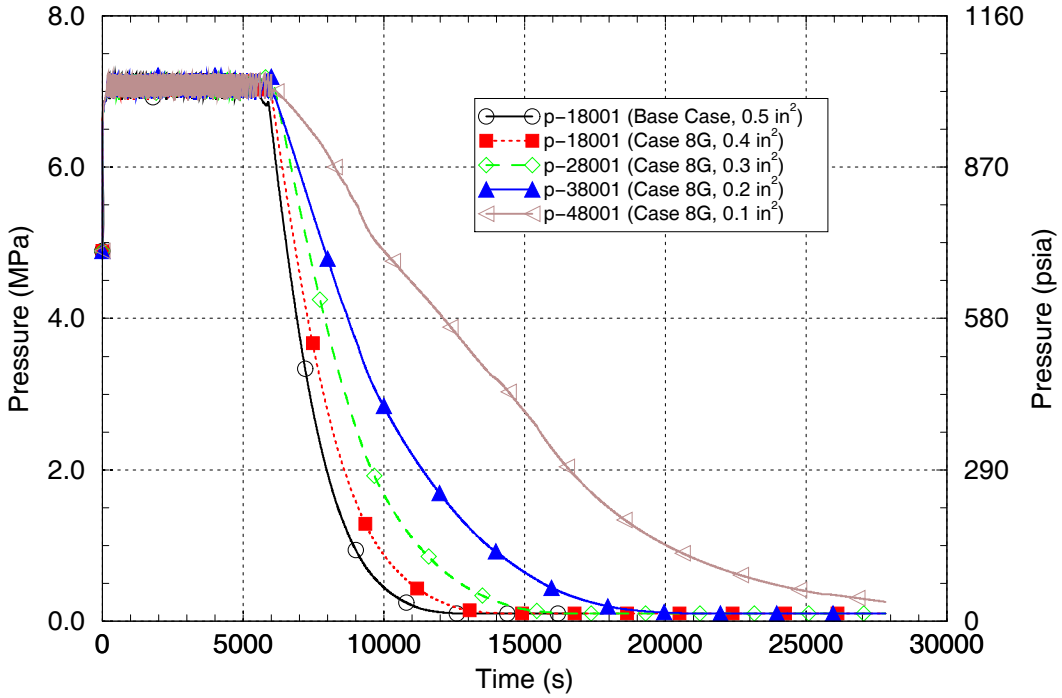

Figure 62. SG Secondary Pressures for the SG Secondary Leakage Sensitivity Cases.

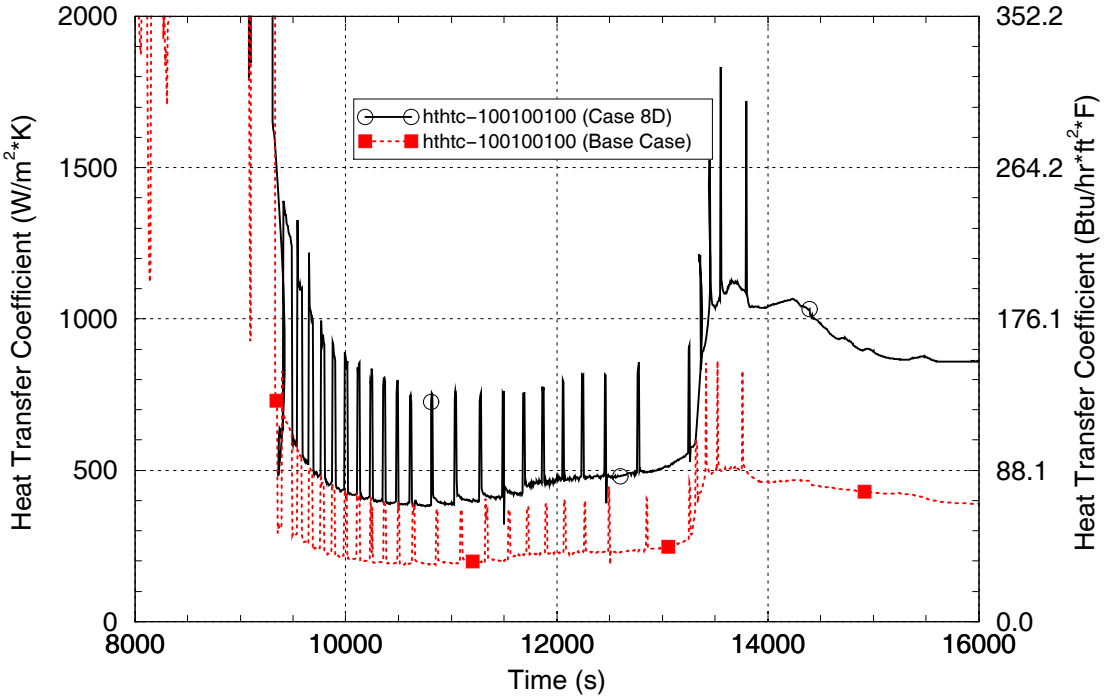

Figure 63. Hot Leg 1 Inside Surface Heat Transfer Coefficient for the Hot Leg and Surge Line Heat Transfer Sensitivity Cases.

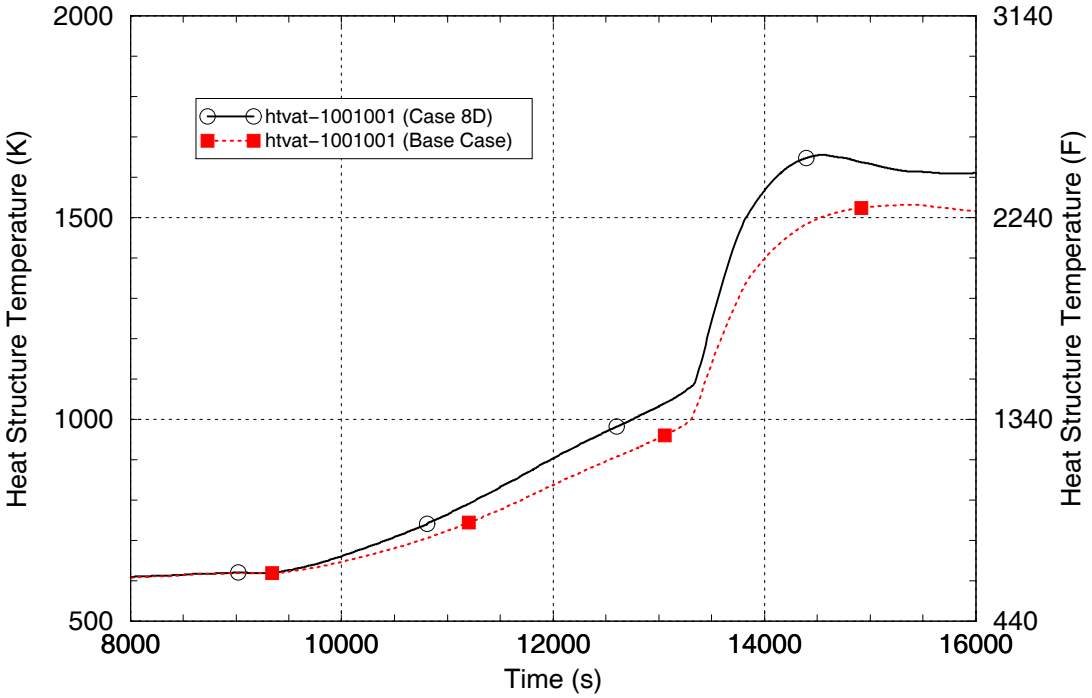

Figure 64. Hot Leg 1 Wall Temperature for the Hot Leg and Surge Line Heat Transfer Sensitivity Cases.

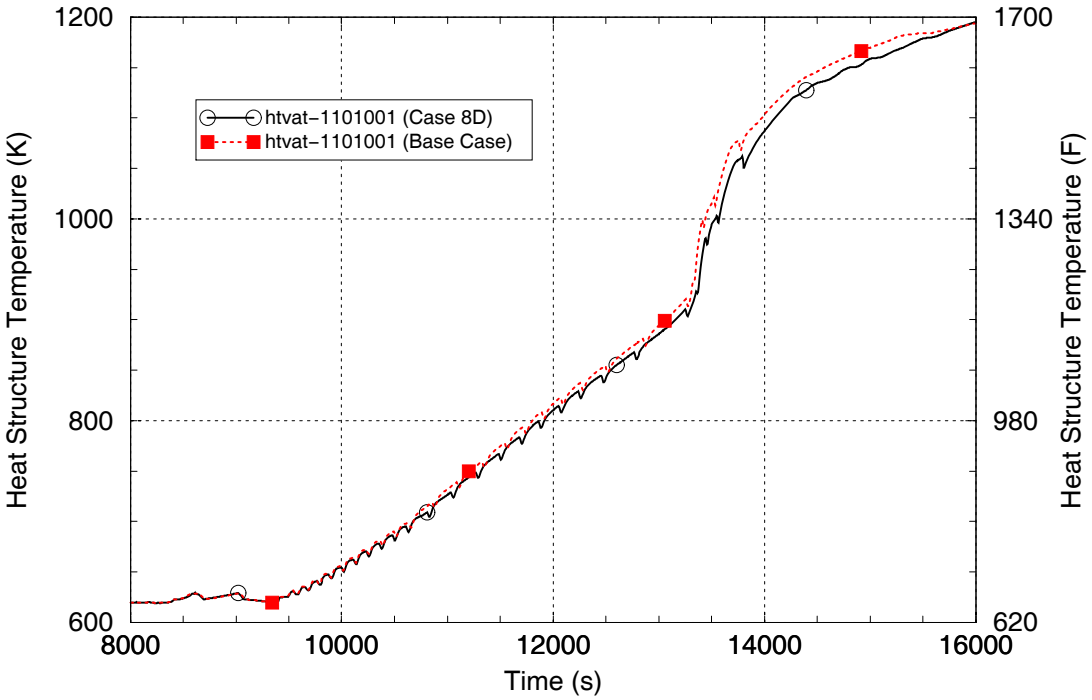

Figure 65. SG 1 Hot Average Tube Wall Temperature for the Hot Leg and Surge Line Heat Transfer Sensitivity Cases.

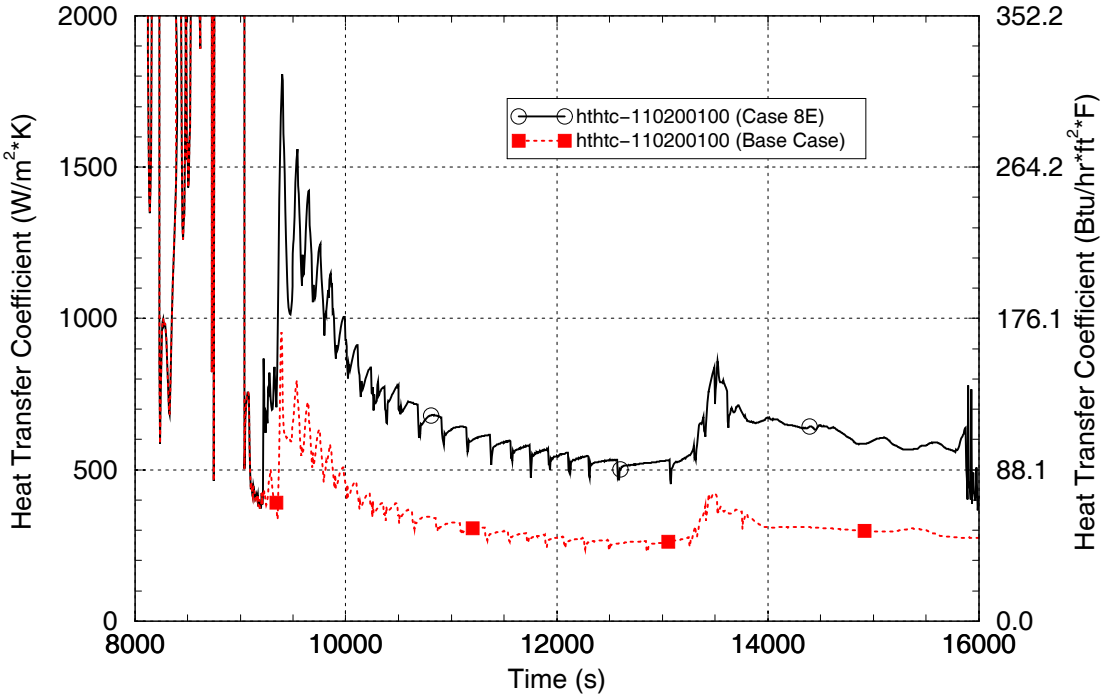

Figure 66. SG 1 Tubesheet Heat Transfer Coefficient for the Tubesheet Heat Transfer Sensitivity Cases.

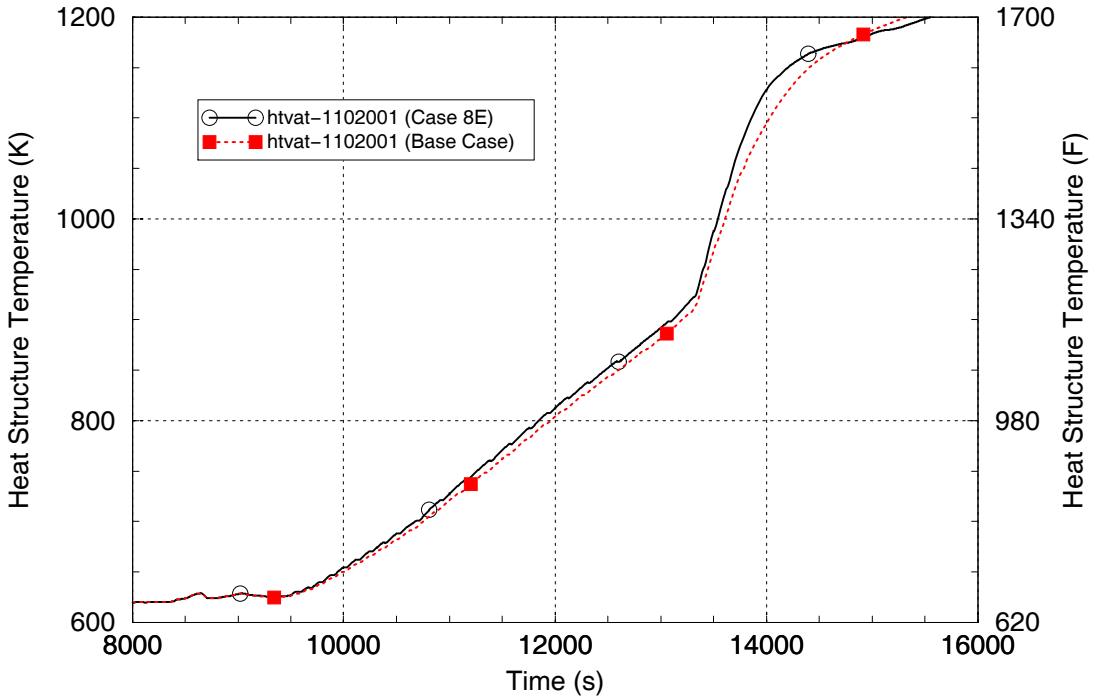

Figure 67. SG 1 Tubesheet Wall Temperature for the Tubesheet Heat Transfer Sensitivity Cases.

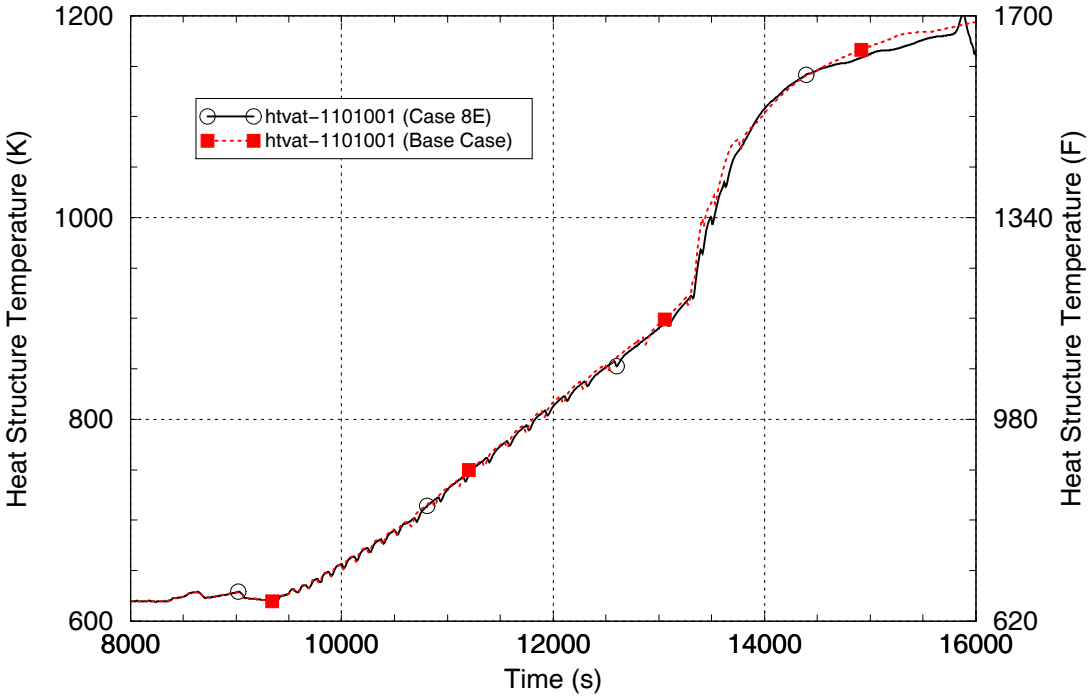

Figure 68. SG 1 Hot Average Tube Wall Temperature for the Tubesheet Heat Transfer Sensitivity Cases.

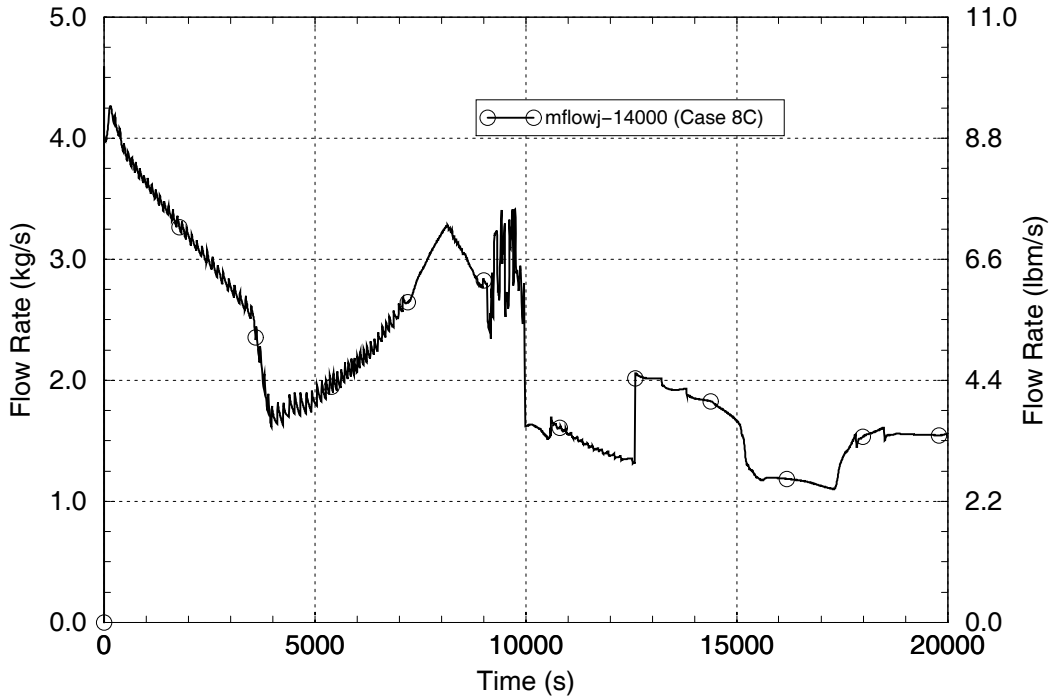

Figure 69. Tube Leak Rate for the SG Tube Leakage Sensitivity Case.

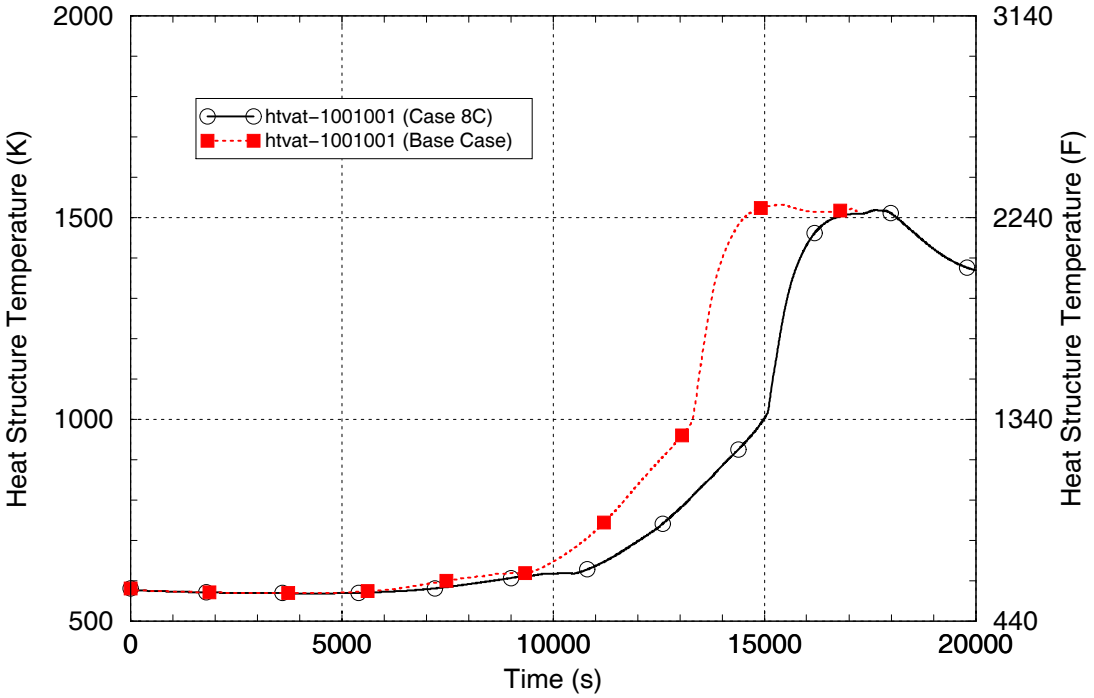

Figure 70. Hot Leg 1 Upper Section Wall Temperature for the SG Tube Leakage Sensitivity Case.

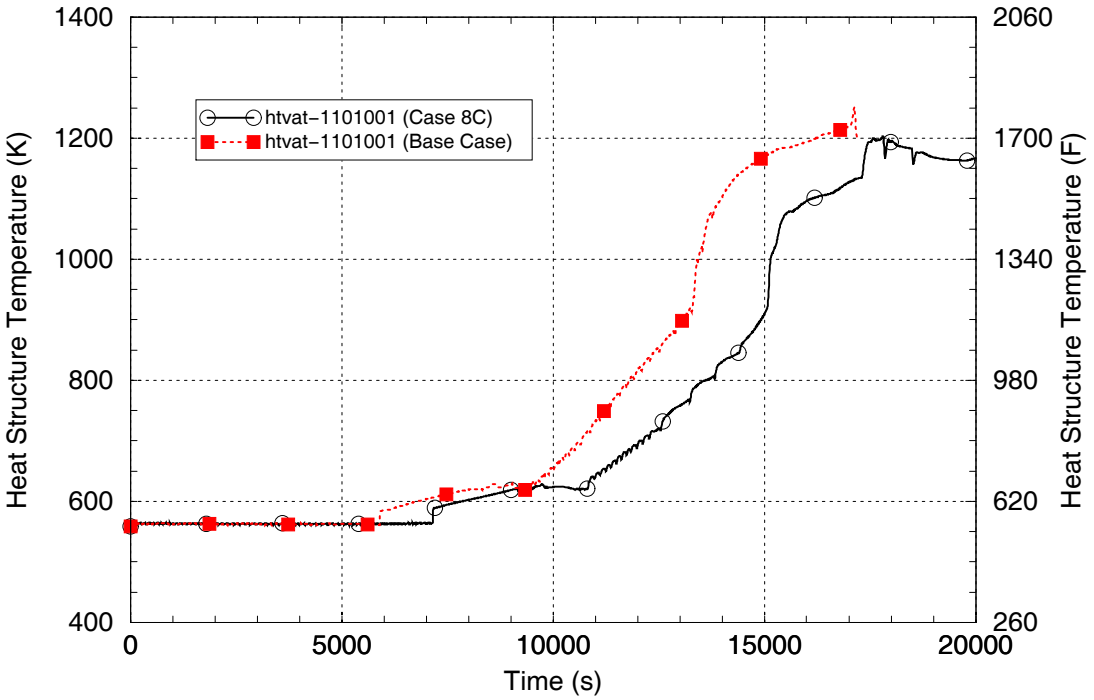

Figure 71. SG 1 Average Tube Wall Temperature for the SG Tube Leakage Sensitivity Case.

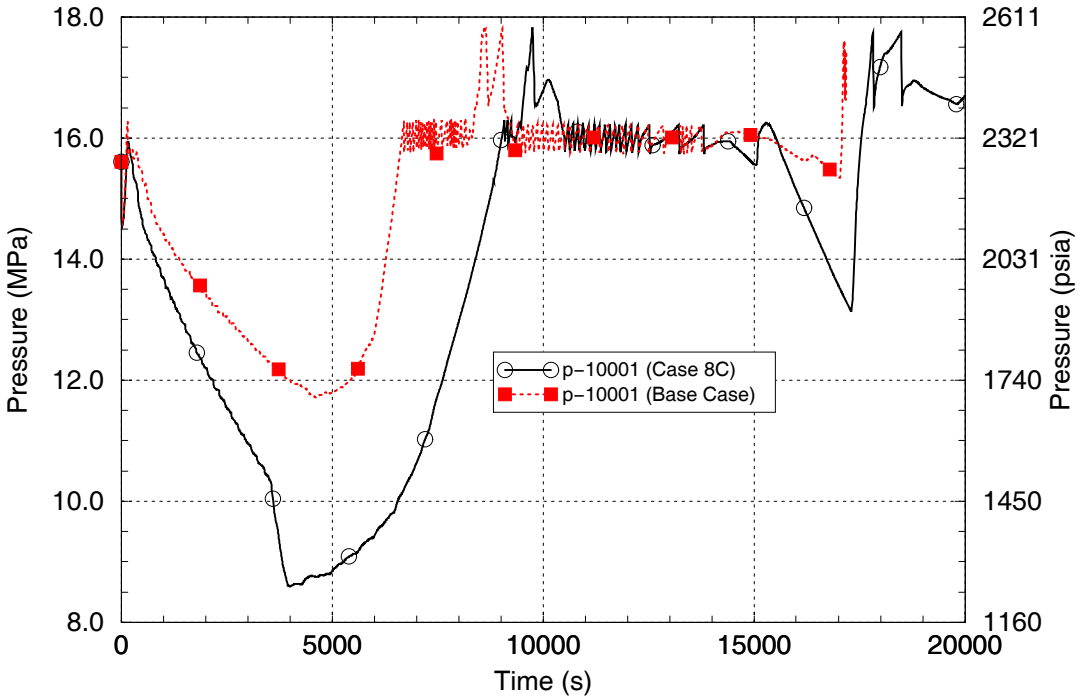

Figure 72. Hot Leg Pressure for the SG Tube Leakage Sensitivity Case.

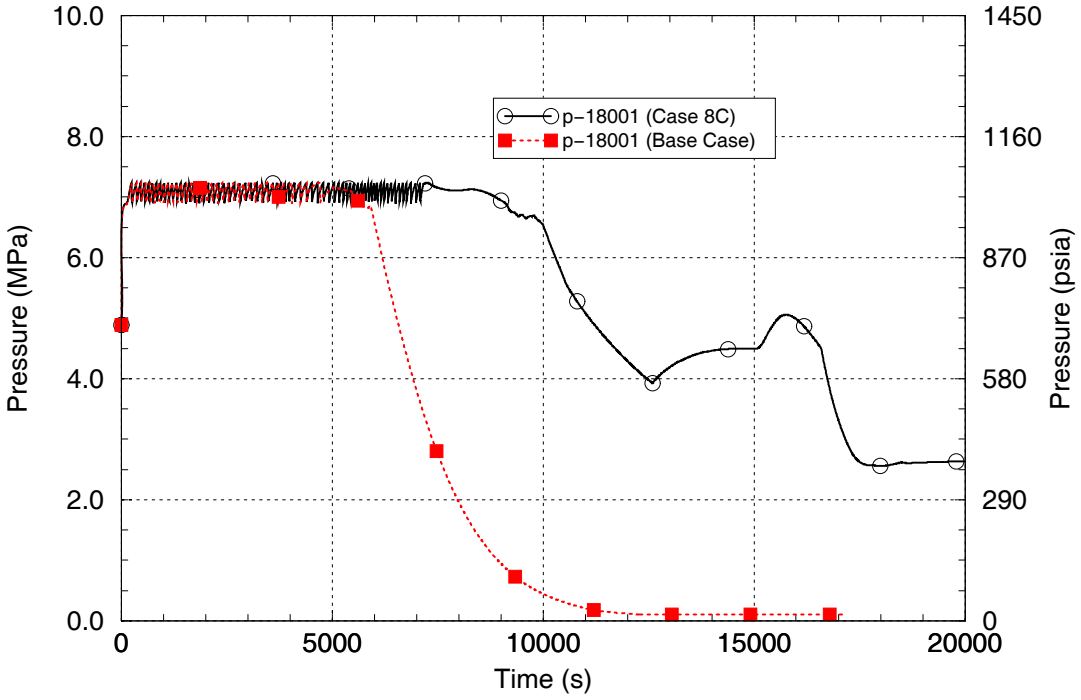

Figure 73. SG 1 Secondary Pressure for the SG Tube Leakage Sensitivity Case.

7.0 ESTIMATES OF UNCERTAINTIES IN THE CALCULATION OUTPUT

Section 7.1 describes the method used to estimate the uncertainties in the SCDAP/RELAP5-calculated responses for the key output parameters (the dependent variables). The method compares the output from the SCDAP/RELAP5 base case calculation and sensitivity calculations performed to evaluate the changes in the dependent variables resulting from variations in the independent variables (which are parameters deemed by the PIRT evaluation to be important for the simulation of the dependent variables). The uncertainty evaluation results are described in Section 7.2

7.1 Method for Estimating Uncertainties

The eight dependent variables for the uncertainty study are the key parameters used by the project stress analysts and probabilistic risk assessment analysts:

- Failure margin for average SG tube
- Failure margin for hottest SG tube
- Average SG tube metal temperature
- Hottest SG tube metal temperature
- Hot leg steam temperature
- Hot leg piping wall inner surface heat transfer coefficient
- Pressurizer surge line steam temperature
- Pressurizer surge line piping wall inner surface heat transfer coefficient

The exact descriptions (location, evaluation time, smoothing process, etc.) selected for each of the dependent variables are provided in Section 5.1.

The PIRT identified 15 parameters important for the plant thermal-hydraulic response; these are the independent variables for the uncertainty study. For each PIRT parameter, the thermal-hydraulic phenomena, the event sequence assumptions and progression, the current SCDAP/RELAP5 modeling, experience from prior sensitivity analyses and prior SCDAP/RELAP5 assessments were evaluated. From these evaluations, the list of 19 sensitivity runs in Table 8 was developed to generate statistics needed for the uncertainty evaluation. The sensitivity runs incorporate variations into the model that cover the expected ranges of the important PIRT parameters. The sensitivity run output for the temperatures, heat transfer coefficients and SG tube failure margins is then compared against the corresponding output from the base case calculation and the differences are used to estimate the uncertainties in the dependent variables.

A paper by Macdonald, Clark and Strachan (Reference 31) describes methods for assessing the uncertainty in simulation of building energy and environmental responses. The situation described in the paper is analogous in many respects to the subject analysis of this report. A model of the physical building is assembled (similar to the SCDAP/RELAP5 plant model) consistent with the geometry, materials, and initial and boundary conditions. To characterize the building performance, the model is run using simulation software (similar to the

SCDAP/RELAP5 computer code) to represent the physical processes, such as flow of heat and moisture.

Reference 31 indicates that the traditional and most widely-used methods for assessing uncertainty are based on sensitivity analysis. Sensitivity analysis allows assessing the relationship between variations in input parameters and resulting variations in the output predictions. The sources of uncertainty affecting the model need to be identified and quantified, which for this application has been accomplished through the PIRT and subsequent evaluations related to the PIRT parameters. Reference 31 describes a differential sensitivity analysis method which is adopted here. This method requires a base case simulation in which the input parameters are set to represent their best-estimate conditions. The simulation is then repeated with one input parameter varied to represent its expected extreme variation in one direction and the effect on the output variables are noted. The method assumes linearity, which means that variation of the input parameter in the opposite direction results in corresponding opposite variations in the output variables.

A differential sensitivity analysis is not optimized for the number of simulations required and does not identify parameter interactions, for which factorial designs could be used. In this analysis, the number of uncertain parameters is ten and 19 sensitivity runs have been performed in addition to the base case run. A full factorial analysis for ten parameters would require 1,024 SCDAP/RELAP5 runs, although fractional factorial design approaches could reduce the number of runs somewhat. An alternate approach for addressing parameter interactions using Bayesian Networks (also involving additional sensitivity runs) could be used.

Given the complexity of performing SCDAP/RELAP5 runs, it was judged for this project that expanding the number of runs past 20 cannot be justified at this time for economic reasons. Instead, maximum use is made of the 19 sensitivity runs to determine rough estimates for the uncertainties in the temperatures, heat transfer coefficients and SG tube failure margins. These rough uncertainty estimates will be provided to the stress and probabilistic risk analysts. Should it later be found that the uncertainties in the thermal-hydraulic results dominate the uncertainties in the overall project results, then the additional effort to use a fractional factorial or Bayesian Network approach for addressing the interactions among the parameters may be justified.

It is assumed that the set of sensitivity runs is normally distributed (i.e., based on a Gaussian distribution with the shape of the “bell curve”) around the base case run.

Reference 32 provides the following formula for the standard deviation, σ_x, of N readings of parameter x around a mean value, m:

$$\sigma_x = \{ [1.0 / (N - 1.0)] \sum_{i=1}^{N} (x_i - m)^2 \}^{0.5}$$

For our application, N (the number of sensitivity runs) is 19, the x_i are the values for the dependent variable output variables from the sensitivity runs and m is the corresponding values for the dependent variables from the output of the base case run. The primary results from the

uncertainty study are the values for σ_x, representing rough estimates for the standard deviations of the SCDAP/RELAP5 calculated results, for the eight dependent variables (the SG tube failure margins, temperatures and wall heat transfer coefficients). For this report, the standard deviations in the dependent variables are reported first using the above approach.

Next, for some of the x_i parameters, there are indications that the distribution around the base case values may not be symmetric. For example, plant operating experience suggests that it is more likely that our base case calculation is underpredicting, rather than overpredicting, the heat loss from the RCS into the containment. The effects of modifying the standard deviation calculation in the following manner, which introduces weighting factors, w_i, to account for known unsymmetrical behavior, are evaluated:

$$\sigma_x = \{ [1.0 / (N - 1.0)] \sum_{i=1}^{N} [w_i (x_i - m)^2] \}^{0.5}$$

This weighting-factor approach introduces, in a simplistic way, the concept of distributions in the independent variables, such as featured in factorial, response surface approaches to uncertainty evaluation. For this report, the standard deviations in the dependent variables are also reported using this second, weighting-factor approach.

Finally, consideration is added that the 20 runs (base case and 19 sensitivity cases) collectively, rather than the base case alone, represent the true mean. With this approach, the total uncertainty includes the effects of uncertainty in the mean itself, not just an uncertainty due to distribution around the mean. From Reference 32 the uncertainty in the mean σ_m is given by:

$$\sigma_m = \sigma_x / N^{0.5}$$

For the purposes here a revised total standard deviation, σ, is developed by combining the uncertainty in the mean with the uncertainty of the distribution around that mean:

$$\sigma = [\sigma_m^2 + \sigma_x^2]^{0.5} = \sigma_x [(1.0 / N^{0.5})^2 + 1.0^2]^{0.5}$$

For N = 20, this becomes: $\sigma = 1.025\ \sigma_x$

The standard deviations provided in this report are therefore calculated using both unweighted and weighted approaches, with and without application of a multiplier that considers the uncertainty in the mean.

7.2 Uncertainty Estimate Results

The SCDAP/RELAP5-calculated results for the eight dependent variables (temperatures, heat transfer coefficients and SG tube failure margins) for the station blackout base case run and the 19 sensitivity runs are shown in Tables 10 and 11. For each sensitivity run, the differences between the results for the sensitivity and base case runs are taken for each dependent variable. Tables 17 and 18 compile the differences between the sensitivity and base case run results. The

differences are calculated by subtracting the base case dependent variable values from the corresponding sensitivity run dependent variable values.

As identified in the tables, the differences listed for certain runs reflect adjustments made to the output data from the SCDAP/RELAP5 sensitivity case calculations. The runs for Cases 2A and 2B were performed to consider ±15% variations in the hot leg discharge coefficient. It was subsequently judged that larger variations are needed to bound the expected ranges for that parameter. The differences shown for Cases 2A and 2B represent twice the differences calculated between those runs and the base case run, thereby effectively representing ±30% variations in the hot leg discharge coefficient. The differences shown for Cases 4A and 4B (variations in the fuel rod oxidation power) were adjusted to account for slight changes seen in the calculated response as a result of implementing the model features needed to perform the sensitivity runs (see discussion for PIRT Parameter B1 in Section 5.2). The differences shown for Case 7A (61 gpm per pump shaft seal leakage after two hours) reflect adjustments, based on interpolation of results, to represent a 41-gpm RCP shaft seal leakage rate assumption (see discussion for PIRT Parameter C2 in Section 5.2).

For each of the dependent variables, the relative magnitudes of the differences associated with the sensitivity cases in Tables 17 and 18 reflect their influence on the overall uncertainty. For three of the dependent variables (average SG tube failure margin, average SG tube wall temperature and hottest SG tube wall temperature), the uncertainties from many independent variables contribute relatively-equally to the overall uncertainty. For the other five dependent variables, the overall uncertainty is dominated by the contributions from only a few of the independent variables. When the number of dependent variables for which the individual contributions are considered dominant are counted, the following cases are seen to have the most important effect on the overall uncertainties (in decreasing order of importance): Case 5A (50% decrease in reactor vessel internal circulation rate), Case 4B (50 % decrease in fuel rod oxidation power) and Case 7A (RCP shaft seal leakage increased to 41 gpm per pump at two hours).

Standard deviations are calculated for each of the eight dependent variables using the methods described in Section 7.1. The standard deviation results shown in Table 19 are calculated with four different approaches: using equal-weighting and biased-weighting of the independent-variable terms and with and without considering the effects of uncertainty in the mean.

The biased-weighting approach takes advantage of information, where available, regarding the likelihoods of the variation of a parameter in one direction versus the other direction. Pertinent information may be available from plant operating experience, the assessment of SCDAP models against specific severe accident experiments and the assessment of RELAP5 models against a much larger set of general reactor safety-related thermal-hydraulic experiments. The scheme by which biased weighting is applied in this analysis is described as follows.

For most of the independent variables, there was no known basis supporting the weighting of variations in one direction differently than those in the other direction. For the cases in this category (1A, 1B, 2A through 2G, 3A and 3B), weighting factors of 1.0 were used.

For the fuel rod oxidation power sensitivity cases, there are pertinent prior assessments of SCDAP/RELAP5 capabilities for predicting hydrogen generation in nine tests and five experimental facilities (FLHT, PBF, CORA, PHEBIS and ACRR, see Reference 1, Volume 5, Table 3-1). In these assessments, the code underpredicted hydrogen generation in seven tests and overpredicted it in two tests. To account for this underprediction bias, the results for Case 4A (oxidation rate x 1.2) are weighted by (2 x 7 / 9 =) 1.556 and the results for Case 4B (oxidation rate x 0.5) are weighted by (2 x 7 / 9 =) 0.444.

For the vessel internal circulation sensitivity, years of general RELAP5 assessment background suggests that, due to numerical difficulties, the code is much more likely to overpredict circulation rates than to underpredict them. To account for this overprediction bias, the results for Case 5A (50% decrease in vessel circulation rate) are weighted by (2 x 2 / 3 =) 1.333 and the results for Case 5B (100% increase in vessel circulation rate) are weighted by (2 x 1 / 3 =) 0.667.

For the heat loss sensitivity, an EPRI report (Reference 29) indicates that vessel and piping insulation installed in plants is in general performing more poorly than designed. This suggests that a higher RCS heat loss is more likely than a lower RCS heat loss. To account for this bias, the results for Case 6A (2 MW total RCS heat loss) are weighted by (1 x 2 / 3 =) 0.667 and the results for Case 6B (8 MW total RCS heat loss) are weighted by (2 x / 3 =) 1.333.

Finally, for the RCP shaft seal leak sensitivity, $\pm$20 gpm variations around the nominal 21 gpm per pump leakage are assumed. This uncertainty accounts for several factors related to: (1) predicting the correct conditions upstream of the leak, (2) adequately representing the complex geometry of the pump shaft seal configuration and (3) general considerations regarding the prediction capabilities of the RELAP5 critical flow model. Case 7G (1 gpm leakage per pump after two hours) considers that the code might underpredict the leak flow by a factor of (21 / 1 =) 21.0. Case 7A (adjusted for 41 gpm leakage per pump after two hours) considers that the code might overpredict the flow by a factor of (41 / 21 =) 1.95. Since RELAP5 code assessment experience shows no general bias for the code either underpredicting or overpredicting critical flows, the results for these two cases are weighted (90% x 2 =) 1.8 for Case 7A (adjusted for 41 gpm) and (10% x 2 =) 0.2 for Case 7G (1 gpm).

The results for the standard deviations calculated with equal weighting and biased weighting of the sensitivity case results are seen to generally be similar. For only three of the dependent variables (hot leg wall inside surface heat transfer coefficient, pressurizer surge line steam temperature and pressurizer surge line wall inside surface heat transfer coefficient) are the differences in the standard deviations obtained with equal-weighting and biased-weighting greater than 10%. The greatest difference is only 22%. Since the weighted approach provides results which take advantage of various additional assessment, modeling and plant operation experiences, the use of the standard deviations calculated using the weighted approach is recommended.

Finally, since the total number of cases is only 20, the approach which applies a 1.025 multiplier to consider effects related to the uncertainties in the mean values for the dependent variables is recommended.

The recommended results for the standard deviations in the eight dependent variables are shown in the right-hand column of Table 19.

Table 17. Compilation of Differences Between the SCDAP/RELAP5-Calculated Results from the Sensitivity and Base Case Runs for the SG Tube Failure Margin and SG Tube Temperature Dependent Variables.

Case Number and Description of the Variation	Difference in SG 1 Hottest Tube with 1.0 Multiplier Failure Time – First Primary Failure Time (s)	Difference in SG 1 Average Tube Stress Multiplier for Tube Failure Coincident with First Primary Failure (-)	Difference in SG 1 Average Tube Structure Temperature (K)	Difference in SG 1 Hottest Tube Structure Temperature (K)
Case 1A, Pressurizer PORV and SRV flow areas x 1.3	0.02	-0.03	1.33	-0.08
Case 1B, Pressurizer PORV and SRV flow areas x 0.7	4.99	0.01	-0.78	-0.91
Case 2A (adjusted), Hot Leg Discharge Coefficient x 1.3	0.04	-0.37	35.32	28.98
Case 2B (adjusted), Hot Leg Discharge Coefficient x 0.7	40.00	0.57	-43.71	-42.46
Case 2C, recirculation ratio = 2.3	-14.99	0.08	-7.10	8.02
Case 2D, recirculation ratio = 1.7	19.98	-0.08	6.88	-22.54
Case 2E, mixing fractions = 0.95	9.99	0.40	-34.95	-13.62
Case 2F, mixing fractions = 0.75	-4.98	-0.29	31.31	7.49
Case 2G, assumed hot/cold tube split = 50%/50%	15.00	0.11	-7.84	-22.32
Case 3A, SG tube wall outside surface HTC x 5.0	120.02	0.25	-20.96	-66.66
Case 3B, SG tube wall outside surface HTC x 0.5	-5.02	-0.03	2.07	8.87
Case 4A (adjusted), fuel rod oxidation power x 1.2	-14.98	0.06	-3.23	0.47
Case 4B (adjusted), fuel rod oxidation power x 0.5	64.94	-0.19	9.26	-50.06
Case 5A, vessel internal circulation rate x 0.5	-104.98	0.18	-22.49	-82.11
Case 5B, vessel internal circulation rate x 2.0	65.01	-0.13	10.10	-8.30
Case 6A, 2 MW total RCS heat loss	14.97	0.02	-3.74	-4.65
Case 6B, 8 MW total RCS heat loss	-99.98	-0.18	19.04	11.01
Case 7A (adjusted), 41 gpm pump seal leakage after 2 hours	-27.50	0.11	-11.93	-29.73
Case 7G, 1 gpm pump leakage after 2 hours	15.00	-0.02	1.32	-5.04

Table 18. Compilation of Differences Between the SCDAP/RELAP5-Calculated Results from the Sensitivity and Base Case Runs for the Hot Leg and Surge Line Temperature and Heat Transfer Coefficient Dependent Variables.

Case Number and Description of the Variation	Difference in Hot Leg 1 Steam Temperature (K)	Difference in Hot Leg 1 Wall Inside Surface HTC (W/m^2-K)	Difference in Surge Line Steam Temperature (K)	Difference in Surge Line Wall Inside Surface HTC (W/m^2-K)
Case 1A, Pressurizer PORV and SRV flow areas x 1.3	-4.12	11.40	5.25	71.44
Case 1B, Pressurizer PORV and SRV flow areas x 0.7	-2.23	-10.23	-2.45	-36.03
Case 2A (adjusted), Hot Leg Discharge Coefficient x 1.3	-62.60	11.71	-24.78	20.45
Case 2B (adjusted), Hot Leg Discharge Coefficient x 0.7	-63.00	-47.42	-52.80	-30.15
Case 2C, recirculation ratio = 2.3	-46.67	1.13	-23.86	70.79
Case 2D, recirculation ratio = 1.7	-46.23	-18.86	-24.19	-19.90
Case 2E, mixing fractions = 0.95	-50.94	-15.23	-20.80	26.32
Case 2F, mixing fractions = 0.75	4.27	15.04	-4.04	52.12
Case 2G, assumed hot/cold tube split = 50%/50%	12.30	-15.78	3.98	-47.96
Case 3A, SG tube wall outside surface HTC x 5.0	-38.13	-9.30	-19.28	8.94
Case 3B, SG tube wall outside surface HTC x 0.5	-25.01	-9.95	-18.03	-26.87
Case 4A (adjusted), fuel rod oxidation power x 1.2	-9.26	15.71	-4.89	57.40
Case 4B (adjusted), fuel rod oxidation power x 0.5	-98.33	-125.20	-98.42	-247.09
Case 5A, vessel internal circulation rate x 0.5	-172.77	-42.22	-124.27	-22.12
Case 5B, vessel internal circulation rate x 2.0	24.48	-0.33	32.69	36.53
Case 6A, 2 MW total RCS heat loss	-11.97	-8.00	-8.23	-28.26
Case 6B, 8 MW total RCS heat loss	-36.20	-4.09	-47.52	-0.46
Case 7A (adjusted), 41 gpm pump seal leakage after 2 hours	-22.41	-29.25	-122.72	-105.55
Case 7G, 1 gpm pump leakage after 2 hours	-40.73	-1.86	-12.28	71.64

Table 19. Standard Deviations for the Dependent Variables Calculated Using Four Methods.

Parameter and Units	Standard Deviations Approach 1 Equal Weighting Base Case = Mean	Standard Deviations Approach 2 Equal Weighting Uncertainty in the Mean Effects Included	Standard Deviations Approach 3 Biased Weighting Base Case = Mean	**Recommended** Standard Deviations Approach 4 Biased Weighting Uncertainty in the Mean Effects Included
1.0-Multiplier Hottest Tube Failure Margin [Hottest Tube Failure Time – First Primary Piping Failure Time] (s)	51.60	52.87	53.57	54.89
Average Tube Failure Margin [Stress Multiplier for Tube Failure Coincident with First Primary Failure]	0.227	0.233	0.228	0.234
Average SG Tube Wall Temperature (K)	19.98	20.47	20.43	20.93
Hottest SG Tube Wall Temperature (K)	32.36	33.16	33.67	34.50
Hot Leg Steam Temperature (K)	58.16	59.60	60.00	61.48
Hot Leg Wall Inside Surface Heat Transfer Coefficient (W/m^2-K)	35.37	36.24	29.06	29.78
Pressurizer Surge Line Steam Temperature (K)	52.45	53.75	58.50	59.94
Pressurizer Surge Line Wall Inside Surface Heat Transfer Coefficient (W/m^2-K)	75.61	77.48	64.56	66.15

8.0 CONCLUSIONS

Standard deviations have been developed for the uncertainties in eight important output parameters (the dependent variables, which are SG tube failure margins, temperatures and heat transfer coefficients) for SCDAP/RELAP5 simulations of station blackout severe accident events in a Westinghouse PWR. The standard deviations are obtained using a sensitivity-study method employing 19 sensitivity runs in addition to the base-case run.

Standard deviations are calculated through four different approaches, using equal-weighting and biased-weighting of the independent-variable contributions to uncertainty, and with and without consideration of the uncertainties in the means. Since a weighted approach provides results which take advantage of various additional assessment, modeling and plant operation experiences, the use of the standard deviations calculated using the weighted approach are recommended. Since the total number of cases is only 20, the calculation approach which applies a 1.025 multiplier in order to include the consideration that there is an uncertainty in the mean values for the dependent variables is also recommended.

The base-case values, the evaluation times and the recommended standard deviations for the eight dependent variables are listed in Table 20.

Twelve additional SCDAP/RELAP5 sensitivity cases were also run to evaluate various modeling, plant configuration and event-sequence issues unrelated to evaluation of the uncertainties.

Table 20. Base Case Values and Recommended Standard Deviations for the Dependent Variables.

Parameter and Units	Evaluation Time for Base Case Value (s)	Base Case Value	Recommended Standard Deviation
Hottest SG Tube Failure Margin [1.0 Stress Multiplier Hottest Tube Failure Time – First Primary Piping Failure Time], s	Not Applicable	-155	54.89
Average SG Tube Failure Margin [Stress Multiplier for Tube Failure Coincident with First Primary Piping Failure], dimensionless	Not Applicable	2.10	0.234
Average SG Tube Wall Temperature, K	13,630	1021.7	20.93
Hottest SG Tube Wall Temperature, K	13,630	1239.6	34.50
Hot Leg Steam Temperature, K	13,517	1776.0	61.48
Hot Leg Wall Inside-Surface Heat Transfer Coefficient, W/m^2-K	13,517	423.1	29.78
Pressurizer Surge Line Steam Temperature, K	13,517	1373.0	59.94
Pressurizer Surge Line Wall Inside-Surface Heat Transfer Coefficient, W/m^2-K	13,517	490.9	66.15

9.0 REFERENCES

1. L. J. Siefken et al., *SCDAP/RELAP5/MOD3.3 Code Manual,* NUREG/CR-6150, INEL-96/0422, Revision 2, Idaho National Engineering and Environmental Laboratory, January 2001.
2. D. L. Knudson, L. S. Ghan, and C. A. Dobbe, *SCDAP/RELAP5 Evaluation of the Potential for Steam Generator Tube Ruptures as a Result of Severe Accidents in Operating Pressurized Water Reactor*s, Idaho National Engineering and Environmental Laboratory, EXT-98-00286, Revision 1, September 1998.
3. Westinghouse Four-Loop Plant Design Differences Letter Report (title pending review).
4. L. W. Ward and V. V. Palazov, *Sequence Variations, Task 3.2: Accident Sequence Variations*, Information Systems Laboratories, Inc., ISL-NSAD-NRC-01-004, September 2001.
5. L. W. Ward and V. V. Palazov, *Sequence Variations, Task 3.3: Potential Conservatisms*, Information Systems Laboratories, Inc., ISL-NSAD-NRC-01-004 (Draft) , March 2002.
6. L. W. Ward, *Tube-to-Tube Temperature Variations During the Station Blackout Event, Task 3.5: Tube-to-Tube Temperature Variations*, Information Systems Laboratories, Inc., ISL-NSAD-TR-02-03, (Draft) August 2002.
7. W. A. Stewart, et al., "Natural Circulation Experiments for PWR High Pressure Accidents," EPRI Project No. RP2177-5, Westinghouse Electric Corp., December 1992.
8. Westinghouse Four-Loop Plant Revised Base Case Calculation Letter Report (title pending review).
9. Westinghouse Four-Loop Plant Sensitivity Evaluation Report (title pending review).
10. Westinghouse Four-Loop Plant Base Case Calculation for the Station Blackout Uncertainty Study (title pending review).
11. F. R. Larson and J. Miller, "A Time Temperature Relationship for Rupture and Creep Stress," *Transactions of the ASME*, July 1952, pp. 765-775.
12. "Minutes of PIRT Meeting on Containment Bypass Issue," C. D. Fletcher, Information Systems Laboratories, Inc., email to PIRT meeting participants, October 13, 2005.
13. Minutes, Advisory Committee on Reactor Safeguards, Joint Materials and Metallurgy and Thermal-Hydraulic Subcommittees Meeting, "Steam Generator Action Plan," February 3-4, 2004, Rockville MD.
14. S. J. Leach and H. Thompson, "An Investigation of Some Aspects of Flow into Gas Cooled Reactors Following an Accidental Depressurization," *Journal of British Nuclear Energy Society*, Vol. 14, No. 3, 1975, pp. 243-250.
15. N. Zuber and J. Findlay, "Average Volumetric Concentrations in Two-Phase Flow Systems, *Journal of Heat Transfer*, Vol. 87, 1965, pp. 453-568.
16. I. Kataoka and M. Ishii, "Drift Flux Model for Large Diameter Pipe and New Correlations for Pool Void Fraction," *International Journal of Heat and Mass Transfer*, Vol. 30, 1987, pp. 1927-1939.
17. C. D. Fletcher, D. A. Prelewicz and W. C. Arcieri, "RELAP5/MOD3.2.2Gamma Assessment for Pressurized Thermal Shock Applications," NUREG/CR-6857, Information Systems Laboratories, Inc., October 2004.
18. L. Erickson, et al., "The Marviken Full-Scale Critical Flow Tests Interim Report: Results from Test 22," MXC222, March 1979.

19. L. Erickson, et al., "The Marviken Full-Scale Critical Flow Tests Interim Report: Results from Test 24," MXC224, May 1979.
20. D. L. Gills and J. M. Carpenter, "Experimental Data Report for LOFT Nuclear Small Break Experiment L3-7," Idaho National Engineering Laboratory, EG&G Idaho, Inc., NUREG/CR-1570, August 1980.
21. P. D. Bayless and J. M. Devine, "Experiment Data Report for LOFT Large Break Loss of Coolant Experiment L2-5," Idaho National Engineering Laboratory, NUREG/CR-2826, EGG-2210, August 1982.
22. P. D. Bayless, J. B. Marlow and R. H. Averill, "Experiment Data Report for LOFT Nuclear Small Break Experiment L3-1," Idaho National Engineering Laboratory, NUREG/CR-1145, EGG-2007, January, 1980.
23. ISP-26, OECD/NEA/CSNI International Standard Problem No. 26, ROSA-IV LSTF Cold-Leg Small-Break LOCA Experiment, Comparison Report, OECD Nuclear Energy Agency, NEA/CSNI/R(91)13, February 1992.
24. T. F. Habib, et al., "Multiloop Integral System Test (MIST): MIST Facility Functional Specification," NUREG/ CR-5670, April, 1991.
25. J. A. Klingenfus and M. V. Parece, "Multiloop Integral Systems Test, Final Report," NUREG/CR-5395, December 1989.
26. F. W. Dittus and L. M. K. Boelter, "Heat Transfer in Automobile Radiators of the Tubular Type," *Publications in Engineering*, Vol. 2, University of California, Berkeley, 1930, pp. 443-461.
27. "American National Standard For Decay Heat Power in Light Water Reactors," ANSI-5.1-1979, American Nuclear Society, 1979.
28. Kraftwerk Union AG, "Upper Plenum Test Facility, Test No. 1, Fluid-Fluid Mixing Test," R515/87/09, April 1987.
29. EPRI Report NP-2694, Research Project No. 1730-1, "Control of Containment Air Temperature: An Industry Survey and Insulation Test," Final Report, October 1982.
30. Evaluation Report of Westinghouse Four-Loop Plant RCP Seal Models (title pending review).
31. I. A. Macdonald, J. A. Clarke and P. A. Stracham, "Assessing Uncertainty in Building Simulation," *Proceedings of Building Simulation '99*, Kyoto, Japan, September 13-15, 1999, Vol. 2, pp. 683-690.
32. L. Riley, "Random or Statistical Uncertainties, Estimating Uncertainties," http://webpages.ursinus.edu/lriley/ref/unc/unc.html, Ursinus College, Collegeville, Pensylvania, January 10, 2006.

APPENDIX A - SUMMARY OF ADDITIONAL DATA PROVIDED ON DVDS

The data provided electronically on the DVDs accompanying this report is summarized as follows:

Cover Letter and Attachment

PDF electronic files of the cover letter and attachment of this transmittal.

Standard Files for the SCDAP/RELAP5 Station Blackout Base Case Calculation Described in Section 3 and the Sensitivity Calculations Described in Section 6.

Input, output and demux plot files are provided for each of the four calculation steps. For the base case, input files are named uncbasesX.i and printed output files are named uncbasesX.o (where "X" is the calculation step number, 1 through 4). The demux file, containing all plotted data covering the full period of Steps 1 through 4, is named uncbases4.dmx.

For the sensitivity cases the input and output file names are similar, except that "uncbase" is replaced with the sensitivity case identifier.

Supplemental Data for the Revised SCDAP/RELAP5 Station Blackout Base Case Calculation Described in Section 3 and the Sensitivity Calculations Described in Section 6

To facilitate analyses performed by others in the project, additional output data channels have been stripped from the demux output files and stored separately. The additional data channels stored are listed in Tables A-1 through A-11.

The list includes all known data requests from other analysts in the project; please advise should you need additional data from the calculations.

Table A-1. Supplemental Pressure Data.

Channel Identifiers PCCCNN P = Pressure CCC = Component Number NN = Axial Cell Number Units: Pa	Location
p10001	Hot Leg 1 upper section, cell adjacent to the reactor vessel
p11001	SG 1 average tube, inside lowermost active cell
p12204	Cold Leg 1, adjacent to the reactor vessel
p15307	Pressurizer surge line, cell adjacent to hot leg
p16001	Containment
p18001	SG 1 steam dome pressure
p20001	Hot leg 2 upper section, cell adjacent to the reactor vessel
p21001	SG 2 average tube, inside lowermost active cell
p22204	Cold Leg 2, cell adjacent to the reactor vessel
p28001	SG 2 steam dome pressure
p38001	SG 3 steam dome pressure
p48001	SG 4 steam dome pressure

Table A-2. Supplemental Steam Temperature Data.

Channel Identifiers TempgCCCNN Tempg = Steam Temperature CCC = Component Number NN = Axial Cell Number **Cntrlvar76X3**[1] X = 1 through 9 Units: K	Location
tempg10001 through tempg10005	Hot Leg 1 upper section, axial cells 1 (at reactor vessel end) through 5 (at SG end)
tempg10101 through tempg10105	Hot Leg 1 lower section, axial cells 1 (at SG end) through 5 (at reactor vessel end)
tempg 10501	SG 1 hot inlet plenum
tempg10601	SG 1 mixing inlet plenum
tempg 10701	SG 1 cold inlet plenum
tempg11003 through tempg11013	SG 1 hot average tube, axial cells 3 (just above tubesheet) through 13 (at top of the U-bend)
tempg112003through tempg112013	SG 1 hottest tube, axial cells 3 (just above tubesheet) through 13 (at top of the U-bend). Component 112, not shown on diagrams, see Reference 8, Section 2.10.
tempg 12201 through tempg12204	Cold Leg 1 from the pump discharge to the reactor vessel
tempg15301 through tempg15307	Pressurizer surge line, axial cells 1 (at pressurizer end) through 7 (at hot leg end)
tempg16001	Containment – this is the sink temperature used for the primary and secondary system heat losses
tempg20001 through tempg20005	Hot Leg 2 upper section, axial cells 1 (at reactor vessel end) through 5 (at SG end)
tempg20101 through tempg20105	Hot Leg 2 lower section, axial cells 1 (at SG end) through 5 (at reactor vessel end)
tempg21003 through tempg21013	SG 2 hot average tube, axial cells 3 (just above tubesheet) through 13 (at top of the U-bend)
tempg22201 through tempg22204	Cold Leg 2 from the pump discharge to the reactor vessel
tempg56101	Exit of average core channel
Cntrlvar7603, Cntrlvar7613, Cntrlvar7623, Cntrlvar7633, Cntrlvar7643, Cntrlvar7653, Cntrlvar7663, Cntrlvar7673, Cntrlvar7683, Cntrlvar7693,	Hot Leg 1 upper and lower section steam temperatures. X = 0, 2, 4, 6, 8 for upper section from reactor vessel toward the SG and X = 1, 3, 5, 7, 9 for lower section also from reactor vessel toward the SG. See Footnote 1.

1 – Control variables 76X3 represent the Hot Leg 1 steam temperatures to be used in conjunction with the control variable 8X0Y convection-only heat transfer coefficients described in Note 5 of Table A-4.

Table A-3. Supplemental Wall Temperature Data.

Channel Identifiers HttempCCCGNNNXX Httemp = Wall Temperature CCCG = Component/Geometry Number NNN = Axial Heat Structure Number XX = Mesh Point Number Units: K	Location
httemp1001001XX through httemp1001005XX	Hot Leg 1 upper section wall, connected to hot leg Component 100, Cell 1 (NNN = 001, reactor vessel end) through Cell 5 (NNN = 005, SG end). Mesh points range from 1 (XX = 01) on inside surface to 9 (XX = 09) on outside surface.
httemp1011001XX through httemp1011005XX	Hot Leg 1 lower section wall, connected to hot leg Component 101, Cell 1 (NNN = 001, SG end) through Cell 5 (NNN = 005, reactor vessel end). Mesh points range from 1 (XX = 01) on inside surface to 9 (XX = 09) on outside surface.
httemp1051001XX	SG 1 hot inlet plenum wall, XX=1 for inside surface and XX=6 for outside surface.
httemp1061001XX	SG 1 mixing inlet plenum wall, XX=1 for inside surface and XX=6 for outside surface.
httemp1071001XX	SG 1 cold inlet plenum wall, XX=1 for inside surface and XX=6 for outside surface.
httemp1101001XX through httemp1101011XX	SG 1 average tube wall, connected to tube Component 110, Cell 3 (NNN = 001, just above tubesheet) through Cell 13 (NNN = 011, at U-bend). Only channels for surface mesh points are included, XX = 01 for inside surface and XX = 09 for outside surface.
httemp1121001XX through httemp1121011XX	SG 1 hottest tube wall, connected to hottest tube Component 112, Cell 3 (NNN = 001, just above tubesheet) through Cell 13 (NNN = 011, at U-bend). Only channels for surface mesh points are included, XX = 01 for inside surface and XX = 09 for outside surface. Component 112, not shown on diagrams, see Reference 8, Section 2.10.
httemp1531001XX through httemp1531007XX	Pressurizer surge line wall, connected to surge line Component 153, Cell 1 (NNN = 001, pressurizer end) through Cell 7 (NNN = 007, hot leg end). Mesh points range from 1 (XX = 01) on inside surface to 9 (XX = 09) on outside surface.

httemp2001001XX through httemp2001005XX	Hot Leg 2 upper section wall, connected to hot leg Component 200, Cell 1 (NNN = 001, reactor vessel end) through Cell 5 (NNN = 005, SG end). Mesh points range from 1 (XX = 01) on inside surface to 9 (XX = 09) on outside surface.
httemp2011001XX through httemp2011005XX	Hot Leg 2 lower section wall, connected to hot leg Component 201, Cell 1 (NNN = 001, SG end) through Cell 5 (NNN = 005, reactor vessel end). Only channels for surface mesh points are included, XX = 01 for inside surface and XX = 09 for outside surface.
httemp2071001XX	SG 2 cold inlet plenum wall, XX=1 for inside surface and XX=6 for outside surface.
httemp2101001XX through httemp2101011XX	SG 2 average tube wall, connected to tube Component 210, Cell 3 (NNN = 001, just above tubesheet) through Cell 13 (NNN = 011, at U-bend). Only channels for surface mesh points are included, XX = 01 for inside surface and XX=09 for outside surface.
httemp222100101	Cold Leg 2 inside surface temperature at reactor coolant pump discharge.

Table A-4. Supplemental Heat Transfer Coefficient Data.

Channel Identifiers IMPORTANT: SEE FOOTNOTES FOR USE OF THIS DATA **Cntrlvar7XX2** Heat Transfer Coefficient[1] XX = 01 through 17 **Cntrlvar73XX** Heat Transfer Coefficient[2] XX = 01 through 17 **TestdaXX** Heat Transfer Coefficient[3] XX = 01 through 17 **HthtcCCCGNNNSS** Heat Transfer Coefficient[4] CCCG = Component/Geometry Number NNN = Axial Heat Structure Number SS = Surface Identifier **Cntrlvar8X0Y** Heat Transfer Coefficient[5] X = 1 through 5 Y = 3 or 6 Units: W/m^2-K	Location
Convection-Only Heat Transfer Coefficient cntrlvar7012, cntrlvar7022, cntrlvar7032, cntrlvar7042, cntrlvar7052	Inside surface of Hot Leg 1 upper section wall, connected to hot leg Component 100, Cell 1 (XX = 01, reactor vessel end) through Cell 5 (XX = 05, SG end).
Convection-Only Heat Transfer Coefficient Cntrlvar7062, cntrlvar7072, cntrlvar7082, cntrlvar7092, cntrlvar7102	Inside surface of Hot Leg 1 lower section wall, connected to hot leg Component 101, Cell 1 (XX = 06, SG end) through Cell 5 (XX = 10, reactor vessel end).
Convection-Only Heat Transfer Coefficient cntrlvar7112, cntrlvar7122, cntrlvar7132, cntrlvar7142, cntrlvar7152, cntrlvar7162, cntrlvar7172	Inside surface of pressurizer surge line wall, connected to surge line Component 1531, Cell 1 (XX = 11, pressurizer end) through Cell 7 (XX = 17, hot leg end).

Steam-Wall Radiation Only Heat Transfer Coefficient cntrlvar7301, cntrlvar7302, cntrlvar7303, cntrlvar7304, cntrlvar7305	Inside surface of Hot Leg 1 upper section wall, connected to hot leg Component 100, Cell 1 (XX = 01, reactor vessel end) through Cell 5 (XX = 05, SG end).
Steam-Wall Radiation Only Heat Transfer Coefficient cntrlvar7306, cntrlvar7307, cntrlvar7308, cntrlvar7309, cntrlvar7310	Inside surface of Hot Leg 1 lower section wall, connected to hot leg Component 101, Cell 1 (XX = 06, SG end) through Cell 5 (XX = 10, reactor vessel end).
Steam-Wall Radiation Only Heat Transfer Coefficient cntrlvar7311, cntrlvar7312, cntrlvar7313, cntrlvar7314, cntrlvar7315, cntrlvar7316, cntrlvar7317	Inside surface of pressurizer surge line wall, connected to surge line Component 1531, Cell 1 (XX = 11, pressurizer end) through Cell 7 (XX = 17, hot leg end).
testda1, testda2, testda3, testda4, testda5	Inside surface of Hot Leg 1 upper section wall, connected to hot leg Component 100, Cell 1 (XX = 01, reactor vessel end) through Cell 5 (XX = 05, SG end).
testda6 testda7, testda8, testda9, testda10	Inside surface of Hot Leg 1 lower section wall, connected to hot leg Component 101, Cell 1 (XX = 06, SG end) through Cell 5 (XX = 10, reactor vessel end).
testda11, testda12, testda13, testda14, testda15, testda16, testda17	Inside surface of pressurizer surge line wall, connected to surge line Component 1531, Cell 1 (XX = 11, pressurizer end) through Cell 7 (XX = 17, hot leg end).
hthtc1001001SS through hthtc1001005SS	Hot Leg 1 upper section wall, connected to hot leg Component 100, Cell 1 (NNN = 001, reactor vessel end) through Cell 5 (NNN = 005, SG end). Surface identifier is SS = 00 on inside surface and SS = 01 on outside surface.
hthtc1011001SS through hthtc1011005SS	Hot Leg 1 lower section wall, connected to hot leg Component 101, Cell 1 (NNN = 001, SG end) through Cell 5 (NNN = 005, reactor vessel end). Surface identifier is SS = 00 on inside surface and SS = 01 on outside surface.
hthtc105100100	SG 1 hot inlet plenum wall, inside surface.
hthtc106100100	SG 1 mixing inlet plenum wall, inside surface.
hthtc107100100	SG 1 cold inlet plenum wall, inside surface.

hthtc1101001SS through hthtc1101011SS	SG 1 average tube wall, connected to tube Component 110, Cell 3 (NNN = 001, just above tubesheet) through Cell 13 (NNN = 011, at U-bend). Surface identifier is SS = 00 on inside surface and SS = 01 on outside surface.
hthtc1121001SS through hthtc1121011SS	SG 1 hottest tube wall, connected to hottest tube Component 112, Cell 3 (NNN = 001, just above tubesheet) through Cell 13 (NNN = 011, at U-bend). Surface identifier is SS = 00 on inside surface and SS = 01 on outside surface. Component 112, not shown on diagrams, see Reference 8, Section 2.10.
hthtc1531001SS through hthtc1531007SS	Pressurizer surge line wall, connected to surge line Component 153, Cell 1 (NNN = 001, pressurizer end) through Cell 7 (NNN = 007, hot leg end). Surface identifier is SS = 00 on inside surface and SS = 01 on outside surface.
hthtc2001001SS through hthtc2001005SS	Hot Leg 2 upper section wall, connected to hot leg Component 200, Cell 1 (NNN = 001, reactor vessel end) through Cell 5 (NNN = 005, SG end). Surface identifier is SS = 00 on inside surface and SS = 01 on outside surface.
hthtc2011001SS through hthtc2011005SS	Hot Leg 2 lower section wall, connected to hot leg Component 201, Cell 1 (NNN = 001, SG end) through Cell 5 (NNN = 005, reactor vessel end). Surface identifier is SS = 00 on inside surface and SS = 01 on outside surface.
hthtc2101001SS through Hthtc2101011SS	SG 2 average tube wall, connected to tube Component 210, Cell 3 (NNN = 001, just above tubesheet) through Cell 13 (NNN = 011, at U-bend). Surface identifier is SS = 00 on inside surface and SS = 01 on outside surface.
Convection-Only Heat Transfer Coefficient Cntrlvar8103, cntrlvar8203, cntrlvar8303, cntrlvar8403, cntrlvar8503	Inside surface of Hot Leg 1 upper section wall (Y = 3), connected to hot leg Component 100, Cell 1 (X = 1, reactor vessel end) through Cell 5 (X = 5, SG end).
Convection-Only Heat Transfer Coefficient Cntrlvar8106, cntrlvar8206, cntrlvar8306, cntrlvar8406, cntrlvar8506	Inside surface of Hot Leg 1 lower section wall (Y = 6), connected to hot leg Component 101, Cell 5 (X = 1, reactor vessel end) through Cell 1 (X = 5, reactor SG end). Note that the axial numbering convention for this set of control variables is in the reverse direction of the lower hot leg section cell numbering.

1 – The control variable (cntrlvar) parameters 70X2 and 71X2 listed in this table represent the convection-only heat transfer coefficient for use in ABAQUS analyses of the Hot Leg 1 and pressurizer surge line regions. These heat transfer coefficients contain no contribution from steam-to-wall or wall-to-wall radiation heat transfer. Based on CFD analysis, these heat transfer coefficients include a 50% enhancement in the normal SCDAP/RELAP5 convection heat transfer in the upper and lower hot leg sections.

2 – The control variable (cntrlvar) parameters 73XX listed in this table represent the heat transfer coefficient due only to steam-to-wall radiation heat transfer for use in ABAQUS analyses of the Hot Leg 1 and pressurizer surge line regions. These heat transfer coefficients contain no contribution from convection or wall-to-wall radiation heat transfer.

3 – The developmental assessment test (testda) parameters listed in this table represent the convection-only portion of the SCDAP/RELAP5 calculated heat transfer coefficient (parameter hthtc, see Note 4) for the Hot Leg 1 and pressurizer surge line regions. These heat transfer coefficients do not include the 50% enhancement for the hot leg described in Note 1. The testda parameters are provided only for reference should the data needs for the ABAQUS input later change.

4 – Parameter hthtc represents the combination of the convective and (where applied) steam-to-wall thermal radiation processes, but does not include effects of wall-to-wall thermal radiation process (where applied). For ABAQUS analysis of the Hot Leg 1 and pressurizer surge line region, the cntrlvar parameters described in Note 1 are to be used (the hthtc parameters are provided only for reference). For analyses in regions other than the hot leg and pressurizer surge line (for example, steam generator tube analyses), the hthtc parameters should be used.

5 – Additional control variables were developed in order to represent different expected heat transfer coefficient behavior in Hot Leg 1 during periods when pressurizer relief valves are open than when they are closed. Control variables 8X0Y represent the Hot Leg 1 convection-only steam-to-wall heat transfer coefficient response. During periods when all pressurizer relief valves are closed these control variables have the same values as the original convection-only heat transfer coefficients given by control variables 7XX2 and described in Note 1 above. During periods when any pressurizer relief valve (PORV or SRV) is open, these control variables represent convection-only heat transfer coefficients based on the net, co-current flows toward the surge line connection in the upper and lower Hot Leg 1 sections using the Dittus-Boelter correlation without the enhancement described in Note 1. The heat transfer coefficient responses provided by control variables 8X0Y include the effects of switching back and forth between the two processes, depending on the current status of the pressurizer relief valves. Note that when applying control variables 8X0Y as the heat transfer coefficients, the steam temperatures given by control variables 76X3 should be used (rather than the SCDAP/RELAP5 calculated cell steam temperatures), see Table A-2. The steam temperatures represented by control variables 76X3 also include the effects of switching between separated or combined hot leg flows based on the pressurizer valve status.

Table A-5. Supplemental Heat Flux Data.

Channel Identifiers HtrnrCCCGNNNSS or HftotCCCGNNNSS Htrnr or Hftot = Heat Flux[1] CCCG = Component/Geometry Number NNN = Axial Heat Structure Number SS = Surface Identifier Units: W/m^2	Location
hftot1001001SS through hftot1001005SS or htrnr1001001SS through htrnr1001005SS	Hot Leg 1 upper section wall, connected to hot leg Component 100, Cell 1 (NNN = 001, reactor vessel end) through Cell 5 (NNN = 005, SG end). Surface identifier is SS = 00 on inside surface and SS = 01 on outside surface. Use parameter Hftot for inner surface and parameter Htrnr for outer surface
hftot1011001SS through hftot1011005SS or htrnr1011001SS through hthtc1011005SS	Hot Leg 1 lower section wall, connected to hot leg Component 101, Cell 1 (NNN = 001, SG end) through Cell 5 (NNN = 005, reactor vessel end). Surface identifier is SS = 00 on inside surface and SS = 01 on outside surface. Use parameter Hftot for inner surface and parameter Htrnr for outer surface
htrnr105100100	SG 1 hot inlet plenum wall, inside surface.
htrnr106100100	SG 1 mixing inlet plenum wall, inside surface.
htrnr107100100	SG 1 cold inlet plenum wall, inside surface.
htrnr1101001SS through htrnr1101011SS	SG 1 average tube wall, connected to tube Component 110, Cell 3 (NNN = 001, just above tubesheet) through Cell 13 (NNN = 011, at U-bend). Surface identifier is SS = 00 on inside surface and SS = 01 on outside surface.
htrnr1121001SS through htrnr1121011SS	SG 1 hottest tube wall, connected to hottest tube Component 112, Cell 3 (NNN = 001, just above tubesheet) through Cell 13 (NNN = 011, at U-bend). Surface identifier is SS = 00 on inside surface and SS = 01 on outside surface. Component 112, not shown on diagrams, see Reference 8, Section 2.10.
htrnr1531001SS through htrnr1531007SS	Pressurizer surge line wall, connected to surge line Component 153, Cell 1 (NNN = 001, pressurizer end) through Cell 7 (NNN = 007, hot leg end). Surface identifier is SS = 00 on inside surface and SS = 01 on outside surface.

hftot2001001SS through hftot2001005SS or htrnr2001001SS through htrnr2001005SS	Hot Leg 2 upper section wall, connected to hot leg Component 200, Cell 1 (NNN = 001, reactor vessel end) through Cell 5 (NNN = 005, SG end). Surface identifier is SS = 00 on inside surface and SS = 01 on outside surface. Use parameter Hftot for inner surface and parameter Htrnr for outer surface.
hftot2011001SS through hftot2011005SS or htrnr2011001SS through hthtc2011005SS	Hot Leg 2 lower section wall, connected to hot leg Component 201, Cell 1 (NNN = 001, SG end) through Cell 5 (NNN = 005, reactor vessel end). Surface identifier is SS = 00 on inside surface and SS = 01 on outside surface. Use parameter Hftot for inner surface and parameter Htrnr for outer surface.
htrnr2101001SS through htrnr2101011SS	SG 2 average tube wall, connected to tube Component 210, Cell 3 (NNN = 001, just above tubesheet) through Cell 13 (NNN = 011, at U-bend). Surface identifier is SS = 00 on inside surface and SS = 01 on outside surface.

1 – Parameter htrnr represents the combined heat flux from convection and steam-to-wall thermal radiation (where applied) processes. Parameter hftot represents the combined heat flux from convection, steam-to-the wall thermal radiation (where applied) and wall-to-wall thermal radiation (where applied) processes. Both parameter htrnr and hftot include the effect of the multiplier placed on the combination of hot leg convection and steam-to-wall heat transfer intended to represent the enhancement of the convection portion of the heat transfer.

Table A-6. Supplemental Average Wall Temperature Data.

Channel Identifiers HtvatCCCGNNN Htvat = Ave. Temperature CCCG = Component/Geometry Number NNN = Axial Heat Structure Number Units: K	Location
htvat1001001 through htvat1001005	Hot Leg 1 upper section wall, connected to hot leg Component 100, Cell 1 (NNN = 001, reactor vessel end) through Cell 5 (NNN = 005, SG end).
htvat1011001 through htvat1011005	Hot Leg 1 lower section wall, connected to hot leg Component 101, Cell 1 (NNN = 001, SG end) through Cell 5 (NNN = 005, reactor vessel end).
htvat1101001 through htvat1101011	SG 1 average tube wall, NNN = 001 at tube sheet, NNN = 011 at U bend.
htvat1121001 through htvat1121011	SG 1 hottest tube wall, NNN = 001 at tube sheet, NNN = 011 at U bend.
htvat1221001	Cold Leg 1 wall adjacent to the reactor coolant pump discharge.
htvat1531007	Pressurizer surge line at hot leg end.
htvat2001001 through htvat2001005	Hot Leg 2 upper section wall, connected to hot leg Component 200, Cell 1 (NNN = 001, reactor vessel end) through Cell 5 (NNN = 005, SG end).
htvat2011001 through htvat2011005	Hot Leg 2 lower section wall, connected to hot leg Component 101, Cell 1 (NNN = 001, SG end) through Cell 5 (NNN = 005, reactor vessel end).
htvat2101001 through htvat2101011	SG 2 average tube wall, NNN = 001 at tube sheet, NNN = 011 at U bend.

Table A-7. Supplemental Mass Flow Rate Data.

Channel Identifiers MflowjCCCXX Mflowj = Mass Flow Rate CCC = Component Number XX = Junction Number Units: kg/s	Location
mflowj12203	Cold Leg 1, near the reactor vessel.
mflowj12500	Reactor Coolant Pump 1 shaft seal leak.
mflowj22203	Cold Leg 2, near the reactor vessel.
mflowj22500	Reactor Coolant Pump 2 shaft seal leak.

Table A-8. Supplemental Liquid Temperature Data.

Channel Identifiers TempfCCCXX Tempf = Liquid Temperature CCC = Component XX = Volume Number Units: K	Location
tempf12204	Cold Leg 1, cell adjacent to the reactor vessel.
tempf22204	Cold Leg 2, cell adjacent to the reactor vessel.

Table A-9. Supplemental Velocity Data

Channel Identifiers VelfCCCXX VelgCCCXX Velf = liquid velocity Velg = vapor velocity CCC = Component Number XX = volume number Units: m/s	Location
velf12204	Cold Leg 1 liquid velocity in cell adjacent to reactor vessel.
velg12204	Cold Leg 1 vapor velocity in cell adjacent to reactor vessel.
velf22204	Cold Leg 2 liquid velocity in cell adjacent to reactor vessel.
velg22204	Cold Leg 2 vapor velocity in cell adjacent to reactor vessel.

Table A-10. Supplemental Void Fraction.

Channel Identifiers VoidgCCCXX VoidgjCCCXX Voidg = Volume Void Voidgj = Junction Void CCC = Component XX = Volume or Junction Number Units: dimensionless	Location
voidg12204	Cold Leg 1, cell adjacent to reactor vessel.
voidgj12500	Reactor Coolant Pump 1 at the shaft seal leak location.
voidg22204	Cold Leg 2, cell adjacent to reactor vessel.
voidgj22500	Reactor Coolant Pump 2 at the shaft seal leak location.

Table A-11. Supplemental Pressurizer Relief Valve Status Indicator.

Channel Identifier Units: dimensionless	Data Format
cntrlvar7400	This control variable describes the status of the pressurizer PORVs and SRVs. The control variable has a value of 1.0 if any pressurizer PORV or SRV is open. The control variable has a value of 0.0 if all pressurizer PORVs and SRVs are closed. See Footnote 5 of Table A-4.